Quantum Geometry of Correlated Many-Body States

By

Ankita Chakrabarti

PHYS10201304001

The Institute of Mathematical Sciences, Chennai

A thesis submitted to the

Board of Studies in Physical Sciences

In partial fulfillment of requirements

For the Degree of

DOCTOR OF PHILOSOPHY

of

HOMI BHABHA NATIONAL INSTITUTE

July, 2019

Homi Bhabha National Institute

Recommendations of the Viva Voce Committee

As members of the Viva Voce Committee, we certify that we have read the dissertation prepared by Ankita Chakrabarti entitled "Quantum geometry of correlated many-body states" and recommend that it maybe accepted as fulfilling the thesis requirement for the award of Degree of Doctor of Philosophy.

V. Ravindran Date: 13/12/19

Chairman: V. Ravindran

S. R. Hassan Date: 13/12/19

Guide/Convener: S. R. Hassan

Sibasish Ghosh Date: 13/12/19

Member 1: Sibasish Ghosh

Date: 13/12/19

Member 2: Rajesh Ravindran

Date: 13/12/19

Member 3: V. S. Nemani

SUBHRO BHATTACHARJEE Date: 13/12/19

External Examiner:

Final approval and acceptance of this dissertation is contingent upon the candidate's submission of the final copies of the dissertation to HBNI.

I hereby certify that I have read this dissertation prepared under my direction and recommend that it may be accepted as fulfilling the dissertation requirement.

Date: 13/12/19

Place: Chennai

S. R. Hassan

Guide

STATEMENT BY AUTHOR

This dissertation has been submitted in partial fulfillment of requirements for an advanced degree at Homi Bhabha National Institute (HBNI) and is deposited in the Library to be made available to borrowers under rules of the HBNI.

Brief quotations from this dissertation are allowable without special permission, provided that accurate acknowledgement of source is made. Requests for permission for extended quotation from or reproduction of this manuscript in whole or in part may be granted by the Competent Authority of HBNI when in his or her judgement the proposed use of the material is in the interests of scholarship. In all other instances, however, permission must be obtained from the author.

Ankita Chakrabarti

Ankita Chakrabarti

DECLARATION

I, hereby declare that the investigation presented in the thesis has been carried out by me. The work is original and has not been submitted earlier as a whole or in part for a degree / diploma at this or any other Institution / University.

Ankita Chakrabarti

Ankita Chakrabarti

DEDICATIONS

To Nirmala Srivastava

&

My Family

ACKNOWLEDGEMENTS

I am thankful to every person who has been kind and helpful to me in this journey.

Now starting with my personal list of people who have influenced and shaped my journey. The first person has to be my advisor Prof. S. R. Hassan. He has made me confront all my deepest academic fears in this journey and trained me to be brave. What I will take back will definitely be the tremendous love and passion for work which he has.

I am deeply indebted to Prof. Sibasish Ghosh for always being approachable and helpful. He has been the anchor in turbulent times both at the academic front or otherwise, coming up with the best possible solutions.

Working with Prof. Shankar has been a very nice experience. The discussions with him have always brought clarity. Prof. Mukul Laad has always been very encouraging and the discussions during the coursework has been very educative. I definitely enjoyed my initial academic discussions with Luckshmy. I learned a lot about coding from her. Her endless energy at work inspired me to get started. All my seniors Archana, Arya and Prosenjit have been helpful. I can't thank Jilmy enough for helping me out always with her warm positive presence. Indumathi maa'm has been a motherly presence. The Sahaja Yoga community in Chennai has been a big source of strength. My teacher Dr. Samir Kumar Paul will always continue to inspire me. He was the first person to make mathematics understandable and lovable for me.

Now coming to people who have been at the recieving end of my endless rants. The biggest inspiration in my life is my mother. My parents and my husband Gaurav have been with me in the toughest and ugliest moments. They believed in me when I was unable to believe in myself. My brother has taught me to cherish the fact of being different and enjoying one's own individuality. My family back in Punjab has been a source of strength.

List of Publications arising from the thesis

- **Published**

1. **Quantum geometry of correlated many-body states**

   S. R. Hassan, R. Shankar and Ankita Chakrabarti

   Physical Review B **98**, 235134 (2018)

2. **Intrinsic and extrinsic geometries of correlated many-body states**

   Ankita Chakrabarti, S. R. Hassan and R. Shankar.

   Physical Review B **99**, 085138 (2019)

- **Sent for Publication**

1. **Theory of optimal transport and the structure of many-body states**

   S. R. Hassan, Ankita Chakrabarti and R. Shankar.

   arXiv : 1905.13535v1 [cond-mat.str-el]

Ankita Chakrabarti
ANKITA CHAKRABARTI

List of presentations and participations at conferences

- *SERC School on Topology and Condensed Matter Physics*
  Ramakrishna Mission Vivekanda Educational and Research Institute,
  Nov 23-Dec 12, 2015.

- Poster presentation, *Emergent Phenomena in Classical and Quantum Systems*,
  S. N. Bose National Centre for Basic Sciences, Kolkata,
  February 26-28, 2018.

- Talk, *IMSc Workshop on Quantum Metrology and Open Quantum Systems*,
  Kodaikanal Solar Observatory, August 27-31st, 2018.

Contents

List of Figures

Synopsis

Introduction

The discovery of the quantum Hall effect has initiated a foray of research activities investigating ideas of geometry to understand and characterise the phases of many electron systems in the last few decades. The relevance of quantum geometry for condensed matter systems was first brought into limelight when Thouless, Kohmoto, Nightingale and den Njis in a pioneering paper [1] pointed out that for non interacting electrons in a magnetic field and a periodic potential, if the quasi-momenta were chosen as the parameters parameterising the single particle states, then the quantised Hall conductivity could be identified with the Chern invariant which is the integral of the Berry curvature (BC) over the Brillouin zone (BZ). The anomalous component of the fermion velocity, perpendicular to the acceleration as discovered by Karplus and Luttinger [3] has been found to be a physical manifestation of the BC [4, 5, 16]. Haldane further showed in his famous work [5] that the BC can occur even without an external magnetic field if time-reversal symmetry is broken. This leads to topological Fermi liquids and Chern insulators. The quantum metric was shown to provide a natural variational parameter for anisotropic fractional quantum Hall states [7].

Another deeply interesting direction of investigation of quantum geometry in condensed matter system over the past few decades has been the the geometric theory of the insulating state [8]. In 1964, in his milestone paper [9], Walter Kohn proposed the idea that all

metal to insulator transitions, including strongly correlated interacting solids, are characterised by the structural transformation of the ground state in the insulating phase. This idea was substantiated years later by developments in quantum geometry [10, 11, 12, 13]. After the development of the modern theory of polarisation in 1993 [14], the polarisation was connected to the Berry phase [10, 11]. In 1999 Resta and Sorella provided the definition of many-electron localisation deeply rooted in theory of polarisation [12]. These ideas were generalised and put on a firmer foundation by the work of Souza, Wilkens and Martin [13] who used a generating function approach to provide expressions for polarisation and localisation length in terms of the centre of mass of the many-body wavefunction. The organisation of the electron in the ground state in the insulating phase as proposed by Kohn was captured by the second moment of the pair correlation function, called the localisation tensor, which was identified to be the integral of a quantum metric over the Brillouin Zone (BZ)[15] and found to be finite in the insulating phase and divergent in the metallic phase [12, 13]. Thus, quantum geometry has thrown new light on the theory of quantum phase transitions by characterising the phases of the many-body system beyond the Landau theory of complete characterisation of the many-body state (and thus the phases of the system) by its symmetries.

The inner product of the Hilbert space, which is the basis of the physical interpretation of states, naturally defines a distance between two states and a geometric phase associated with three states [2]. If there is a subspace of the Hilbert space, parameterised by a set of variables, such that the distances and geometric phases are smooth functions of the parameters, then they define a quantum metric and the so called Berry curvature (BC) in the parameter space [23, 24]. In all the works discussed above, the quantum distances between two quasi-momenta, the geometric phase associated with three quasi-momenta and the corresponding quantum metric and BC on the BZ is defined in terms of single-particle states and used to characterize the quantum geometry of mean-field states. The quantum geometry, namely, quantum distances and geometric phases in terms of physical parameters such as the quasi-momenta, has not been formulated beyond the mean field

many-body wavefunctions, until now.

In this thesis I have looked into generalizations of the study of quantum geometry for correlated many-body wave functions. When generalising to correlated systems, global quantities like the integral of the BC over the BZ (the Chern invariant) and the integral of the quantum metric over the BZ (the localization tensor) can be defined in terms of the response of the system to changes in the boundary conditions [16]. To define local quantities, namely the quantum distance between two quasi-momenta and the geometric phase associated with three quasi-momenta, one approach has been to define these quantities in terms of the zero frequency limit of the Euclidean Green's function [17, 18, 19, 20, 21, 22].

In this thesis, a new formalism is introduced to obtain the induced quantum distance on the space of physical parameters such as the quasi-momenta [25], where the quantum distance for the correlated system is defined in terms of the static correlation functions and is purely a ground state property, in contrast to the previous Green's function approach [17, 18, 19, 20, 21, 22]. This formalism has been applied to the simple but non-trivial model of correlated fermions with nearest-neighbour repulsion on a one-dimensional lattice, the so called one-dimensional $t - V$ model, at half-filling [26, 27]. The distance matrix or the matrix of the quantum distances in the space of the quasi-momenta is then computed numerically using exact diagonalization and the above distance matrix is studied in the context of the metal-insulator transition observed in the above model. This thesis further pursues the question: what geometric quantity constructed from the above distance matrix captures the metal-insulator transition [29] brought about by strong electron correlations? We seek an answer by analysing the intrinsic and extrinsic geometries of the correlated many-body state. Finally, the thesis looks into the characterisation of the above Mott transition by a detailed analysis of optimal transport theory in the context of the quantum geometry of the correlated many-body state [30].

Quantum geometry of correlated many-body states

In our work [25] we have proposed, for any many-body state, a definition of the quantum distance between physical parameters, such as the quasi-momenta, in terms of static correlation functions.

The building blocks of many body states are single-particle states. A complete set of single-particle states can be labeled by some set of parameters that we refer to as the spectral parameters. The spectral parameters are completely general: they could be quasi-momenta in periodic systems, positions labelling Wannier orbitals, parameters labelling the eigenfunctions of some confining potential like in a quantum dot or an optical trap. Our proposed definition of quantum distances on the space of spectral parameters is in terms of the expectation value of certain operators that we call the exchange operators. The wavefunction, in principle, is completely characterised in terms of correlation functions. The exchange operator can be written in terms of the fermion creation and annihilation operators and thus the distances can be written in terms of static correlation functions. For one-band models these are the four-point corrrelation functions.

Our definition of the quantum distance satisfies all the basic properties of a distance including triangle inequalities (proved using Ptolemy inequality [31]) and when applied to the mean field states it reduces to the standard definition in terms of single-particle states. Thus, our formalism provides a geometric characterisation of the correlated many-body state. Moreover, since our definition of the quantum distances is in terms of the expectation values of the exchange operators, it is a purely kinematic one. As a consequence, if the state being investigated is the ground state of a system, then the geometry defined is manifestly a ground state property.

We apply our definition to the time-reversal and parity invariant one-dimensional $t - V$ model where we can concentrate on the quantum distances because we do not expect any geometric phase effects. The spectral parameters are choosen to be the quasi-momenta. The distance matrices at strong coupling have been studied analytically and the metal-

insulator transition is studied by heuristic analysis of the properties of the numerical distance matrices obtained by exact diagonalization for different values of the interaction strength V. The finite system that we are studying does not have a phase transition, but only a crossover from the metallic to the insulating regime as V is increased. We observe that the metallic regime is characterized by a clustering of the distances, either very small or close to 1. It also shows signals of sharp Fermi points. As V increases the distances spread and the Fermi points are washed out.

We have illustrated this behaviour in three ways.

- By examining the distances from a fixed point (chosen to be $k = -\pi$) to all the others. This shows very sharp changes at the Fermi points at low V, which smoothen out at large V.

- By examining the nearest-neighbour distances and constructing a representation of these on a unit circle. This representation clearly shows clustering at small V, which gets washed out at large V.

- By examining the triangles formed by the distances between three quasi momenta. The triangles are of two types, both have finite areas in the insulating regime, which drastically reduce in the metallic regime.

In all three cases discussed above the crossover happens around $V = 2 - 4$. Since previous studies [28] have established that the metal-insulator transition occurs at $V = 2$, we conclude that the “clustering-declustering" feature that we observe in the distance matrix is indeed characterizing the metal-insulator crossover. Our formalism yields non-trivial results even for partially filled single band systems. Thus, unlike the single particle formalism, it is capable of probing the quantum geometry of metallic phases as well as insulating ones.

Intrinsic and extrinsic geometries of correlated many-body states

In our work [29], which is sequel to the previous work [25], we attempt to find ways to characterize the quantum geometry of many-fermion states in terms of its distance matrix. Although we do not have a general answer, we compute the different geometric quantities that characterize the ground state of the one dimensional $t - V$ model, which exhibits a transition from metallic Luttinger liquid to a CDW insulator at $V/t = 2$. We then analyse how they differ in the two regimes.

We first explored an intrinsic geometry approach and studied a discrete notion of the intrinsic curvature. We studied finite size systems using exact diagonalization where the quasi-momenta are discrete and finite and therefore techniques of discrete geometry are needed to study the system. We used the defintion of the curvature in a discrete setting as proposed by Ollivier [32, 33], called the Ollivier-Ricci Curvature. To compute the Ollivier-Ricci curvature we need to compute a new distance function on the above discrete point set of the BZ called the Wasserstein distance, which is obtained from the matrix of the quantum distances by applying the mathematical theory of optimal transport [34] and computed using the standard techniques of linear programming. The metallic regime is characterised by non-uniform curvature, which sharply changes around the Fermi point, while the insulating regime is found to be homogenous, characterised by uniform curvatures. Thus, the Ollivier Ricci curvature is found to be distinctly different in both phases and is able to capture the metal-insulator transition.

The extrinsic geometry of the state is studied by analysing the exact and approximate embedding of the distance matrix in Euclidean spaces [35, 36, 37, 40, 38, 39]. We show that the distance matrices of mean-field states can always be embedded in a finite-dimensional Euclidean space. The analytic calculations for exact embedding at strong coupling reveals that the isometric embedding of the distance matrix corresponds to an embedding

dimension which scales as the system size and hence is not finite in the thermodynamic limit. By contrast, for the metal at $V = 0$, the distance matrix can be isometrically embedded in one dimension. For the distance matrices obtained numerically for interaction values $V > 0$, the exact embedding reveals the same result as that in the latter case. So, for correlated states, in contrast to the mean-field states, the dimension of embedding Euclidean space for the isometric embedding of the distance matrix diverges as the system size. Using tools of approximate embedding [40, 38, 39], we showed that the distance matrix however can be embedded in a finite dimensional Euclidean space with small error or average distortion in the metallic regime. This is not possible in the insulating regime.

We also look at the Euclidean embedding of the Wasserstein distance matrix and we find that it can be approximately embedded in a one dimensional space in the metallic regime. Further, well within the insulating regime, it can be embedded in a finite-dimensional Euclidean space with relatively small error and average distortion. Thus, the approximate embedding sharply characterises the metal-insulator transition. Moreover, it can be used to visualise the embedding in the metallic as well as insulating regimes by looking at the embedded vectors (in three or lower dimension). Thus, the approximate embedding of the Wasserstein distance seems to provide a method to obtain an approximate smooth surface in a finite dimensional Euclidean space for correlated states, which we have further illustrated by presenting the shapes given by the vector configurations obtained by low average distortion in both the regimes.

An intriguing fact from the above findings is that the approximate embedding of the Wasserstein distance matrix seems to be more physically revealing than those of the distance matrix, although it apparently seemed to contain no information about the state. Thus, the Wasserstein distance and the underlying optimal transport theory needs a deeper investigation in the context of the quantum geometry of correlated many-body states.

Study of quantum geometry of correlated states using the theory of optimal transport

This work [30] completes our sequence of three papers on a new approach to quantum geometry of strongly correlated fermionic systems. We address the question: what geometric quantity constructed from the above quantum distance matrix can provide a better characterisation of the correlated many-body state and thus the phases of the system?

Our proposed definition of quantum distances on the space of spectral parameters is in terms of the expectation value of certain operators that we call the exchange operators. The spectral parameters can be labelled by an integer, $i = 1, ..., L$. Starting from a general many-particle state $|\Psi\rangle$ we define a set of states, $|(i, j)\rangle$, associated with a (unordered) pair of spectral parameters (i, j) and obtained by the action of the exchange operators, $\hat{E}_{ij}$, $|(i, j)\rangle \equiv \hat{E}_{ij}|\Psi\rangle$.

The states $|(i, j)\rangle$ span a subset of the many-particle Hilbert space which we call the geometric Hilbert space (GHS) and denote by H_g . The matrix of quantum distances between the spectral parameters (i, j), $d(i, j)$ is defined in terms of the Hilbert-Schmidt distance in H_g .

$$d(i, j)^2 = 1 - |\langle\Psi|(i, j)\rangle|^2 \tag{1}$$

We analyse the above distance matrix in terms of distance distributions defined at each point in the BZ, $m_i(j)$,

$$m_i(j) \equiv \frac{d(i, j)}{\sum_{j=1}^{L} d(i, j)}. \tag{2}$$

We then look for a notion of distance between any two distributions m_i and m_j, by applying the mathematical theory of optimal transport [34], which gives a definition for the distance

between any two distributions m_i and m_j as,

$$W^2(m_i, m_j) = \inf_{\pi} \sum_{k,l=1}^{L} d^2(k,l)\pi_{ij}(k,l). \tag{3}$$

Where $\pi_{ij}(k,l)$ is a joint distribution whose left marginal is m_i and right marginal is m_j and $W^2(m_i, m_j)$ is the so called Wasserstein distance. Finding the above distance involves finding an optimal joint distribution function $\pi^*_{ij}(k,l)$ which minimises the sum defined on the RHS in Eq. 3. Computation of the Wasserstein distance from the given distance matrix is done numerically by linear programming.

We define a mixed state obtained from the optimal joint distribution $\pi^*_{ij}(k,l)$,

$$\rho(\pi^*_{ij}) \equiv \sum_{k,l} \pi^*_{ij}(k,l)\rho_{kl}, \tag{4}$$

where the pure state density matrices, $\rho_{ij},\ i > j$ and ρ_0 are

$$\rho_{ij} \equiv |(i,j)\rangle\langle(i,j)|, \quad \rho_0 \equiv |\Psi\rangle\langle\Psi|.$$

The above distance in Eq. 3 can then be rewritten as

$$W^2(m_i, m_j) = (1 - Tr\rho_0\rho(\pi^*_{ij})) = (\frac{1}{2}Tr(\rho_0 - \rho(\pi^*_{ij}))^2 + \frac{1}{2}(1 - Tr\rho^2(\pi^*_{ij}))). \tag{5}$$

Thus the Wasserstein distance can be expessed in terms of quantities defined on H_g.

From numerical and analytic results (at strong coupling), we find that the Wasserstein distance in the insulating phase becomes zero in the thermodynamic limit and is non-zero in the metallic phase. So this distance provides a sharp geometric characterisation of the state and thus the phases of a system.

Starting from the L distance distribution functions $\{m_i\}$, we now ask for some appropriate average distribution function representing the configuration of the above L distributions. This can be done by further application of the optimal transport theory, by minimisation of the following function,

$$J(\rho^*) = \frac{1}{L}\sum_{i=1}^{L} W_\gamma(m_i, \rho^*).$$

Here ρ^* is a single distribution function called the barycenter and $J(\rho^*)$ is the average Wasserstein distance between ρ^* and the L starting distance distributions. The barycenter is found to be a function on the BZ that can potentially sharply distinguish between the metallic and insulating phases. We have also identified a single parameter, the average Wasserstien distance between the barycenter and all the distance distributions, which sharply distinguishes between the metallic and insulating phases.

Bibliography

[1] D. J. Thouless, M. Kohmoto, M. P. Nightingale, and M. den Nijs, *Phys. Rev. Lett.*, vol. 49, p. 405, (1982).

[2] N. Mukunda and R. Simon, *Annals of Physics*, vol. 228, p. 205, (1993).

[3] R. Karplus and J. M. Luttinger, Phys. Rev. 95, 1154 (1954).

[4] G. Sundaram and Q. Niu *Physical Review B*, vol. 59, no. 23, p. 14915, (1999).

[5] F. Haldane *Physical review letters*, vol. 93, no. 20, p. 206602, (2004).

[6] D. Xiao, M.-C. Chang, and Q. Niu, Rev. Mod. Phys. 82, 1959 (2010).

[7] F. D. M. Haldane, "Topology and geometry in quantum condensed matter," 2012. PCCM/PCTS Summer School, July 23-26, 2012.

[8] R. Resta *The European Physical Journal B-Condensed Matter and Complex Systems*, vol. 79, no. 2, p. 121, (2011).

[9] Walter Kohn, *Phys. Rev.*, vol. 133, no. 1A, p. A171–A181, (1964).

[10] R. Resta, *Berry Phase in Electronic Wave Functions*,

[11] R. Resta, *Phys. Rev. Lett.*, vol. 80, p. 1800, (1998).

[12] R. Resta and Sandro Sorella, *Phys. Rev. Lett.*, vol. 82, p. 370, (1999).

[13] I. Souza, T. Wilkens, and R. M. Martin, *Phys. Rev. B*, vol. 62, p. 1666, (2000).

[14] R. D. King-Smith and David Vanderbilt, *Phys. Rev. B(R)*, vol. 47, p. 1651, (1993).

[15] C. Sgiarovello, M. Peressi, and R. Resta, *Phys. Rev. B*, vol. 64, p. 115202, (2001).

[16] G. Sundaram and Q. Niu, *Phys. Rev. B*, vol. 59, p. 14915, (1999).

[17] Z. Wang, X.-L. Qi, and S.-C. Zhang, *Phys. Rev. Lett.*, vol. 105, p. 256803, (2010).

[18] Z. Wang and S.-C. Zhang, *Phys. Rev. X*, vol. 2, p. 031008, (2012).

[19] L. Wang, X. Dai, and X. C. Xie, *Phys. Rev. B*, vol. 84, p. 205116, (2011).

[20] V. Gurarie, *Phys. Rev. B*, vol. 83, p. 085426, (2011).

[21] K.-T. Chen and P. A. Lee, *Phys. Rev. B*, vol. 84, p. 205137, (2011).

[22] Z. Wang, X.-L. Qi, and S.-C. Zhang, *Phys. Rev. B*, vol. 85, p. 165126, (2012).

[23] P. V. Sriluckshmy, A. Mishra, S. R. Hassan and R. Shankar, *Phys. Rev. B 89*, vol. 045105, (2014).

[24] J. P. L. Faye, D. SÃl'nÃl'chal, and S. R. Hassan, *Phys. Rev.B*, vo. 89, p. 115130, (2014).

[25] S. R. Hassan, R. Shankar, and Ankita Chakrabarti, *Phys. Rev. B*, vol. 98, p. 235134, (2018).

[26] C. N. Yang and C. P. Yang, *Phys. Rev.*, vol. 150, p. 321, (1966).

[27] M. A. Cazalilla, R. Citro, T. Giamarchi, E. Orignac, and M. Rigol, *Rev. Mod. Phys.*, vol. 83, p. 1405, (2011).

[28] R. Shankar, *International Journal of Modern Physics B*, vol. 04, p. 2371, (1990).

[29] Ankita Chakrabarti, S. R. Hassan and R. Shankar, *Phys. Rev. B*, vol. 99, p. 085138, (2019).

[30] "Metals,insulators and the theory of optimal transport",
S. R. Hassan, Ankita Chakrabarti and R. Shankar.
Manuscript under preparation and to be submitted soon.

[31] I. J. Schoenberg, *Ann. Math.*, vol. 41, p. 715, (1940).

[32] Y. Ollivier, *Journal of Functional Analysis*, vol. 256, p. 810, (2009).

[33] Y. Ollivier, Probabilistic Approach to Geometry, Vol. 57 (*Mathematical Society of Japan*, 2010).

[34] C. Villani, Optimal Transport: Old and New , 2009th ed., Grundlehren der mathematischen Wissenschaften (Springer, 2008).

[35] B. Loisel and P. Romon, *Axioms*, vol. 3, p. 119, (2014).

[36] I. J. Schoenberg, Annals of Mathematics 38, 787 (1937).

[37] L. Liberti and C. Lavor, *International Transactions in Op- erational Research*, vol. 23, (2015).

[38] P. Indyk and J. Matousek, in Handbook of Discrete and Computational Geometry (CRC Press, 2004), p. 177-196.

[39] Y. Rabinovich, Proceedings of the Thirty-fifth Annual ACM Symposium on Theory of Computing, STOC '03, 456 (2003).

[40] D. B. Skillicorn, Understanding Complex Datasets: Data Mining with Matrix Decompositions (CRC press, 2008), p. 9-87.

Chapter 1

Introduction

The geometrical aspect of quantum mechanics has been a subject of active research ever since Berry's discovery[1] of the geometric phase in 1984. The Berry phase is the gauge-invariant total phase picked up by the quantum state along a closed path. It is a geometrical object, which can be expressed in terms of local geometric observables in the space of variables parameterising the quantum states. It can be expressed as a line integral over a loop in parameter space or as a surface integral of the Berry curvature over the surface having the loop as a boundary.

Why should condensed matter physicists be bothered with quantum geometry?

Because the physical manifestations of the geometry of the quantum states in condensed matter systems has been spectacular.
Quantum geometry first captured the attention of condensed matter physicists with the pathbreaking discovery of Thouless et al.[2] in the quantum Hall effect.
In two-dimensional crystals, where the Fermi energy lies in a gap between Landau levels, the quantized Hall conductivity is connected to the topological invariance of energy bands[2, 3, 4]. The transverse Hall conductivity is given by a topological invariant, the Chern number, which is the quantized geometric phase obtained as integral multiples of 2π. It is the integral of the Berry curvature of an energy band over the full Brillouin zone.

Quantum geometry thus provides an explanation for the quantization of the transverse Hall conductivity and also its robustness and insensitivity to small changes in the material's properties.

Haldane showed that the Hall effect can also be induced by the band structure in the absence of magnetic field by constructing a tight-binding model on a honey-comb lattice with zero net flux per unit cell[5]. So, non-zero Chern numbers can also be observed without magnetic field if the time-reversal symmetry is broken, giving birth to the concept of Chern insulators. An unquantized geometric phase effect observed in condensed matter systems is the anomalous quantum Hall effect. In the study of large spontaneous Hall current in a ferromagnet in response to an electric field, the Karplus-Luttinger anomalous velocity[6] has been reinterpreted and identified with the Berry curvature[7, 8, 9, 10] in a new geometrical theory.

A modern theory of polarization in electronic structure theory[11, 12] has been developed, where the change in polarization of crystalline solids has been connected to the Berry phase of the electronic wavefunction.

For inspecting the geometry of a quantum state we have discussed the study of the geometric phase. A complementary aspect of the study of geometry of quantum states is the study of the quantum distances between the states (defined later in Eq (1.9)) and the corresponding induced differential metric in the space of parameters. The integral of the quantum metric over the parameter space, the localisation tensor, characterises the insulating state in a geometrical theory[13]. The quantum metric was also shown to provide a natural variational parameter for anisotropic fractional quantum Hall states [14].

Quantum geometry has been shown to be a natural consequence of quantum kinematics[15]. It is very powerful in characterising the phases of a system, as we found for quantum Hall systems or for the metal-insulator transition. So the study of the geometry of the many-body state in the study of quantum phase transitions, is indispensable.

1.1 Quantum geometry of non-interacting electrons

Let us investigate the quantum geometry of a system of electrons in a periodic potential, for a perfect crystalline solid. Owing to the discrete lattice translational symmetry, the quasi-momenta defining the Brillouin zone (BZ) is a natural choice of parameters.

The hamiltonian for a n_b tight-binding model for a d dimensional lattice has the simple form,

$$\hat{H} = \sum_{\mathbf{k}\in BZ,\alpha,\beta} h_{\alpha,\beta}(\mathbf{k}) C^{\dagger}_{\alpha\mathbf{k}} C_{\beta\mathbf{k}}. \tag{1.1}$$

α, β label the n_b number of orbitals. The quasi-momenta $\mathbf{k}$ are d dimensional vectors $\mathbf{k} = (k^1, k^2, \ldots k^d)$, taking values in the BZ.

Diagonalisation of $n_b \times n_b$ matrix $h(\mathbf{k})$ gives the single particle eigenstates,

$$h_{\alpha,\beta}(\mathbf{k}) u^n_\beta(\mathbf{k}) = \epsilon^n(\mathbf{k}) u^n_\alpha(\mathbf{k}),\ n = 1, \cdots n_b. \tag{1.2}$$

$$\Rightarrow h(\mathbf{k}) u^n(\mathbf{k}) = \epsilon^n(\mathbf{k}) u^n(\mathbf{k}) \tag{1.3}$$

The eigenstates of $\hat{H}$ are,

$$|n\mathbf{k}\rangle = u^n_\alpha(\mathbf{k}) |\mathbf{k}, \alpha\rangle \tag{1.4}$$

$$\hat{H}|n\mathbf{k}\rangle = \epsilon^n(\mathbf{k}) |n\mathbf{k}\rangle. \tag{1.5}$$

The single particle states $u^n(\mathbf{k})$ are parametrised by the quasi-momenta $\mathbf{k}$. They sit in the projective Hilbert space, where all states $\{e^{i\phi} u^n(\mathbf{k})\}$ are equivalent because the phase $e^{i\phi}$ is not physically measurable. All the above states of the Hilbert space differing from each other by an arbitrary (gauge-dependent) phase factor, are representated by the density matrix $\rho^n(\mathbf{k}) = u^n(\mathbf{k}) (u^n(\mathbf{k}))^{\dagger}$, in the projective Hilbert space. This space is a complex manifold $\mathbb{CP}_{n_b-1}$ for the above n_b level system.

Each point on the BZ has a corresponding image $\rho^n(\mathbf{k})$ in $\mathbb{CP}_{n_b-1}$, representing the nth band . Thus each band will correspond to a surface in $\mathbb{CP}_{n_b-1}$. Quantum geometry pro-

vides geometric characterisation of this surface in terms of the quantum distance and the geometric phase, which we define next.

All observable physical quantities are functions on projective Hilbert space. These can expressed in terms of the so called Bargmann invariants[16, 15, 17] which are constructed from the inner products of the single particle states. For every band, with every ordered sequence of m points in the Brillouin zone $\{\mathbf{k}\} = (\mathbf{k}_1, \mathbf{k}_2, \ldots, \mathbf{k}_m)$, we can associate a corresponding m^{th} order Bargmann invariant. It is defined in terms of the density matrices of the single particle states.

The second order Bargmann invariant is defined as,

$$\mathcal{B}^2(\mathbf{k}_1, \mathbf{k}_2) \equiv \left(u^{n\dagger}(\mathbf{k}_1)u^n(\mathbf{k}_2)\right)\left(u^{n\dagger}(\mathbf{k}_2)u^n(\mathbf{k}_1)\right) \equiv \mathrm{Tr}\left(\rho^n(\mathbf{k}_1)\rho^n(\mathbf{k}_2)\right). \tag{1.6}$$

The third order Bargmann invariant is defined as,

$$\mathcal{B}^3(\mathbf{k}_1, \mathbf{k}_2, \mathbf{k}_3) \equiv \left(u^{n\dagger}(\mathbf{k}_1)u^n(\mathbf{k}_3)\right)\left(u^{n\dagger}(\mathbf{k}_3)u^n(\mathbf{k}_2)\right)\left(u^{n\dagger}(\mathbf{k}_2)u^n(\mathbf{k}_1)\right) \equiv \mathrm{Tr}\left(\rho^n(\mathbf{k}_1)\rho^n(\mathbf{k}_2)\rho^n(\mathbf{k}_3)\right). \tag{1.7}$$

The general m^{th} order Bargmann invariant is associated with an ordered sequence of m states, $\{u^n(\mathbf{k})\} \equiv (u^n(\mathbf{k}_1), u^n(\mathbf{k}_2), \ldots, u^n(\mathbf{k}_m))$. It is defined as follows,

$$\mathcal{B}^m \equiv \mathrm{Tr}\left(\rho^n(\mathbf{k}_1)\rho^n(\mathbf{k}_2)\ldots\rho^n(\mathbf{k}_m)\right). \tag{1.8}$$

The Bargmann invariants have a geometric interpretation in terms of quantum distances and geometric phases[15, 17].

This allows us to define an induced distance between any two points in the Brillouin zone and a geometric phase associated with every loop in it.

The quantum distance, $d(\mathbf{k}_i, \mathbf{k}_j)$, is defined in terms of the second order Bargmann invariant as follows:

$$d(\mathbf{k}_i, \mathbf{k}_j) \equiv \sqrt{1 - \left(\mathcal{B}^2(\mathbf{k}_i, \mathbf{k}_j)\right)^{\alpha}}. \tag{1.9}$$

The above distances satisfy all the properties of a metric for $\alpha \geq 0.5$.

The geometric phase associated with the loop $\{\mathbf{k}\}$ corresponds to the geometric phase in the projective Hilbert space defined by the ordered sequence of states, $\{u^n(\mathbf{k})\}$. It is defined in terms of the phase of the corresponding m^{th} order Bargmann invariant defined in Eq. (1.8).

The "loop" in question is defined as the union of the segments, $(u^n(\mathbf{k}_i), u^n(\mathbf{k}_{i+1}))$ with $u^n(\mathbf{k}_{m+1}) \equiv u^n(\mathbf{k}_1)$. This identification could not have been possible if the phases of the Bargmann invariants did not satisfy additive laws by construction. A loop can be expressed as a union of several smaller loops. The sum of the phases of the Bargmann invariants associated with the smaller loops should match the phase of the full loop. This is ensured by the additive law satisfied by them.

We assume that the surface corresponding to the single particle states in $\mathbb{CP}_{n_b-1}$ is a smooth surface. We can thus define a differential quantum metric in the BZ from the distance between two infinitesimally seperated states and a geometric phase associated with infinitesimal loops.

So, the quantum geometry is studied in terms of the single particle states with the quasi-momenta as the physical parameters. These states connect the BZ and the Hilbert space. For non-interacting or mean-field cases the many-body ground state is given by the Slater determinant constructed from the single particle states. Consequently, the geometrical observables can be explicitly expressed in terms of the single-particle states.

1.2 Life in Correlated Scenario

In case of narrow bands like partially filled d and f shells, the effect of electron interactions cannot be neglected, leading to inclusion of interaction terms in the Hamiltonian. Electron interactions lead to interesting physical phenomena like Mott transitions, unconventional superconductivity, to name a few. The physics of correlated electrons have fascinated condensed matter physicists for past few decades.

However, the simplest interaction term being a quartic term, the Hamiltonian is no longer quadratic in the Fermionic operators (like in the tight-binding models) and life becomes complicated. For a better understanding let us have a look at the example of a simple and popular model of correlated electrons.

The Hamiltonian for a single-orbital Hubbard model on d dimensional hypercubic lattice of N sites is,

$$\hat{H} = -t \sum_{\langle i,j\rangle,\sigma} \left(C^{\dagger}_{i\sigma} C_{j\sigma} + H.c. \right) + U \sum_{i} n_{i\uparrow} n_{i\downarrow} = H_{band} + H_U. \tag{1.10}$$

The first term corresponds to the kinetic energy due to nearest neighbour hopping and the second term gives the onsite Coulomb repulsion, where $n_{i\sigma} = C^{\dagger}_{i\sigma} C_{i\sigma}$.

The Fourier transform is defined as follows :

$$C_{\mathbf{k}\sigma} = \frac{1}{N^{d/2}} \sum_{i} e^{i\mathbf{k}.\mathbf{r}_i} C_{i\sigma}. \tag{1.11}$$

The kinetic energy term is given by

$$H_{band} = -t \sum_{\mathbf{k},\sigma} \left(\sum_{i=1}^{d} \{ e^{-k_i a} + e^{k_i a} \} \right) C^{\dagger}_{\mathbf{k}\sigma} C_{\mathbf{k}\sigma} = \sum_{\mathbf{k}} \epsilon(\mathbf{k}) C^{\dagger}_{\mathbf{k}\sigma} C_{\mathbf{k}\sigma} \tag{1.12}$$

where, $\epsilon(\mathbf{k}) = -4t \sum_{i=1}^{d} \cos(k_i a)$. We get back the familiar form in Eq. (1.1) and studies of Sec. (1.1) holds through.

However, the interaction term is quite complicated and not diagonal in the quasi-momenta:

$$H_U = \frac{U}{N^d} \sum_{\mathbf{k}} \sum_{\mathbf{q}} \sum_{\mathbf{q}_1} C^{\dagger}_{\mathbf{k}+\frac{\mathbf{q}}{2}\uparrow} C^{\dagger}_{\mathbf{k}-\frac{\mathbf{q}}{2}\downarrow} C_{\mathbf{k}-\frac{\mathbf{q}_1}{2}\downarrow} C_{\mathbf{k}+\frac{\mathbf{q}_1}{2}\uparrow} \,. \tag{1.13}$$

Clearly, the quasi-momentum is no longer a good quantum number. The many-body state is complex and does not have a simple form like the Slater determinant constructed from the single particle states.

We cannot think of a map from the Hilbert space to the BZ defined by the single-particle states.

So how to generalize the concepts of quantum geometry studied in Sec. (1.1) for correlated electrons?

This is the primary question we investigate in this thesis.

An existing approach has been to consider the parameters in the wavefunction to be a "flux" or "twist" in the electronic Hamiltonian. The "twist" in question affects the eigenvalues and eigenvectors of the many-body quantum state depending on the chosen boundary conditions[9].

The linear response of the many-body wavefunction to an infinitesimal twist and the distance between the (infinitesimally) twisted and untwisted ground states are then studied.

Souza et. al.[18] showed that the localization tensor, which characterises the insulating state, can be written as an average over the space of twisted boundary conditions of a metric defined on the manifold of ground states of the system with twisted boundary conditions.

Note first that the space of twists is not a space of physical parameters. The second point to note is that local geometric quantities like the quantum distances between any two points, or the geometric phase associated with a triplet of points in the parameter space, remain inaccessible.

Only global averaged quantities, like the integral of the Berry curvature (the Chern in-

variant) and the integral of the quantum metric (the localization tensor) over the space of parameters, can be studied.

To define the local quantities, namely the induced quantum distance between two quasi-momenta and the geometric phase associated with three quasi-momenta, there exists a Green's function approach [19, 20, 21, 22, 23, 24]. In this approach these quantities have been defined in terms of the zero frequency limit of the Euclidean Green's function.

We have proposed a new formalism to generalize the concepts of quantum geometry to correlated many-body states.

1.3 Motivation and the spirit of our formalism

Let us begin with a question addressed by Walter Kohn long back in 1964[25]. Is the metal-insulator transition captured by some features of the ground state alone?
The transition does not involve any change of symmetries, hence, cannot be studied with Landau's approach[26] of the presence or absence of long range order of local order parameters in the ground state.
The conventional approach for band insulators has involved an analysis of the low lying excited states of the spectrum. However, quantum Hall insulators and Chern insulators which we discussed earlier are characterised by topological invariants. We also find in Nature correlated Mott insulators and Anderson insulators as an effect of disorder. Can there be some uniform way of characterising the insulating state of matter?

Kohn argued that insulating states are characterised by the fact that they are insensitive to changes in the boundary conditions. He further stated that the class of many-body wavefunctions that were insensitive to changes in the boundary conditions were of the form,

$$\Psi(\mathbf{x}_1, \ldots, \mathbf{x}_N) = \sum_{M=-\infty}^{\infty} \Phi_M(\mathbf{x}_1, \ldots, \mathbf{x}_N). \tag{1.14}$$

In the above equation each of the functions $\Phi_M(\mathbf{x}_1, \ldots, \mathbf{x}_N)$ are localised around points in the many particle configuration space, and have an exponentially small overlap in the thermodynamic limit. His hypothesis was that the ground state wavefunction of all insulating states is representated by the above form.
Finding such functions starting from the many-body wavefunction in practice is very difficult. Even starting from any known ground state wavefunction decomposing it into the above sum (on the rhs of Eq. (1.14)) is a very difficult task. So how to quantify this qualitative difference of organisation of electrons as proposed by Kohn?

This idea was quantitatively substantiated years later using concepts of quantum geometry [27, 28, 29, 18, 30]. The organisation of the electron in the ground state in insulating phase as proposed by Kohn was captured by the second moment of the pair correlation function, called the localisation tensor[29]. It is found to be finite in insulating phase and divergent in the metallic phase[29, 18]. Interestingly it is a geometrical object which was identified to be the integral of quantum metric over the Brillouin Zone (BZ)[31, 32].

Much of the motivation for our work comes from these developments.
In this thesis a new formalism to generalize the concepts of quantum geometry to correlated many-body states has been presented.
In this formalism we are able to define quantum distances in the space of physical variables labelling the single particle states, like the quasi-momenta. Our definition of the quantum distances are in terms of the static correlation functions.
The many-body state as we know is completely characterized by the static correlation functions. We have cast them in a geometrical framework pretty much in the spirit of Resta and Sorella's work[29], where the localization tensor, which is the second moment of the pair correlation function, was the central geometric object.

This thesis further discusses methods to construct geometrical observables starting from the collection of the quantum distances. We propose observables which can give geometric characterisation of the above space of distances obtained from the many-body state.

The formalism has been applied to a correlated model of spinless Fermions with nearest neighbour repulsion in one dimension, the $t - V$ model [33, 34, 35]. At half-filling, this model exhibits a Mott transition. The efficiency of geometrical observables constructed in our theory, in characterising the metallic and insulating phases, has been supported with results.

1.3.1 Outline of the Chapters

In this section we summarize the content of each chapter of this thesis.

- In Chapter 2 the basic concepts of quantum geometry is discussed.
- Chapter 3 illustrates in detail the concepts developed in Chapter 2 in context of the tight-binding models and mean field many-body states.
- Our new formalism to study the quantum geometry of correlated many-body states has been introduced and discussed rigorously in Chapter 4. The construction of the quantum distances has been detailed.
- The collection of quantum distances in the space of parameters labelling single-particle states which we call the spectral parameters, gives us a new geometrical object which is a collection of points and distances. We refer to this collection as the space of distances and briefly introduce mathematical tools to analyse this space of distances in Chapter 5. These tools have been analysed in much more detail in the next chapters of the thesis.

  In the later part of this chapter we apply our formalism to the $t - V$ model. The efficiency of the tools introduced has been illustrated with the quantum distances of this model computed using exact diagonalization, henceforth.
- In Chapter 6 the Euclidean embedding of the quantum distances are discussed. It is a method to study the extrinsic geometry of the correlated many-body states.

We ask for coordinates of a collection of points in Euclidean space, such that their interconnecting distances are the quantum distances.

- Chapter 7 discusses the application of optimal transport theory to construct a new metric called the Wasserstein distances, which are obtained by averaging over the space of spectral parameter and very efficient in characterising the phases.

- Chapter 8 further discusses application of optimal transport theory to locate a single geometric observable, the Wasserstein barycenter, which can capture the phases of the many-body state.

- In Chapter 9 the construction of a discrete notion of Ricci curvature called the Ollivier-Ricci curvature is discussed. The study of Ollivier-Ricci curvature reveals intrinsic geometric properties of the many-body state.

- We finally conclude the thesis with Chapter 10.

Chapter 2

Basic Concepts of Quantum Geometry

This chapter is a brief prelude which introduces the basic concepts of quantum geometry. The states of a quantum system belong to the projective Hilbert space as briefly discussed in Sec. (1.1). First we familiarise ourselves with the projective Hilbert space (a terminology encountered many times in this thesis).

The physical interpretation of quantum states introduces an inner product which induces a natural geometry in this space. The basic geometric objects which we study are the distances between any two states and the geometric phases associated with loops.

2.1 The projective Hilbert space

The central idea is that the phase of a normalised vector $|\psi\rangle$ in the Hilbert space is gauge-dependent and arbitrary. It does not matter in physical measurements. The phase becomes gauge-invariant and thus measurable only when we have a closed loop, which was Berry's important observation [1].

The collection of all vectors $\{e^{i\phi}|\psi\rangle\}$ in the Hilbert space, which is also popularly referred to as a ray, is equivalent to just a point in the projective Hilbert space.

All physically measurable observables are independent of the gauge or choice of the phase

factor and are thus functions on the projective Hilbert space. This many-to-one correspondence from the Hilbert space vectors to the rays in the projective Hilbert space, is defined in terms of the density matrices. The pure state density matrices are defined as follows,

$$\rho(\psi) = \frac{|\psi\rangle\langle\psi|}{\langle\psi|\psi\rangle}. \tag{2.1}$$

We can see they are in one-to-one correspondence with the rays because they cannot differentiate $e^{i\phi}|\psi\rangle$ from $|\psi\rangle$. They satisfy the properties,

$$\rho^2 = \rho \ , \mathrm{Tr}\rho = 1. \tag{2.2}$$

Let us look at the simplest example of a two-level system. Any normalized vector has the general form

$$|\,\omega, \theta, \phi\,\rangle = e^{i\omega}\left(\cos\tfrac{\theta}{2}|\,0\,\rangle + e^{i\phi}\sin\tfrac{\theta}{2}|\,1\,\rangle\right). \tag{2.3}$$

In the above equation, the basis states $|\,n\,\rangle$, $n = 0, 1$, represent an orthonormal basis. Amongst the above three general parameters ω, θ, ϕ, the physical state is independent of the phase $e^{i\omega}$. The corresponding density matrices $\rho(\theta, \phi)$ have the form,

$$\begin{aligned} \rho(\theta,\phi) &= |\,\omega,\theta,\phi\,\rangle\langle\,\omega,\theta,\phi\,| \\ &= \frac{1}{2}(I + \hat{n}.\vec{\sigma}), \end{aligned} \tag{2.4}$$

where I is the identity matrix, $\vec{\sigma}$ are the three Pauli spin matrices and $\hat{n}$ are the unit vectors corresponding to points on a sphere given by

$$\hat{n} = \sin\theta\cos\phi\ \hat{x} + \sin\theta\sin\phi\ \hat{y} + \cos\theta\ \hat{z}. \tag{2.5}$$

Thus the projective Hilbert space for a two level system is a 2-sphere, known as the Bloch sphere.

For a N level system, a general vector $|z\rangle$ can be expanded in an orthonormal basis $\{|n\rangle\}$, $n = 1..., N$, as follows,

$$|z\rangle = \sum_{n=1}^{N} (z_r^n + i z_i^n)|n\rangle. \tag{2.6}$$

Corresponding density matrices are given by

$$\rho(z) = \frac{|z\rangle\langle z|}{\langle z|z\rangle}. \tag{2.7}$$

The projective Hilbert space thus corresponds to a manifold called the complex projective space $\mathbb{CP}_{N-1}$, parameterised by $2N - 2$ real parameters.

2.1.1 Illustration with 2-band models

In this section, we look at two simple 2-band tight-binding models: (a) the $t - t'$ model in one-dimension and (b) the honeycomb lattice in two dimension, for an illustration of the mapping from the parameter space (the BZ) to the projective Hilbert space (the Bloch sphere in this case). The mapping is defined in terms of single particle eigenstates (as discussed in Sec. (1.1)).

t-$t^{'}$ model

Consider the simple model of spinless fermions hopping on a one-dimensional lattice with staggered hopping amplitudes t and t'. The above model is a two-orbital model where the the hopping amplitude (within an unit cell) is t and (between two unit cells) t'. We label the two orbitals as α and β. The Hamiltonian is

$$H = -t \sum_{\mathbf{I}} (C^\dagger_{\mathbf{I}\alpha} C_{\mathbf{I}\beta} + H.c.) - t' \sum_{\langle \mathbf{I},\mathbf{J}\rangle} (C^\dagger_{\mathbf{I}\alpha} C_{\mathbf{J}\beta} + H.c.) \quad = \quad H_1 + H_2 \tag{2.8}$$

where $C^\dagger_{\mathbf{I}\alpha}(C_{\mathbf{I}\alpha})$ creates (annihilates) a fermion corresponding to the orbital α (in a Wannier function basis) located at site $\mathbf{I}$, specified by coordinate $\mathbf{R}_I = n\mathbf{e}_1,\ n = 1, \cdots, N$.

The Fourier transform can be defined as,

$$C_{\mathbf{k}\alpha} = \frac{1}{\sqrt{N}} \sum_{\mathbf{I}} e^{i\mathbf{k}.\mathbf{R_I}} C_{\mathbf{I}\alpha}, \tag{2.9}$$

where $\mathbf{k} = k\mathbf{e}_1$, $k \in [-\pi, \pi)$.

Using the identity

$$\sum_{\mathbf{I}} e^{i(\mathbf{k_1}-\mathbf{k_2}).\mathbf{R_I}} = N\delta_{\mathbf{k_1},\mathbf{k_2}}, \tag{2.10}$$

we get

$$H_1 = -t \sum_{\mathbf{k}\in BZ} (C^{\dagger}_{\mathbf{k}\alpha} C_{\mathbf{k}\beta} + H.c.) \tag{2.11}$$

$$H_2 = -t' \sum_{\mathbf{k}\in BZ} (e^{-i\mathbf{k}.\delta} C^{\dagger}_{\mathbf{k}\alpha} C_{\mathbf{k}\beta} + e^{i\mathbf{k}.\delta} C^{\dagger}_{\mathbf{k}\beta} C_{\mathbf{k}\alpha}) \tag{2.12}$$

where $\delta = \mathbf{e}_1$.

The above calculation gives us the following 2×2 Hamiltonian matrix

$$h(k) = \begin{pmatrix} 0 & t + t'e^{ik} \\ t + t'e^{-ik} & 0 \end{pmatrix}. \tag{2.13}$$

Diagonalising the above Hamiltonian and putting $t = 1$, we get the energy values for the positive and negative energy bands as follows,

$$\epsilon^{\pm}(k) = \pm\sqrt{(1-t')^2 + 4t' cos^2(k/2)} \tag{2.14}$$

and the corresponding eigenstates are

$$u^{\pm}(k) = \frac{1}{\sqrt{2}} \begin{pmatrix} \pm e^{i\phi(k)} \\ 1 \end{pmatrix}, \tag{2.15}$$

$$\phi(k) = \tan^{-1}\left(\frac{t' \sin k}{1 + t' \cos k}\right) \tag{2.16}$$

The corresponding density matrices are found to be

$$\rho^{\pm}(k) = \frac{1}{2}\begin{pmatrix} 1 & \pm e^{i\phi(k)} \\ \pm e^{-i\phi(k)} & 1 \end{pmatrix}. \tag{2.17}$$

Comparing the above with the density matrix $\rho(\theta, \phi)$ for a two-level system given by Eq. (2.4), we get the coordinates (θ, ϕ) on the Bloch sphere of the state corresponding to the bands for every quasi-momenta in the BZ as the following,

$$\theta^{\pm} = \frac{\pi}{2}, \quad \phi^{\pm} = \phi^{\pm}(k) = \tan^{-1}\left(\frac{\pm t' \sin k}{1 + t' \cos k}\right). \tag{2.18}$$

Therefore, the states always lie on the equator. There are two cases, $t > t'$ and $t < t'$.

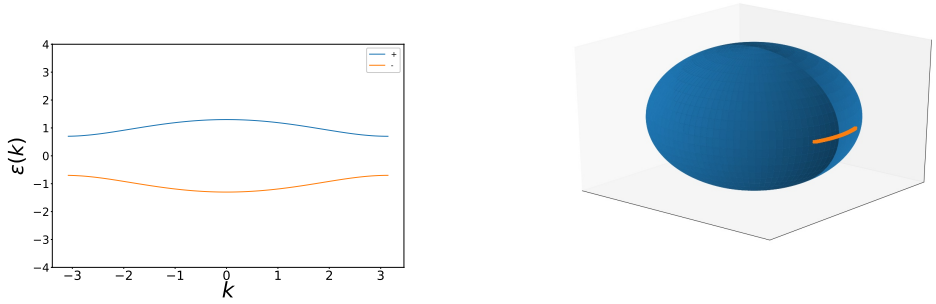

Figure 2.1: The figure at the left represent the energy bands on the BZ for $t = 1, t' = 0.3$, for a lattice of 1000 sites. The image of the BZ on the Bloch sphere for the positive energy band for above choice of parameters is demonstrated in the figure at the right. The states map to an arc on the equator. The map is not one to one. The states for the negative energy band will map to the antipodal points on the Bloch sphere.

$t > t'$. The observations in this regime are

1. The image of the BZ on the Bloch sphere is an arc on the equator.
2. Two points in the BZ gets mapped to the same point on the Bloch sphere and the map is not one to one.

$t < t'$. The observations in this regime are

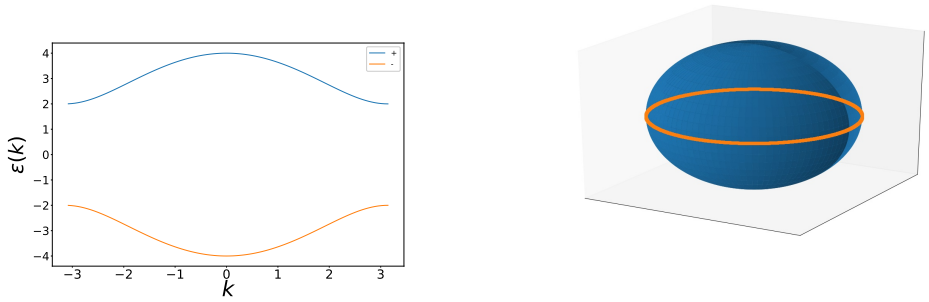

Figure 2.2: The energy bands for $t = 1, t' = 3.0$, for a lattice of 1000 sites is presented at the figure at the left. The states map to a curve on the Bloch sphere which winds around the equator once, as demonstrated in the figure at the right.

1. The map is one to one, with every point having an unique image.
2. The curve in the Bloch sphere corresponding to the positive enery eigenstates winds around the equator once.

For $t = t'$ the energy bands touch at $k = -\pi$, the mapping to the Bloch sphere is not well defined at this point and the hamiltonian $h(k) = 0$. This is a point of topological transition for this model.

Honeycomb lattice

The honeycomb lattice is a diatomic triangular Bravais lattice, where the basis vectors are given by

$$\mathbf{e}_1 = \frac{1}{2}\mathbf{x} + \frac{\sqrt{3}}{2}\mathbf{y} \tag{2.19}$$

$$\mathbf{e}_2 = \frac{1}{2}\mathbf{x} - \frac{\sqrt{3}}{2}\mathbf{y}. \tag{2.20}$$

Let us consider a staggered onsite potential V and next nearest neighbour hopping t of spinless Fermions. The orbitals are labelled by α and β. The Hamiltonian is

$$H = -t \sum_{\langle \mathbf{I}, \mathbf{J} \rangle} (C^\dagger_{\mathbf{I}\alpha} C_{\mathbf{J}\beta} + H.c.) + V \sum_{\mathbf{I}} (C^\dagger_{\mathbf{I}\alpha} C_{\mathbf{I}\alpha} - C^\dagger_{\mathbf{I}\beta} C_{\mathbf{I}\beta}) = H_1 + H_2 \tag{2.21}$$

Taking the Fourier transform as defined in Eq. (2.9) and using the identity in Eq. (2.10) we get

$$H_1 = -t \sum_{\delta_i} \sum_{\mathbf{k}} \left((1 + e^{i\mathbf{k}.\delta_i}) C^{\dagger}_{\mathbf{k}\alpha} C_{\mathbf{k}\beta} + H.c. \right) \tag{2.22}$$

$$H_2 = V \sum_{\mathbf{k}} (C^{\dagger}_{\mathbf{k}\alpha} C_{\mathbf{k}\alpha} - C^{\dagger}_{\mathbf{k}\beta} C_{\mathbf{k}\beta}) \tag{2.23}$$

The position of the orbitals are given by $\mathbf{R}_{\mathbf{I}k} = I_1\mathbf{e}_1 + I_2\mathbf{e}_2 + \mathbf{r}_k$, $k = \alpha, \beta$ and $\mathbf{r}_k = \pm\frac{\sqrt{3}}{8}\mathbf{y}$ for $k = \alpha$ and $k = \beta$ respectively. For the nearest neighbours, $\mathbf{R}_{\mathbf{J}\beta}$ is given by $\mathbf{R}_{\mathbf{J}\beta} = \mathbf{R}_{\mathbf{I}\alpha} + \delta_{\mathbf{i}}$, where $\delta_1 = \mathbf{e_1}$, $\delta_2 = -\mathbf{e_2}$. The vectors in the BZ can be written in the form

$$\mathbf{k} = k_1\mathbf{G}_1 + k_2\mathbf{G}_2. \tag{2.24}$$

$\{\mathbf{G}_i\}$ are the reciprocal lattice vectors and using Eq. (3.5) we have the following hamiltonian matrix,

$$h(k) = \begin{pmatrix} V & z \\ z^* & -V \end{pmatrix} \tag{2.25}$$

$$z = t\,(1 + \cos k_1 + \cos k_2) + i\,t\,(\sin k_1 - \sin k_2) \tag{2.26}$$

The energies of the bands are then given by

$$\epsilon^{\pm}(\mathbf{k}) = \pm\sqrt{|\,z\,|^2 + V^2} = \pm\epsilon(\mathbf{k}). \tag{2.27}$$

The corresponding density matrices are found to be

$$\rho^{\pm}(k) = \frac{1}{2}\begin{pmatrix} 1 \pm \frac{V}{\epsilon} & \pm\frac{z}{\epsilon} \\ \pm\frac{z^*}{\epsilon} & 1 \mp \frac{V}{\epsilon} \end{pmatrix}. \tag{2.28}$$

Comparing the density matrices with Eq. (2.4), the coordinates of the states corresponding to the bands on the Bloch sphere as

$$\theta^{\pm}(\mathbf{k}) = \cos^{-1}\left(\frac{V}{\epsilon(\mathbf{k})}\right) \tag{2.29}$$

$$\phi^{\pm}(\mathbf{k}) = \tan^{-1}\left(\frac{Im(z)}{Re(z)}\right) \tag{2.30}$$

Let us look at the band surfaces in $BZ \otimes \epsilon(\mathbf{k})$ and the states on the Bloch sphere in two different cases in Figs. (2.3, 2.4).

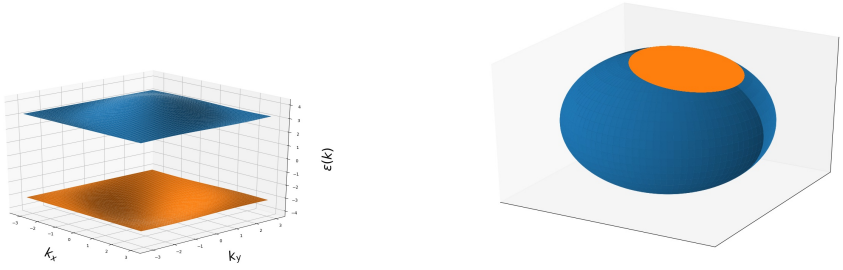

Figure 2.3: (a) $V > t$; The figure at the left represent the energy bands on the BZ for $t = 1, V = 3.0$, for a 300×300 square lattice. The image of the BZ on the Bloch sphere for the positive energy band for above choice of parameters is demonstrated in the figure at the right. The states map to a small region around the north pole.

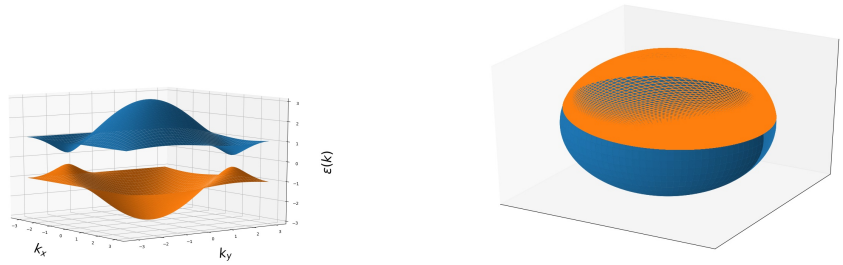

Figure 2.4: (b)$V < t$; The figure at the left represent the energy bands on the BZ for $t = 1, V = 0.3$, for a 300×300 square lattice. The image of the BZ on the Bloch sphere for the positive energy band for above choice of parameters is demonstrated in the figure at the right. The states map to points covering the complete northern hemisphere.

When $V = 0$, the bands touch at the Dirac points $k_1, k_2 = \pm(\frac{2\pi}{3}, \frac{2\pi}{3})$ and $h(k) = 0$ at these

points. The coordinates of these points on the Bloch sphere is ill defined and the states for all other k collapse to the equator.

2.2 Distances and geometric phases in terms of the Bargmann invariants

For any two quantum states ψ_1 and ψ_2, any physically measurable quantity should be unaffected by phase transformations of the vectors.

For example, the phase difference $\delta_{1,2}$ between the above states in terms of their overlap is,

$$e^{i\delta_{1,2}} = \frac{\langle\psi_1|\psi_2\rangle}{|\langle\psi_1|\psi_2\rangle|} \tag{2.31}$$

$$\delta_{1,2} = -Im\ log(\langle\psi_1|\psi_2\rangle). \tag{2.32}$$

This phase, of course, is not gauge invariant and not of any interest for physical measurements. But the modulus square of the inner product of the two vectors is one such quantity which is of physical interest. It can be expressed in terms of the density matrices of the states as follows,

$$|\ \langle\psi_1|\psi_2\rangle\ |^2 = \mathrm{Tr}(\ \rho(\psi_1)\rho(\psi_2)\ ). \tag{2.33}$$

For three physical states, ψ_1, ψ_2, ψ_3, we can similarly propose a complex invariant,

$$\langle\psi_1|\psi_2\rangle\langle\psi_2|\psi_3\rangle\langle\psi_3|\psi_1\rangle = \mathrm{Tr}\left(\ \rho(\psi_1)\rho(\psi_2)\rho(\psi_3)\ \right), \tag{2.34}$$

which was first introduced by Bargmann as a way to distinguish unitary and antiunitary transformations[16]. Higher order generalisations give complex invariants called n^{th} order Bargmann invariants associated with any ordered sequence of n states,

$\{\psi\} \equiv (\psi_1, \psi_2, \ldots, \psi_n)$, defined as,

$$\mathcal{B}^n \equiv \mathrm{tr}\left(\rho(\psi_1)\rho(\psi_2)\ldots\rho(\psi_n)\right). \tag{2.35}$$

The physical observables can be expressed in terms of the Bargmann invariants. The quantum distances and geometric phases are defined in terms of the Bargmann invariants.

2.2.1 Quantum distances

The distances between two states, $D(\psi_1, \psi_2)$, are defined in terms of the second order Bargmann invariant $\mathcal{B}^2(\psi_1, \psi_2)$ which is defined in Eq. (2.33). It corresponds to the length of the segment (ψ_1, ψ_2) in the projective Hilbert space and is defined to be

$$D(\psi_1, \psi_2) \equiv \sqrt{1 - \left(\mathcal{B}^2(\psi_1, \psi_2)\right)^{\alpha}}. \tag{2.36}$$

While the above definition automatically implies,

$$D(\psi_i, \psi_i) = 0, \tag{2.37}$$

$$D(\psi_i, \psi_j) = D(\psi_j, \psi_i). \tag{2.38}$$

The Triangle inequality

$$D(\psi_i, \psi_j) + D(\psi_j, \psi_k) \geq D(\psi_i, \psi_k) \tag{2.39}$$

is satisfied for the choice $\alpha \geq 0.5$, in Eq. (2.36).

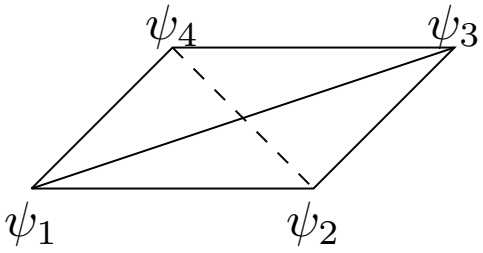

Figure 2.5: Triangulation of a four-vertex loop in the projective Hilbert space.

2.2.2 Geometric Phases

Mukunda and Simon identified the phase of the Bargmann invariant with the geometric phase[15]. Let us denote the phase of the n^{th} order Bargmann invariant by $\Omega^{(n)}$. That is,

$$\mathcal{B}^n(\psi_1, \psi_2, \ldots, \psi_n) = e^{i\Omega^{(n)}} \mid \mathcal{B}^n(\psi_1, \psi_2, \ldots, \psi_n) \mid . \tag{2.40}$$

It follows from the definition in Eq. (2.35) that $\Omega^{(n)}$ obeys additive law.

Let us look at a four-vertex loop in the projective Hilbert space with vertices (ψ_1, ψ_2, ψ_3, ψ_4). From the additive property of the phases,

$$\Omega^{(4)}(\psi_1, \psi_2, \psi_3, \psi_4) = \Omega^{(3)}(\psi_1, \psi_2, \psi_3) + \Omega^{(3)}(\psi_1, \psi_3, \psi_4) \tag{2.41}$$

$$= \Omega^{(3)}(\psi_1, \psi_2, \psi_4) + \Omega^{(3)}(\psi_2, \psi_3, \psi_4). \tag{2.42}$$

The above additive property allows us to write the total geometric phase associated with the four-vertex loop in the projective Hilbert space as a sum of the phases associated with smaller triangles whose union gives the full loop and thus triangulation of the above loop is possible. The above equations (Eqs. (2.41) and (2.42)) give us two possible triangulation as demonstrated in Fig. (2.5). The total geometric phase of the four-vertex loop is independent of the way of triangulation, as we would expect for a physically measurable observable.

Conclusion. The geometric phase associated with a loop in the projective Hilbert space defined by the ordered sequence of states $\{\psi\}$, is identified to be the phase of the n^{th} order Bargmann invariant: the loop under consideration can be defined as the union of the segments (ψ_i, ψ_{i+1}) with $\psi_{n+1} \equiv \psi_1$. The above identification is possible because a loop in the projective Hilbert space can be expressed as the union of several smaller loops: moreover, the geometric phase associated with the full loop is given by the sum of the phases associated with the smaller loops. This is ensured from the additive law satisfied by the phases of the Bargmann invariants.

Chapter 3

Quantum Geometry of Tight Binding Models and Mean Field States

We investigate the quantum geometry of tight binding models and mean field many-body states in this chapter. For translationally symmetric tight binding models, the subspace of the quantum states in the Hilbert space is parameterised by the quasi-momenta that define the Brillouin zone (BZ). Hence, if the quantum distances and geometric phases are smooth functions of the quasi-momenta, they define an induced infinitesimal quantum metric and a Berry curvature (BC) in the BZ.

Let us consider n_b-band tight-binding models of a d-dimensional Bravais lattice, with each unit cell having n_b orbitals centered at

$$\mathbf{R}_{I\alpha} = \mathbf{R}_I + \mathbf{r}_\alpha \ (\alpha = 1, \cdots, n_b), \tag{3.1}$$

where the position of each unit cell is given by, $\mathbf{R}_I = \sum_{i=1}^{d} I_i \mathbf{e}_i$. Here, $\{\mathbf{e}_i\}$ are the d basis vectors.

Let $|\mathbf{R}_{I,\alpha}\rangle$ denote the wavefunction of the orbitals. We further assume they form an or-

thonormal basis,

$$\langle \mathbf{R}_{J,\beta} | \mathbf{R}_{I,\alpha} \rangle = \delta_{\alpha,\beta} \prod_{i=1}^{d} \delta_{I_i J_i} \;\; ; \sum_{\mathbf{R}_{I,\alpha}} |\mathbf{R}_{I,\alpha}\rangle\langle \mathbf{R}_{I,\alpha}| = \hat{I}. \tag{3.2}$$

The Hamiltonian can be expressed as

$$\hat{H} = \sum_{I,\alpha,J,\beta} |\mathbf{R}_{I,\alpha}\rangle h_{\alpha,\beta}(\mathbf{R}_I - \mathbf{R}_J)\langle \mathbf{R}_{J,\beta}|. \tag{3.3}$$

The above Hamiltonian is invariant under lattice translations $\hat{T}_i|\mathbf{R}_{I,\alpha}\rangle = |\mathbf{R}_I + \mathbf{e}_i, \alpha\rangle$. Thus we can have simultaneous eigenstates of $\hat{H}$ and $\hat{T}_i$ labelled by the quasi-momenta taking values in the BZ.

$$|\mathbf{k}, \alpha\rangle = \sum_{\mathbf{I}} e^{i\mathbf{k}.\mathbf{R}_{I\alpha}} |\mathbf{R}_{I\alpha}\rangle \tag{3.4}$$

From the above equation, $|\mathbf{k}, \alpha\rangle \equiv |\mathbf{k} + \mathbf{G}_i, \alpha\rangle$ is satisfied if

$$\mathbf{G}_i.\mathbf{e}_j = 2\pi\delta_{ij}. \tag{3.5}$$

Thus the BZ is a d torus T^d where,

$$\mathbf{k} \sim \mathbf{k} + \mathbf{G}_i, \;\; (i = 1, \cdots, d). \tag{3.6}$$

The Hamiltonian in above basis can be written as

$$\hat{H} = \sum_{\mathbf{k}\in BZ,\, \alpha,\beta} |\,\mathbf{k}, \alpha\rangle\, h_{\alpha,\beta}\,(\mathbf{k})\langle \mathbf{k}, \beta|. \tag{3.7}$$

Diagonalisation of the $n_b \times n_b$ matrix $h(\mathbf{k})$ gives the n_b single particle eigenstates $u^n(\mathbf{k})$ (Eqs. (1.2, 1.3)). The eigenstates and eigenvalues of $\hat{H}$ are given by Eqs. (1.4, 1.5). Each energy level or energy band $\epsilon^n(\mathbf{k})$ is a function in the BZ. In the $d+1$ dimensional space consisting of the BZ and an orthogonal dimension corresponding to the single particle energy, $T^d \otimes \mathbb{R}^1$, the above energy band can be visualized as a d dimensional surface.

There are n_b such surfaces.

Let us now inspect the projective Hilbert space, which is $\mathbb{CP}_{n_b-1}$ for the above n_b level system. The single particle states $u^n(\mathbf{k})$ are parametrised by the quasi-momenta $\mathbf{k}$ in the BZ. Each point on the BZ has a corresponding image $\rho^n(\mathbf{k}) = u^n(\mathbf{k})\,(u^n(\mathbf{k}))^\dagger$ representing the nth band in $\mathbb{CP}_{n_b-1}$. Thus each band will correspond to a surface in $\mathbb{CP}_{n_b-1}$. Quantum geometry provides geometric characterisation of this surface in terms of the quantum distance and the geometric phase.

For every band of states, with every ordered sequence of m points in the Brillouin zone $\{\mathbf{k}\} = (\mathbf{k}_1, \mathbf{k}_2, \ldots, \mathbf{k}_m)$, we can associate a corresponding *mth* order Bargmann invariant defined in terms of the density matrices of the single particle states. This allows us to define an induced distance between any two points in the Brillouin zone and a geometric phase associated with every loop in it.

If the surface in $\mathbb{CP}_{n_b-1}$ is a smooth surface, we can define a differential quantum metric in the BZ from the distance between two infinitesimally seperated states and a geometric phase associated with infinitesimal loops. Equations 2.33 and 2.36 gives the distance between two infinitesimally seperated states corresponding to the nth band, $u^n(\mathbf{k})$ and $u^n(\mathbf{k}+\mathbf{dk})$, as follows:

$$d^2(\mathbf{k}, \mathbf{k}+\mathbf{dk}) = 1 - (\mathrm{Tr}\,(\rho^n(\mathbf{k})\,\rho^n(\mathbf{k}+\mathbf{dk}))\,)^\alpha = \sum_{a,b=1}^{d} g_{ab}\,dk^a\,dk^b \tag{3.8}$$

From the properties of the density matrices,

$$\mathrm{Tr}(\rho^2) = \mathrm{Tr}(\rho) = 1 \Rightarrow \mathrm{Tr}(\rho\delta_a\rho) = 0 \Rightarrow \mathrm{Tr}(\delta_a\rho\delta_b\rho) = -\mathrm{Tr}(\rho\delta_a\delta_b\rho) \tag{3.9}$$

where $\delta_a \equiv \frac{\delta}{\delta k_a}$. Taylor series expansion of $\rho^n(\mathbf{k}+\mathbf{dk})$ (upto the second order) and use of

Eq. (3.9) gives,

$$\begin{aligned} d^2(\mathbf{k}, \mathbf{k}+\mathbf{dk}) &\simeq 1 - \left(1 + \frac{1}{2}\mathrm{Tr}(\,\rho^n \delta_a \delta_b \rho^n\,) dk^a dk^b\right)^{\alpha} \\ &\simeq \frac{\alpha}{2}\,\mathrm{Tr}(\,\delta_a \rho^n \delta_b \rho^n\,)\, dk^a\, dk^b \\ \Rightarrow g_{ab} &= \frac{\alpha}{2}\,\mathrm{Tr}(\delta_a \rho^n \delta_b \rho^n). \end{aligned} \tag{3.10}$$

Now we look at the phase of a 3-vertex Bargmann invariant with the vertices at infinitesimal seperation, as given by Eq. (2.34).

$$\Omega^{(3)}(\mathbf{k}, \mathbf{k}+\mathbf{dk_1}, \mathbf{k}+\mathbf{dk_2}) = \mathrm{Im}\,\ln(\mathrm{Tr}\,(\,\rho^{\mathrm{n}}(\mathbf{k})\,\rho^{\mathrm{n}}(\mathbf{k}+\mathbf{dk_1})\,\rho^{\mathrm{n}}(\mathbf{k}+\mathbf{dk_2}\,))). \tag{3.11}$$

Taylor series expansion of the RHS and use of the properties in Eq. (3.9) as before gives

$$\Omega^{(3)}(\mathbf{k}, \mathbf{k}+\mathbf{dk_1}, \mathbf{k}+\mathbf{dk_2}) = \frac{1}{2i}\,\mathrm{Tr}\,(\,\rho^n(\delta_a\rho^n\delta_b\rho^n - \delta_b\rho^n\delta_a\rho^n)\,)\; dk^a\, dk^b \tag{3.12}$$

This defines an anti-symmetric tensor

$$F_{ab}(\mathbf{k}) \equiv \frac{1}{2i}\mathrm{Tr}\,(\,\rho^n(\delta_a\rho^n\delta_b\rho^n - \delta_b\rho^n\delta_a\rho^n\,)) \tag{3.13}$$

Parameterising the vertices of the triangle by two parameters $\mathbf{k}(s,t)$, we have $\mathbf{k}(s+ds,t) = \mathbf{k}+\mathbf{dk_1}$ and $\mathbf{k}(s,t+dt) = \mathbf{k}+\mathbf{dk_2}$, giving us, $dk_1^a = \delta_s k^a ds$ and $dk_2^a = \delta_t k^a dt$. We can now write Eq. (3.12) in the following form :

$$\begin{aligned} \Omega^{(3)}(\mathbf{k}, \mathbf{k}+\mathbf{dk_1}, \mathbf{k}+\mathbf{dk_2}) &= F_{ab}\,(\mathbf{k})\frac{1}{2}(\delta_s k^a \delta_t k^b - \delta_s k^b \delta_t k^a)\, ds\, dt \qquad (3.14) \\ &= F_{ab}(\mathbf{k})\, dk^a \wedge dk^b \qquad (3.15) \end{aligned}$$

The phase of a 3-vertex Bargmann invariant is found to be an integral of a two-form over a surface whose boundary is given by the triangle under consideration. Any closed curve in the projective Hilbert space can be interpreted as a limit of polygons. Moreover, any

N vertex Bargmann invariant corresponds to a N-sided polygon in the projective Hilbert space : this polygon can be triangulated and the total phase can be obtained by summing over all triangles. Using the above result, we can associate a phase with every closed curve γ in the projective Hilbert space,

$$\Omega(\gamma) = \int_S F_{ab}(\mathbf{k})\, dk^a \wedge dk^b, \tag{3.16}$$

where (a) S is the surface with γ as the boundary and (b) $F_{ab}(\mathbf{k})$ is called the Berry curvature for the nth band.

Quantization The integral of the Berry curvature of a band over the full BZ in two-dimensional tight-binding models is found to be an integral multiple of 2π and identified to be a topological invariant, called the Chern invariant which characterises the band.
The integral of the Berry curvature on the rhs of Eq. (3.16) represents the phase of the Bargmann invariant constructed along the boundary of the surface S. So, if we consider two surfaces S' and S'' having the same boundary, C, the corresponding integrals could differ from each other only by an integral multiple of 2π. So we must have,

$$\int_{S'} F_{ab}(\mathbf{k})\, dk^a \wedge dk^b = \int_{S''} F_{ab}(\mathbf{k})\, dk^a \wedge dk^b + 2n\pi. \tag{3.17}$$

Let us assume the union of S' and S'' gives a closed surface S. A schematic representation is demonstrated in Fig. (3.1). Now we shrink C to a point. In the limiting situation when

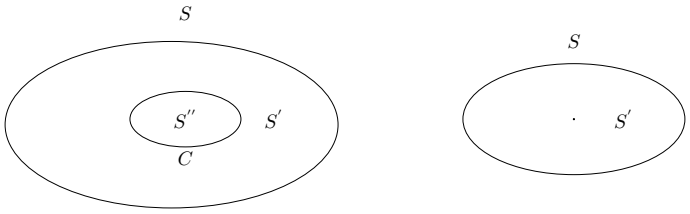

Figure 3.1: Two surfaces S' and S'' having the same boundary C. The union of S' and S'' gives the surface S. For the figure on the right, C has been shrunk to a point giving $S \equiv S'$.

$S \equiv S'$, the integral over S'' should vanish, giving us,

$$\int_{S'} F_{ab}(\mathbf{k})\, dk^a \wedge dk^b = 2n\pi. \tag{3.18}$$

This indicates that the integral of the Berry curvature over any closed surface in the BZ has to be an integral multiple of 2π. However, the value of n in above equation could be zero as well.

There are two-dimensional tight-binding models like the Haldane model where the above integral can be non-zero and changes discontinously across the topological phase transition.

3.1 Quantum geometry of the mean field many-body states

The many-body ground state in a non-interacting or mean field scenario, for the case when the n^{th} band is completely filled and all others completely empty, in terms of the single-particle wavefunctions (introduced in Eq. (1.3)) is as follows,

$$|n\rangle \equiv \prod_{\mathbf{k}} \left(u^n_\alpha(\mathbf{k}) C^\dagger_{\mathbf{k}\alpha} \right) |0\rangle \tag{3.19}$$

where $C_{\mathbf{k}\alpha}|0\rangle = 0$. The Fermion operators satisfy the canonical anti-commutator relations

$$\{C^\dagger_{\mathbf{k}_1\alpha}, C_{\mathbf{k}_2\beta}\} = \delta_{\mathbf{k}_1\mathbf{k}_2}\delta_{\alpha\beta}, \qquad \{C^\dagger_{\mathbf{k}_1\alpha}, C^\dagger_{\mathbf{k}_2\beta}\} = 0, \qquad \{C_{\mathbf{k}_1\alpha}, C_{\mathbf{k}_2\beta}\} = 0. \tag{3.20}$$

The mean field many-body ground state in Eq. (3.19) is not labelled by the quasi-momenta, but has a simple form in terms of the single particle states which are parametrised by the quasi-momenta. This allows us to connect the Bargmann invariants defined in terms of overlap of the single-particle states to the many-body ground state and thus study the induced quantum distances and geometric phase in the BZ, as we shall soon find out in next

section.

3.1.1 Bargmann invariants for mean field states as expectation values of unitary operators

The quantum geometry of a band, namely the quantum distances and the geometric phases defined in terms of the second and third order Bargmann invariants in Eqs. (2.33,2.34) respectively, can be studied in terms of the single particle states. The second order Bargmann invariant can be written as

$$\mathcal{B}^2(\mathbf{k}_1,\mathbf{k}_2) = \left(u^{n\dagger}(\mathbf{k}_1)u^n(\mathbf{k}_2)\right)\left(u^{n\dagger}(\mathbf{k}_2)u^n(\mathbf{k}_1)\right). \tag{3.21}$$

Similarly the third order Bargmann invariant can be expressed as

$$\mathcal{B}^3(\mathbf{k}_1,\mathbf{k}_2,\mathbf{k}_3) = \left(u^{n\dagger}(\mathbf{k}_1)u^n(\mathbf{k}_3)\right)\left(u^{n\dagger}(\mathbf{k}_3)u^n(\mathbf{k}_2)\right)\left(u^{n\dagger}(\mathbf{k}_2)u^n(\mathbf{k}_1)\right). \tag{3.22}$$

The above Bargmann invariants of order two and three defined in Eqs. (3.21,3.22) can interestingly also be casted as expectation values of some suitably defined unitary operators over the mean-field many-body state.

Eq.(3.21) can also be rewritten as

$$\mathcal{B}^2(\mathbf{k}_1,\mathbf{k}_2) = -\langle 0|\left(u^{n\dagger}(\mathbf{k}_1)C_{\mathbf{k}_1}\right)\left(u^{n\dagger}(\mathbf{k}_2)C_{\mathbf{k}_2}\right)\left(C^\dagger_{\mathbf{k}_1}u^n(\mathbf{k}_2)\right)\left(C^\dagger_{\mathbf{k}_2}u^n(\mathbf{k}_1)\right)|0\rangle. \tag{3.23}$$

Let us consider an unitary operator $E(\mathbf{k}_1,\mathbf{k}_2)$ with the following properties

$$E(\mathbf{k}_1,\mathbf{k}_2)\,|\,0\rangle = |\,0\rangle \tag{3.24}$$

$$E(\mathbf{k}_1,\mathbf{k}_2)\,C^\dagger_{\mathbf{k}_1,\alpha}\,C^\dagger_{\mathbf{k}_2\beta}\,E^\dagger(\mathbf{k}_1,\mathbf{k}_2) = -C^\dagger_{\mathbf{k}_2,\alpha}C^\dagger_{\mathbf{k}_1\beta} \tag{3.25}$$

and a two-particle state $|\psi\rangle = \left(C^\dagger_{\mathbf{k}_2} u^n(\mathbf{k}_2)\right)\left(C^\dagger_{\mathbf{k}_1} u^n(\mathbf{k}_1)\right)|0\rangle$. It follows form Eqs. (3.24,3.25) that

$$\mathcal{B}^2(\mathbf{k}_1, \mathbf{k}_2) = \langle\psi \,|\, E(\mathbf{k}_1, \mathbf{k}_2) \,|\, \psi\rangle. \tag{3.26}$$

Moreover, since $E(\mathbf{k}_1, \mathbf{k}_2)$ commutes with all the other fermion creation and annihilation operators, i.e. $(C_{\mathbf{k}\alpha}, C^\dagger_{\mathbf{k}\alpha})$, $\mathbf{k} \neq \mathbf{k}_1, \mathbf{k}_2$, we can write the second order Bargmann invariant as an expectation value of this operator over the many-body groundstate $|n\rangle$ defined in Eq. (3.19).

The action of the above operator $E(\mathbf{k}_1, \mathbf{k}_2)$ on the many-body ground state $|n\rangle$ can be thought of as an exchange of fermions at quasi-momenta $\mathbf{k}_1$ and $\mathbf{k}_2$. We name this operator accordingly as the exchange operator and the second order Bargmann invariant can thus be written as the expectation value of the exchange operator over the many-body ground state,

$$\mathcal{B}^2(\mathbf{k}_1, \mathbf{k}_2) = \langle n \,|\, E(\mathbf{k}_1, \mathbf{k}_2) \,|\, n\rangle. \tag{3.27}$$

The operator $E(\mathbf{k}_1, \mathbf{k}_2)$, defined in terms of the fermion creation and annhilation operators as follows,

$$E(\mathbf{k}_1, \mathbf{k}_2) \equiv e^{\frac{\pi}{2}\sum_{\alpha=1}^{n_b}\left(C^\dagger_{\mathbf{k}_1\alpha} C_{\mathbf{k}_2\alpha} - H.c.\right)}, \tag{3.28}$$

does satisfy Eqs. (3.24,3.25).

The third order Bargmann invariant defined in Eq. (3.22) can be rewritten as,

$$\mathcal{B}^3(\mathbf{k}_1, \mathbf{k}_2, \mathbf{k}_3) = \langle 0|\left(u^{n\dagger}(\mathbf{k}_1) C_{\mathbf{k}_1}\right)\left(u^{n\dagger}(\mathbf{k}_2) C_{\mathbf{k}_2}\right)\left(u^{n\dagger}(\mathbf{k}_3) C_{\mathbf{k}_3}\right)\left(C^\dagger_{\mathbf{k}_1} u^n(\mathbf{k}_3)\right)\left(C^\dagger_{\mathbf{k}_3} u^n(\mathbf{k}_2)\right)\left(C^\dagger_{\mathbf{k}_2} u^n(\mathbf{k}_1)\right)|0\rangle.$$

Repeating above procedure, we construct an unitary operator $C(\mathbf{k}_1, \mathbf{k}_2, \mathbf{k}_3)$, such that,

$$\begin{aligned} C(\mathbf{k}_1, \mathbf{k}_2, \mathbf{k}_3)|0\rangle &= |0\rangle, \\ C(\mathbf{k}_1, \mathbf{k}_2, \mathbf{k}_3) C^\dagger_{\mathbf{k}_3\alpha} C^\dagger_{\mathbf{k}_2\beta} C^\dagger_{\mathbf{k}_1\gamma} C^\dagger(\mathbf{k}_1, \mathbf{k}_2, \mathbf{k}_3) &= C^\dagger_{\mathbf{k}_1\alpha} C^\dagger_{\mathbf{k}_3\beta} C^\dagger_{\mathbf{k}_2\gamma}. \end{aligned} \tag{3.29}$$

Moreover, we can construct C as a product of the exchange operators,

$$C(\mathbf{k}_1, \mathbf{k}_2, \mathbf{k}_3) = E(\mathbf{k}_1, \mathbf{k}_3)E(\mathbf{k}_3, \mathbf{k}_2). \tag{3.30}$$

The above procedure can be followed even for higher order Bargmann invariants.
The same result can be generalised for arbitrary number of filled bands just like the above case of one completely filled band (details in the Appendix).

Therefore, we conclude that for many-body mean field states, the Bargmann invariants can be thought of as expectation values of the exchange operator and higher order cyclic products of the exchange operators. Thus the quantum distances and the geometric phases can be expressed in terms of expectation values of some suitably defined unitary operator.

Chapter 4

Quantum Geometry of Correlated Many-body States

The immediate question which arises is: how to generalize the framework of quantum geometry discussed so far, for *correlated* many-body states?
The previous chapter hints at the following hypothesis. The induced quantum distance for any general many-body state in a space of single particle quantum numbers, which label the single particle spectrum, can be more generally defined in terms of expectation values of suitably defined unitary operators. For the mean field states, we called them the exchange operators. The same can perhaps also be proposed for geometric phases by suitably defining an unitary operator. In mean field states, this operator happened to be products of the exchange operators.

Hence, by the above scheme the study of quantum geometry of the correlated many-body state, in a space of physical parameters (in analogy to the BZ in case of tight binding models), might indeed be possible. We can generalize the definition of the quantum distances and geometric phases in terms of expectation values of some appropriately defined unitary operator. But for this scheme to work, the distances should satisfy all the properties of a metric and the geometric phases should satisfy the additive law. In our new formal-

ism, we accomplish this task: we study the quantum geometry of correlated many-body states by proposing a valid definition of the quantum distances in the space of spectral parameters, for a general correlated many-body state. The quantum distances are defined in terms of expectation values of unitary operators which we call the exchange operators. These expectation values are in fact the static correlation functions of the system. While the geometric phases defined in terms of product of the exchange operators do not satisfy the additive law, our scheme leaves a future possible direction of work to track down a correct operator. We proceed with a detailed examination of the quantum distances.

4.1 Quantum distances for correlated states

We define induced quantum distances amongst the single particle spectral parameters like the quasi-momenta which label the single particle state, by appropriately defining an exchange operator and taking the expectation value of this operator over the many-body state.

4.1.1 The exchange operators

The many-body state can always be written in a Fock basis expansion and the exchange operators are defined by their action on the Fock basis having the following form

$$|\{n\}\rangle = \prod_{\mathbf{k},\alpha} \left(C^{\dagger}_{\mathbf{k}\alpha}\right)^{n_{\mathbf{k}\alpha}} |0\rangle, \qquad C^{\dagger}_{\mathbf{k}\alpha} C_{\mathbf{k}\alpha} |\{n\}\rangle = n_{\mathbf{k}\alpha} |\{n\}\rangle. \tag{4.1}$$

Here, $n_{\mathbf{k},\alpha}$ refers to the occupation numbers of the mode $(\mathbf{k}, \alpha)$ and $\{n\}$ denotes the collection of all the occupation numbers. For the empty state $|0\rangle$, $n_{\mathbf{k},\alpha} = 0$, for every $\mathbf{k}, \alpha$.

The ordering of the fermionic operators in Eq. (4.1) is very important. We label every

element of the set $(\mathbf{k}, \alpha)$ by a unique integer $m(\mathbf{k}, \alpha)$,

$$C_m \equiv C_{\mathbf{k}\alpha}, \quad n_m \equiv n_{\mathbf{k}\alpha}. \tag{4.2}$$

The ordering corresponding to each basis state is specified by a particular combination of the $n_b \times L^d$ values of $m(\mathbf{k}, \alpha)$ for a d dimensional Bravais lattice with n_b number of orbitals and L^d number of unit cells,

$$|\{n\}\rangle = \prod_{m=1}^{n_b L^d} C_m^\dagger |0\rangle. \tag{4.3}$$

The many-body state $|\psi\rangle$, when expanded in the above basis has a form

$$|\psi\rangle = \sum_{\{n\}} \psi(\{n\}) |\{n\}\rangle. \tag{4.4}$$

As a generalisation of the mean field scenario the exchange operators, $E(\mathbf{k}_1, \mathbf{k}_2)$, are defined as operators that exchanges the occupation numbers of the modes at $\mathbf{k}_1$ and $\mathbf{k}_2$, i.e.,

$$\begin{aligned} E_\alpha(\mathbf{k}_1, \mathbf{k}_2) |\ldots, n_{\mathbf{k}_1\alpha}, \ldots, n_{\mathbf{k}_2\alpha}, \ldots\rangle &\equiv |.., n_{\mathbf{k}_2\alpha}, .., n_{\mathbf{k}_1\alpha}, ..\rangle, & (4.5) \\ E(\mathbf{k}_1, \mathbf{k}_2) &\equiv \prod_{\alpha=1}^{n_b} E_\alpha(\mathbf{k}_1, \mathbf{k}_2). & (4.6) \end{aligned}$$

Some of the properties of the exchange operator which follows immediately from the definition are,

$$\begin{aligned} E^\dagger(\mathbf{k}_1, \mathbf{k}_2) = E^{-1}(\mathbf{k}_1, \mathbf{k}_2) \quad , \quad E^\dagger(\mathbf{k}_1, \mathbf{k}_2) = E(\mathbf{k}_1, \mathbf{k}_2) \\ E^2(\mathbf{k}_1, \mathbf{k}_2) = I \end{aligned} \tag{4.7}$$

4.1.2 The quantum distances

For a general many-particle state $|\psi\rangle$ we define, parallel to the second order Bargmann invariants, a new object: the expectation value of the above exchange operators

$$\tilde{\mathcal{B}}^2(\mathbf{k}_1, \mathbf{k}_2) \equiv \langle\psi|E(\mathbf{k}_1, \mathbf{k}_2)\,|\,\psi\rangle. \tag{4.8}$$

The induced quantum distances between $\mathbf{k}_1$ and $\mathbf{k}_2$, which is usually defined in terms of the second order Bargmann invariant, has been defined as follows:

$$d(\mathbf{k}_1, \mathbf{k}_2) \equiv \sqrt{1 - (\langle\psi|E(\mathbf{k}_1, \mathbf{k}_2)|\psi\rangle)^{\alpha}}. \tag{4.9}$$

The above definition can give valid distances only if they satisfy all the properties of a metric.

From Eqs. (4.5) and (4.6), it follows that,

$$E(\mathbf{k}, \mathbf{k}) = I \Rightarrow d(\mathbf{k}, \mathbf{k}) = 0 \tag{4.10}$$

$$E(\mathbf{k}_1, \mathbf{k}_2) = E(\mathbf{k}_2, \mathbf{k}_1) \Rightarrow d(\mathbf{k}_1, \mathbf{k}_2) = d(\mathbf{k}_2, \mathbf{k}_1). \tag{4.11}$$

So the first two properties of positivity and symmetricity immediately follow.

Before looking into the proof of triangle inequalities, let us re-examine the projective Hilbert space. The following observations are important.

Basis Expansion. A many body wavefunction of a n_h level system is a point in the complex projective space $\mathbb{C}P_{n_h-1}$. We label the single particle eigen states by quantum numbers $\{i\}$, which can be the spin, the quasi-momenta, the position labelling the Warnier orbitals, parameters labelling the eigenfunctions of some confining potential like in a quantum dot or an optical trap. We can expand the many-body state $|\Psi\rangle$ in a direct product

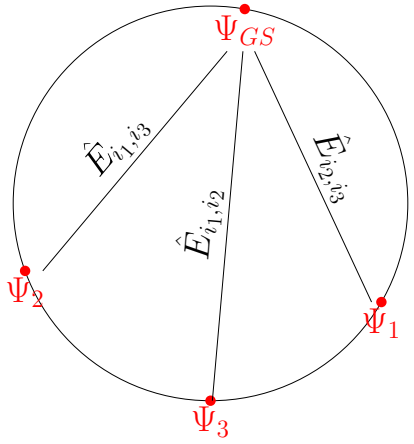

Figure 4.1: Schematic figure for the action of exchange operators in the projective Hilbert space.

basis of the single particle states,

$$|\Psi\rangle = \underbrace{\sum_{i_1,\ldots,i_L} c_{i_1\ldots i_L}}\, |i_1 \otimes i_2 \ldots \otimes i_L\rangle$$
$$= \sum_{j=1}^{n_h} C_j |j\rangle, \quad \left(\sum_j |C_j|^2 = 1\right).$$

New States. The exchange operator $E_{i_l i_m}$ generates a new (normalized) state, $|\Psi'\rangle$, corresponding to an exchange of the quantum numbers i_l and i_m,

$$|\Psi'\rangle = E_{i_l,i_m}|\Psi\rangle.$$

Distance. For the space of quantum numbers $\{i_1, i_2, ..., i_L\}$ (which we refer to as the spectral parameters), the distance $d(i_l, i_m)$ connecting two points (i_l, i_m) is defined in terms of the overlap of $|\Psi\rangle$ and $|\Psi'\rangle$:

$$d(i_l, i_m) = \sqrt{1 - |\langle\Psi'|\Psi\rangle|^\alpha}$$

4.1.3 Satisfaction of Triangle Inequalities

Why are the triangle inequalities not obvious?

We need to prove that

$$d(i_2, i_3) + d(i_3, i_1) \geq d(i_1, i_2). \tag{4.12}$$

So we have three states in the projective Hilbert space generated by the action of the three concerned exchange operators

$$|\Psi_1\rangle \equiv \hat{E}_{i_2,i_3}|\Psi\rangle, \qquad |\Psi_2\rangle \equiv \hat{E}_{i_3,i_1}|\Psi\rangle, \qquad |\Psi_3\rangle \equiv \hat{E}_{i_1,i_2}|\Psi\rangle.$$

The above distances are essentially the distances between the reference many-body state and the above three states in the projective Hilbert space defined in Eqs. (2.33,2.36),

$$d(i_2, i_3) = D(\Psi_1, \Psi) \tag{4.13}$$

$$d(i_3, i_1) = D(\Psi_2, \Psi) \tag{4.14}$$

$$d(i_1, i_2) = D(\Psi_3, \Psi) \tag{4.15}$$

Together, the reference many-body state and above three states form a tetrahedron as

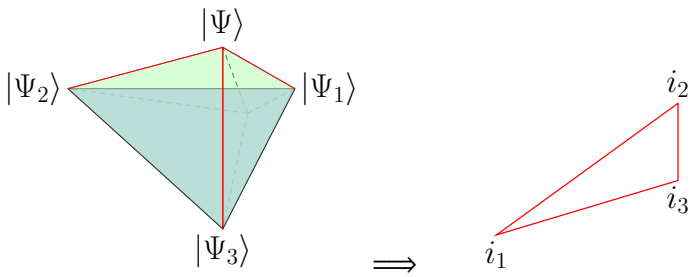

Figure 4.2: The schematic figure for a tetrahedron in the projective Hilbert space being mapped to a new triangle in the spectral parameter space. The corresponding edges are drawn in red colour.

demonstrated in Fig. (4.2). However the triangle under question in the spectral parameter space formed by vertices (i_1, i_2, i_3) with edges $(d(i_2, i_3), d(i_3, i_1), d(i_1, i_2))$ shown in Fig. (4.2), is not a triangle in the Hilbert space.

The question boils down to whether the above three edges out of the six edges of the tetrahedron in the projective Hilbert space will always form a valid triangle. Fortunately, the answer to the question is yes! It follows from a famous inequality in geometry attributed to the Greek mathematician Ptolemy. Ptolemy's inequality[36] states that the six distances $d(i, j)$ between any four distinct points $i, j = 1, ...4$ satisfies the following inequalities

$$d(i, j)\, d(k, l) + d(i, k)\, d(j, l) \geq d(i, l) d(j, l). \tag{4.16}$$

The above results holds in any Hilbert space [36].

Therefore, Ptolemy's inequality implies that

$$D(\Psi, \Psi_1)\, D(\Psi_2, \Psi_3) + D(\Psi, \Psi_2)\, D(\Psi_3, \Psi_1) \geq D(\Psi, \Psi_3)\, D(\Psi_1, \Psi_2). \tag{4.17}$$

We can express the distances $D(\Psi_i, \Psi_j)$ (where $i, j = 1, 2, 3$,and $i \neq j$) in terms of overlap of states generated by action of the exchange operators

$$\langle \Psi_1 | \Psi_2 \rangle = \langle \Psi | \hat{E}_{i_2,i_3} \hat{E}_{i_3,i_1} | \Psi \rangle, \quad \langle \Psi_2 | \Psi_3 \rangle = \langle \Psi | \hat{E}_{i_3,i_1} \hat{E}_{i_1,i_2} | \Psi \rangle, \quad \langle \Psi_3 | \Psi_1 \rangle = \langle \Psi | \hat{E}_{i_1,i_2} \hat{E}_{i_2,i_3} | \Psi \rangle.$$

The exchange operators satisfy the following product rules,

$$\hat{E}_{i_2,i_3} \hat{E}_{i_3,i_1} = \hat{E}_{i_3,i_1} \hat{E}_{i_1,i_2} = \hat{E}_{i_1,i_2} \hat{E}_{i_2,i_3}. \tag{4.18}$$

So the base of the tetrahedron in Fig. (4.2) is always an equilateral triangle. This implies that

$$D(\Psi_1, \Psi_2) = D(\Psi_2, \Psi_3) = D(\Psi_3, \Psi_1). \tag{4.19}$$

Using the above result, Eq. (4.17) implies the following: if $D(\Psi_1, \Psi_2) \neq 0$,

$$D(\Psi, \Psi_1) + D(\Psi, \Psi_2) \geq D(\Psi, \Psi_3). \tag{4.20}$$

If $D(\Psi_1, \Psi_2) = 0$, then the three operations give the same state and we have $D(\Psi, \Psi_1) = D(\Psi, \Psi_2) = D(\Psi, \Psi_3)$. Therefore, in this case, the above identity is trivially true.
Thus we have

$$d(i_2, i_3) + d(i_1, i_3) \geq d(i_1, i_2).$$

Hence, the quantum distances defined in terms of the exchange operators do satisfy triangle inequalities and are, therefore, valid distances. Setting $\alpha = 2$ in Eq. (4.9) as our definition of distances, the above proof reduces to the classical problem in Euclidean space, with the standard definition of distance (details provided in Appendix).

4.1.4 Construction of the exchange operators

Let us define the following operators,

$$T^x_\alpha(\mathbf{k}_1, \mathbf{k}_2) \equiv \left(C^\dagger_{\mathbf{k}_1\alpha} C_{\mathbf{k}_2\alpha} + C^\dagger_{\mathbf{k}_2\alpha} C_{\mathbf{k}_1\alpha}\right) \tag{4.21}$$

$$T^y_\alpha(\mathbf{k}_1, \mathbf{k}_2) \equiv \frac{1}{i}\left(C^\dagger_{\mathbf{k}_1\alpha} C_{\mathbf{k}_2\alpha} - C^\dagger_{\mathbf{k}_2\alpha} C_{\mathbf{k}_1\alpha}\right) \tag{4.22}$$

$$T^z_\alpha(\mathbf{k}_1, \mathbf{k}_2) \equiv \left(C^\dagger_{\mathbf{k}_1\alpha} C_{\mathbf{k}_1\alpha} - C^\dagger_{\mathbf{k}_2\alpha} C_{\mathbf{k}_2\alpha}\right). \tag{4.23}$$

for which

$$\left(T^x_\alpha(\mathbf{k}_1, \mathbf{k}_2)\right)^2 = \left(T^y_\alpha(\mathbf{k}_1, \mathbf{k}_2)\right)^2 = \left(T^z_\alpha(\mathbf{k}_1, \mathbf{k}_2)\right)^2 = \left(\rho_\alpha(\mathbf{k}_1) - \rho_\alpha(\mathbf{k}_2)\right)^2, \tag{4.24}$$

where $\rho_\alpha(\mathbf{k}) \equiv C^\dagger_{\mathbf{k}\alpha} C_{\mathbf{k}\alpha}$. Let us consider the unitary operators

$$U_\alpha(\mathbf{k}_1, \mathbf{k}_2) \equiv e^{i\frac{\pi}{2} T^y_\alpha(\mathbf{k}_1, \mathbf{k}_2)}. \tag{4.25}$$

The above operators satisfy the following equations

$$\begin{aligned} U^\dagger_\alpha(\mathbf{k}_1, \mathbf{k}_2)\left(C^\dagger_{\mathbf{k}_1\alpha}\right) U_\alpha(\mathbf{k}_1, \mathbf{k}_2) &= \left(C^\dagger_{\mathbf{k}_2\alpha}\right) \\ U^\dagger_\alpha(\mathbf{k}_1, \mathbf{k}_2)\left(C^\dagger_{\mathbf{k}_2\alpha}\right) U_\alpha(\mathbf{k}_1, \mathbf{k}_2) &= (-1)\left(C^\dagger_{\mathbf{k}_1\alpha}\right). \end{aligned}$$

Hence,

$$
\begin{aligned}
U_\alpha^\dagger(\mathbf{k}_1,\mathbf{k}_2)\left(C_{\mathbf{k}_1\alpha}^\dagger\right)^{n_{\mathbf{k}_1\alpha}} U_\alpha(\mathbf{k}_1,\mathbf{k}_2) &= \left(C_{\mathbf{k}_2\alpha}^\dagger\right)^{n_{\mathbf{k}_1\alpha}} \\
U_\alpha^\dagger(\mathbf{k}_1,\mathbf{k}_2)\left(C_{\mathbf{k}_2\alpha}^\dagger\right)^{n_{\mathbf{k}_2\alpha}} U_\alpha(\mathbf{k}_1,\mathbf{k}_2) &= (-1)^{n_{\mathbf{k}_2\alpha}}\left(C_{\mathbf{k}_1\alpha}^\dagger\right)^{n_{\mathbf{k}_2\alpha}}.
\end{aligned}
$$

Next, consider the action of $U_\alpha^\dagger(\mathbf{k}_1,\mathbf{k}_2)$ on the two particle states $|n_{\mathbf{k}_2\alpha}, n_{\mathbf{k}_1\alpha}\rangle$

$$
\begin{aligned}
U_\alpha^\dagger(\mathbf{k}_1,\mathbf{k}_2)|n_{\mathbf{k}_1\alpha}, n_{\mathbf{k}_2\alpha}\rangle &= U_\alpha^\dagger(\mathbf{k}_1,\mathbf{k}_2)\left(C_{\mathbf{k}_1\alpha}^\dagger\right)^{n_{\mathbf{k}_1\alpha}}\left(C_{\mathbf{k}_2\alpha}^\dagger\right)^{n_{\mathbf{k}_2\alpha}}|0\rangle \\
&= (-1)^{n_{\mathbf{k}_2\alpha}}\left(C_{\mathbf{k}_2\alpha}^\dagger\right)^{n_{\mathbf{k}_1\alpha}}\left(C_{\mathbf{k}_1\alpha}^\dagger\right)^{n_{\mathbf{k}_2\alpha}}|0\rangle \\
&= (-1)^{n_{\mathbf{k}_2\alpha}(1-n_{\mathbf{k}_1\alpha})}\left(C_{\mathbf{k}_1\alpha}^\dagger\right)^{n_{\mathbf{k}_1\alpha}}\left(C_{\mathbf{k}_2\alpha}^\dagger\right)^{n_{\mathbf{k}_2\alpha}}|0\rangle \\
&= (-1)^{n_{\mathbf{k}_2\alpha}(1-n_{\mathbf{k}_1\alpha})}|n_{\mathbf{k}_2\alpha}, n_{\mathbf{k}_1\alpha}\rangle.
\end{aligned}
$$

Defining the following operator,

$$
\tilde{E}_\alpha(\mathbf{k}_1,\mathbf{k}_2) \equiv e^{i\pi(\rho_\alpha(\mathbf{k}_1)(1-\rho_\alpha(\mathbf{k}_2)))}U_\alpha^\dagger(\mathbf{k}_1,\mathbf{k}_2) \tag{4.26}
$$

we have the desired action of the exchange operator on the two particle states,

$$
\tilde{E}_\alpha(\mathbf{k}_1,\mathbf{k}_2)|n_{\mathbf{k}_1\alpha}, n_{\mathbf{k}_2\alpha}\rangle = |n_{\mathbf{k}_2\alpha}, n_{\mathbf{k}_1\alpha}\rangle. \tag{4.27}
$$

The same will hold through for the Fock basis but the fermionic sign needs to be handled carefully. Let us stick to the same convention as specified by labelling the modes as per equation 4.3. We know from the anticommutation relations of Fermion operators, $\left(C_m^\dagger\right)^{n_m}\left(C_l^\dagger\right)^{n_l} = (-1)^{n_m n_l}\left(C_l^\dagger\right)^{n_l}\left(C_m^\dagger\right)^{n_m}$ and we accordingly define a suitable phase factor $e^{i\pi\nu_\alpha(\mathbf{k}_1,\mathbf{k}_2)}$, where

$$
\nu_\alpha(\mathbf{k}_1,\mathbf{k}_2) \equiv (\rho_\alpha(\mathbf{k}_1)+\rho_\alpha(\mathbf{k}_2))\sum_{l=m(\mathbf{k}_1,\alpha)+1}^{m(\mathbf{k}_2,\alpha)-1}\rho_\alpha(\mathbf{k}_l). \tag{4.28}
$$

So the exchange operator defined as,

$$
E_\alpha(\mathbf{k}_1,\mathbf{k}_2) \equiv e^{i\pi\nu_\alpha(\mathbf{k}_1,\mathbf{k}_2)}\tilde{E}_\alpha(\mathbf{k}_1,\mathbf{k}_2) \tag{4.29}
$$

exchanges the occupation numbers of the modes at $\mathbf{k}_1$ and $\mathbf{k}_2$.

Let us simplify the above expression. Expanding the operators $U^{\dagger}_{\alpha}(\mathbf{k}_1, \mathbf{k}_2)$ and the sign factor in the RHS of Eq. (4.26) we get,

$$e^{i\pi(\rho_\alpha(\mathbf{k}_1)(1-\rho_\alpha(\mathbf{k}_2)))} = 1 - 2\left(\rho_\alpha(\mathbf{k}_1)(1-\rho_\alpha(\mathbf{k}_2))\right) \tag{4.30}$$

$$U^{\dagger}_{\alpha}(\mathbf{k}_1, \mathbf{k}_2) = 1 - (\rho_\alpha(\mathbf{k}_1) - \rho_\alpha(\mathbf{k}_2))^2 + iT^{y}_{\alpha}(\mathbf{k}_1, \mathbf{k}_2) \tag{4.31}$$

Using the above equations we get a simpler form for $\tilde{E}_\alpha(\mathbf{k}_1, \mathbf{k}_2)$, which is

$$\tilde{E}_\alpha(\mathbf{k}_1, \mathbf{k}_2) = 1 - (\rho_\alpha(\mathbf{k}_1) - \rho_\alpha(\mathbf{k}_2))^2 + \left(C^{\dagger}_{\mathbf{k}_1\alpha}C_{\mathbf{k}_2\alpha} + C^{\dagger}_{\mathbf{k}_2\alpha}C_{\mathbf{k}_1\alpha} - 2\rho_\alpha(\mathbf{k}_1)\delta_{\mathbf{k}_1\mathbf{k}_2}\right). \tag{4.32}$$

For a one-band model, considering translationally invariant states, the expression for the expectation values of the exchange operators has the following form,

$$\langle E(k_1, k_2)\rangle = 1 - \left\langle \left(C^{\dagger}_{k_1}C_{k_1} - C^{\dagger}_{k_2}C_{k_2}\right)^2 \right\rangle. \tag{4.33}$$

4.1.5 Failure in Generalisation of the Geometric Phase

In Section 3.1.1 we looked into definitions of the Bargmann invariants of third order as well, for the mean-field states, in terms of expectation values of operators which are products of the exchange operators as defined in Eq. (3.30). If the generalisation of the above definition for the geometric phases in terms of the expectation values of the unitary operator defined as the product of the exchange operators is correct for correlated many-body states, then we can also define the geometric phases associated with loops in the spectral parameter.

We have tested whether generalisation of the above scheme is possible for defining the geometric phases in case of correlated many-body states. The algorithm for a numerical check of the satisfaction of the additive law (given by Eqs. (2.41,2.42)) is discussed in

Fig. (4.3).

The probability distribution $P(\theta)$ of obtaining a deviation $\Delta\phi$ from the additive law in

1. We consider states of a four site, one-band, spinless fermionic system at half-filling. The occupation number basis $\{(n_{\mathbf{k_1}}, n_{\mathbf{k_2}}, n_{\mathbf{k_3}}, n_{\mathbf{k_4}})\}$ is choosen, where $n_{\mathbf{k}_i} = 0, 1 \;\; \forall i \in [1, 4]$.

2. We generate $N = 10^6$ random states.

3. We compute the following quantities for each state $|\psi\rangle$:

$$\begin{aligned} \tilde{\mathcal{B}}^3(\mathbf{k}_1, \mathbf{k}_2, \mathbf{k}_3) &= \langle\psi|E(\mathbf{k}_1, \mathbf{k}_3)E(\mathbf{k}_3, \mathbf{k}_2)\,|\psi\rangle \\ &= e^{i\Omega^{(3)}(\mathbf{k}_1,\mathbf{k}_2,\mathbf{k}_3)}\;|\,\langle\psi|E(\mathbf{k}_1, \mathbf{k}_3)E(\mathbf{k}_3, \mathbf{k}_2)\,|\psi\rangle\,| \\ \tilde{\mathcal{B}}^3(\mathbf{k}_1, \mathbf{k}_3, \mathbf{k}_4) &= \langle\psi|E(\mathbf{k}_1, \mathbf{k}_4)E(\mathbf{k}_4, \mathbf{k}_3)\,|\psi\rangle \\ &= e^{i\Omega^{(3)}(\mathbf{k}_1,\mathbf{k}_3,\mathbf{k}_4)}\;|\,\langle\psi|E(\mathbf{k}_1, \mathbf{k}_4)E(\mathbf{k}_4, \mathbf{k}_3)\,|\psi\rangle\,| \;. \end{aligned}$$

4. The total phase ϕ is given by

$$\phi = \Omega^{(3)}(\mathbf{k}_1, \mathbf{k}_2, \mathbf{k}_3) + \Omega^{(3)}(\mathbf{k}_1, \mathbf{k}_3, \mathbf{k}_4). \tag{4.34}$$

5. Similarly we also compute ϕ',

$$\phi' = \Omega^{(3)}(\mathbf{k}_1, \mathbf{k}_2, \mathbf{k}_4) + \Omega^{(3)}(\mathbf{k}_2, \mathbf{k}_3, \mathbf{k}_4). \tag{4.35}$$

6. We then compute the deviation from the additive law (as per Eqs. (2.41,2.42)),

$$\Delta\phi = \phi - \phi' \tag{4.36}$$

7. The probability distribution $P(\theta)$ of obtaining a deviation in the range, $\theta \leq \Delta\phi \leq \theta + \delta\theta$, where $\delta\theta = \frac{\pi}{100}$ is then computed.

Figure 4.3: Algorithm for verifying the satisfaction of additive law.

the range, $\theta \leq \Delta\phi \leq \theta + \delta\theta$, where $\delta\theta = \frac{\pi}{100}$ is shown in Fig. (4.4). We find that the probability distribution function is sharply peaked at $\theta = 0$. But the additive law are not neccesarily satisfied. Infact there are many violations as the probability of the additive law being satisfied is found to be only $\sim 7\%$. So the proposed scheme fails for the above choice (Eq. (4.29)) of unitary operator and we cannot define geometric phases associated

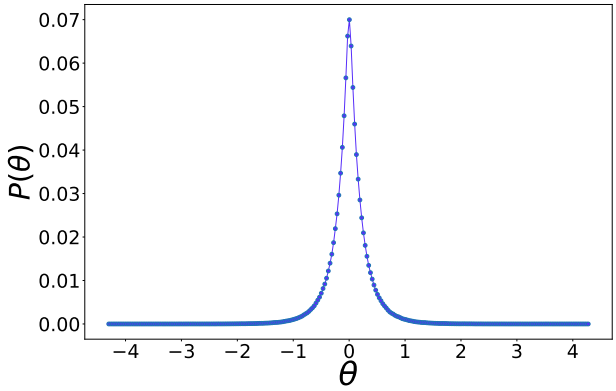

Figure 4.4: The probability distribution $P(\theta)$ of obtaining a deviation $\Delta\phi$ from the additive law in the range, $\theta \leq \Delta\phi \leq \theta + \delta\theta$, where $\delta\theta = \frac{\pi}{100}$.

with loops in spectral parameter space.

4.2 Conclusion

Let us stop and reflect on the findings from our new formalism to study the quantum geometry of correlated many-body states, as we conclude this chapter.

We have been able to give a definition for induced quantum distances in the space of physical parameters like the quasi-momenta which label the single particle states (the spectral parameters) for the correlated many-body states just like in the case of many-body states in a periodic potential. So now we have access to local geometric observables even for the correlated scenario for the very first time. The spectral parameters however could be more generally the spin, the position labelling the Warnier orbitals, parameters labelling the eigenfunctions of some confining potential like in a quantum dot or an optical trap as pointed out already in Sec. (4.1.2).

The proposed definition of quantum distances are in terms of expectation values of the exchange operators. From the explicit form of the operators in Sec.(4.1.4), we know the definition is basically in terms of the static correlation functions. In one band system these being the four-point correlation functions as observed from Eq. (4.33), whereas for

multiband systems they are higher order correlation functions.

So the quantum distances can be obtained by computation of the static correlation functions applying any exact or approximate technique like quantum Monte Carlo methods, DMRG and bosonisation in one dimension, exact diagonalisation for finite systems, perturbation theory and so on.

Studying the geometry of the correlated state now reduces to study of the above collection of quantum distances in spectral parameter space. We apply our formalism to the ground state of the one-dimensional $t - V$ model and discuss the quantum distances in the next chapter. While application to the ground state can throw light on characterisation of the phases of a system in terms of geometry, application to any quantum state is possible in principle, leading to the possibility of applications in quantum dynamical systems as well. The following chapters will elaborate in detail the tools to study the geometry of the state in terms of the quantum distances.

Chapter 5

Space of the Distances

Our formalism introduced in the previous chapter when applied to a correlated system gives a set of distances $\{d(k_i, k_j)\}$, between points in the spectral parameter space $\{k_i\} \in K$, which are basically quantum numbers labelling the single particle states. Therefore, by computing the static correlation functions applying any exact or approximate technique (e.g. quantum Monte Carlo methods, DMRG and bosonisation in one dimension, exact diagonalisation for finite systems, perturbation theory etc.), we obtain a collection of all the interconnecting distances between a set of points, (K, d). The quantum geometry of the correlated many-body state is then studied by analysing the properties of the above space of distances. However, how the distances are related to many-body observables that can be measured in the lab we don't know yet.

How do we explore the rich geometric properties of the above space of distances? In the first part of this chapter, we briefly introduce the mathematical tools needed for this study. In the later part of this chapter, we apply our formalism to the system of spinless fermions in one dimension with nearest-neighbour repulsion, in the half-filled case, the $t-V$ model. This is a one-band model of correlated Fermions which is exactly solvable and exhibits a Mott transition.

We will elaborate these tools in the forthcoming chapters of this thesis, particularly em-

phasizing their efficiency in terms of the capability to give geometric description and characterisation of the metallic and insulating phases of the ground state wavefunction of the one-dimensional $t - V$ model.

Before we proceed, let us examine two basic objects obtained from the space of distances. Extracting geometric information from them will be central to our work.

The distance matrix Let us consider a lattice with L^d sites. The spectral parameters are d dimensional vectors $\mathbf{k}_i = (k_i^1, k_i^2, \ldots k_i^d)$. With every point in the spectral parameter space $\mathbf{k}_i \in \mathbf{k}$, we associate a unique integer i, which runs from 1 to L^d.
So the quantum distances defined as per Eq. (4.9), gives us a $L^d \times L^d$ matrix of distances D whose elements are given by,

$$D(i, j) \equiv \sqrt{1 - |\langle\psi|E(\mathbf{k}_i, \mathbf{k}_j)|\psi\rangle|^\alpha}. \tag{5.1}$$

The study of the quantum geometry of the correlated many-body state is equivalent to extracting geometric information from the above matrix of quantum distances.

The above distance matrix being the fundamental object under inspection, it should reflect the phases of the correlated state. So even a heurestic study of the properties of the distances should be quite insightful for the physics of the model. We will give a detailed illustration of such studies with the distance matrices of the $t - V$ model for different values of the nearest neighbour repulsion V, shortly.

However there are more rigorous and systematic methods to construct geometric invariants starting from the distance matrix, as we will soon find out.

The graph of a state It is particularly helpful to associate a weighted graph $G \equiv (K, e, D)$ with the distance matrix, as the graph of the state. The spectral parameters $\{k_i\} \in K$ can be thought of as the vertices of the graph, a pair of spectral parameters (k_i, k_j)

define an edge $e(i, j)$ and the corresponding quantum distance $D(i, j)$ specifies the weight of each edge.

Fig. (5.1) shows the schematic figure for a graph of a 9-site system.

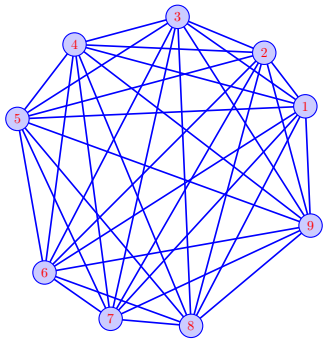

Figure 5.1: The schematic representation of the graph of a 9-site system.

There are several tools studied in the branches of discrete differential geometry, image processing, data mining and machine learning connected to the geometry of a graph. The study of the above graph can also be thought of as a problem in network analysis.

We will develop and analyse tools for studying the geometry of the above graph in vivid details. In the next sections we will introduce the basic ideas and tools involved without going into mathematical details, which we preserve for the upcoming chapters.

5.1 Intrinsic geometry of the state

Intrinsic geometry of the correlated many-body state under inspection can be studied from the intrinsic curvature, which is a fundamental geometric invariant.

The intrinsic curvature is a geometric quantity on the above space of distances, characterising the intrinsic geometry of the space: it is independent of where the space of distances is embedded, and it is computed without assigning any local coordinates to the points.

The problem of treating geometrical properties such as curvature metrically, i.e. of developing a differential geometry without the use of coordinates, has recently received the attention of some mathematicians[37, 38, 39, 40].

In 1827, Gauss in his foundational work[41] in geometry disentangled the two aspects, the intrinsic and extrinsic geometry of surfaces in $\mathbb{R}^3$. He separated the two aspects with the discovery that there exists a curvature measure, later called the Gauss curvature, which is independent of how the surface sits in space and solely depends on the intrinsic geometry of a surface. On the contrary, another curvature measure is the mean curvature which describes the extrinsic geometry, that is, how the surface is embedded in space.

The curvature of curves and surfaces have been studied in differential geometry almost entirely by means of analytic methods which makes it necessary to impose some conditions (e.g. conditions concerning differentiability) upon the entities involved. In a metrical theory the differential geometry can be freed from many of these restrictions, which are often geometrically unessential and serve merely to make the application of differential calculus possible.

Generalisations of the classical curvature or Gauss curvature to the discrete setting includes metric curvatures defined completely from the distances like the Haantjes curvature[42] which is particularly suited for the geometrisation of graphs. More advanced generalisations of the Gaussian curvature include the Wald curvature [43].

In Riemannian geometry, sectional curvature and Ricci curvature are fundamental concepts. There are geometric and topological consequences of bounds on the curvatures, like divergence or convergence of geodesics, vanishing theorems for Betti numbers, convexity properties of distance functions, growth of the volume of distance balls, transportation distance between such balls, bounds for the eigenvalues of the Laplace operator or control of harmonic functions. These properties are often meaningful in the more general framework of metric geometry. Thus recent research projects have turned such properties into axiomatic definitions of curvature bounds in metric geometry and developed generalisations[37, 44, 45, 46, 47, 48, 49] with widespread applicability.

We will be focusing on the generalisation of the Ricci curvature for the graph of the many-body state. In physics we encounter the Ricci curvature in string theory or gen-

eral relativity in the Einstein field equations. Several notions of Ricci curvature such as Ollivier-Ricci curvature[47, 48, 50], Bakry-Emery curvature[45], Entropic curvature introduced by Erbar and Maas[49] and Forman curvature[46], have emerged on graphs in recent years, and are topics of active research.

We will follow the notion of Ricci curvature as introduced by Ollivier[47, 48, 50], called the Ollivier-Ricci curvature. In Riemannian geometry Ricci curvature involves some averaging and contains information about volumes and eigenvalues of a Laplace operator. Therefore, in order to define some kind of generalized Ricci curvature, we need some measure on our space in addition to the metric, that is, the quantum distances. This brings us to optimal transport theory and probability distributions constructed from the distances. We will be discussing the basic mathematical concepts and the efficiency of the Ollivier Ricci curvature in capturing the phases of the ground state in context of the $t - V$ model in Chapter 9.

5.2 Extrinsic geometry of the state

We now come to the study of the extrinsic geometry of the many-body state: we ask whether we can find an Euclidean space where the distances can be embedded. We want to find a set of points, $\{\mathbf{x}_i\} \in \mathbb{R}^m$, in m dimensional Euclidean space such that the Euclidean distances between the points are same as the quantum distances,

$$D(i, j) = |\mathbf{x}_i - \mathbf{x}_j|. \tag{5.2}$$

Some important results of distance geometry[51, 52, 53] (study of geometry with the basic entity being only the distances) allows us to find out if the distance matrix is an allowed matrix of Euclidean distances (EDM) and also the dimension of the Euclidean space and the vector configurations of the points.

5.2.1 Fundamental results in distance geometry

The following theorem, proposed by Isaac Schoenberg in 1935[54], is the main tool to test whether a given distance matrix can be realized via a set of points in the Euclidean space.

Theorem 1 (Schoenberg's Theorem)**.** *The $N \times N$ symmetric matrix D is the EDM of a set of N points $\{\mathbf{x}_1, \cdots, \mathbf{x}_N\} \in \mathbb{R}^m$ if and only if the Gram matrix is a positive semi-definite matrix of rank m.*

The Gram matrix in terms of the distance matrix is

$$G = -\frac{1}{2}(I - \frac{1}{N}ee^T)D^2(I - \frac{1}{N}ee^T) \tag{5.3}$$

where D^2 is the matrix of squared distances: $D^2(i, j) \equiv (D(i, j))^2$. I is the $N \times N$ identity matrix. e is a N-dimensional column vector with all entries equal to 1.

Note that G is the inner product matrix by construction:

$$G(i, j) = \mathbf{x}_i.\mathbf{x}_j = \sum_{n=1}^{d} x_i^n x_j^n = (U\sqrt{\Lambda})(\sqrt{\Lambda}U^T). \tag{5.4}$$

Here, $\mathbf{x}_i$ are m-component column vectors, with components x_i^n, $n = 1, \ldots, m$, which are obtained by diagonalising the real and symmetric Gram matrix.

The volume V_N of a N-simplex with the edges given by the distances $\{D(i, j)\}$ is given in

terms of the Cayley-Menger determinant[55, 56] Δ as follows:

$$\Delta = \text{Det}(C_D), \tag{5.5}$$

$$C_D = \begin{bmatrix} 0 & 1 & 1 & .. & 1 \\ 1 & 0 & D_{1,2} & .. & D_{1,N} \\ \vdots & & & & \\ 1 & D_{N,1} & D_{N,2} & .. & 0 \end{bmatrix} \tag{5.6}$$

$$V_N^2 = \frac{(-1)^{N-1}}{2^N (N!)^2} \Delta \tag{5.7}$$

Next, we state another important theorem due to Bluementhal[57].

Theorem 2 (Bluementhal)**.** *A $N \times N$ distance matrix D is embeddable in $\mathbb{R}^m$ but not $\mathbb{R}^{m-1}$ if and only if: (i) there is a principal $(m+1) \times (m+1)$ submatrix R of D with nonzero Cayley-Menger determinant; (ii) for $\mu \in \{1, 2\}$, every principal $(m+\mu) \times (m+\mu)$ submatrix of D containing R has zero Cayley-Menger determinant.*

Discussion. The dimension of the Euclidean space where the points sit could vary from 1 to $L^d - 1$ for the quantum distance matrix. It will be very interesting to be able to associate "shapes" by obtaining vector configuration for the points in lower dimensions ($1 \leq m \leq 3$), where a visualization is possible. A particularly interesting aspect is the following: we will be able to characterise a correlated many-body state by a surface in a finite dimensional Euclidean space if the embedding dimension does not scale with system size.

In the cases where the rank of the Gram matrix is higher than 3, visualization by isometric embedding will not be possible. But approximate Euclidean embedding methods can save the situation. An approximate Euclidean embedding is possible by applying the concept of distortion[58, 59, 60] or by truncation of the Gram matrix spectrum with a well-defined error estimate[61, 62]. We will discuss these concepts in detail along with demonstrations with the distance matrices of the one dimensional $t - V$ model in Chapter 6.

5.3 Distance distributions and theory of optimal transport

A very powerful way of probing the geometry of the many-body state is by construction of probability distributions from the quantum distances and, ultimately, by applying the powerful theory of optimal transport[63, 64] for a detailed study of the geometry of the distance distributions. The above approach is particularly insightful because it allows us to define geometric observables which are obtained by averaging over the full space of spectral parameters.

5.3.1 Distance distributions

We define probability distributions at every point k_i in the spectral parameter space, $\{m_i(j)\}$, $i = 1, \ldots, L^d$, constructed from normalised distribution of distances of all the points from the above point, as follows:

$$m_i(j) \equiv \frac{D(i,j)}{\sum_{l=1}^{L^d} D(i,l)}. \tag{5.8}$$

The geometry of the graph is very well captured by the geometry of the above distributions, which are basically depicting random walks on the graph with the probabilities being specified by the quantum distances.

Let us look at the motivation behind constructing a space of probability distributions on our space of distances. Choosing the quasi-momenta as spectral parameters, our definition of the distance between two points in the BZ for lattice translation invariant single band model as observed from Eq. (4.33), can be qualitatively thought of as a measure of the difference in the occupancies of these two points. The metallic state is characterised by the different occupancies of the points in the Fermi sea (FS) and those outside it. While on the contrary, deep in the insulating regime, since the kinetic energy is quenched, we

do not expect much difference between the occupancy of the various points in the BZ. Thus, above distributions could be particularly useful in depicting this difference of behaviour in the metallic and insulating states.

5.3.2 Theory of optimal transport

The theory of optimal transport [63, 64, 65, 66, 67, 68, 69] is a concrete quantitative approach for studying the geometry of probability distribution functions. It has been first applied in condensed-matter physics in a very different context, in the study of density functional theory[70, 71]. The theory gives a definition of distances between probability distribution functions[63, 64] and thus allows us to compare a set of distance distribution functions quantitatively. The distance $W_p(m_i, m_j)$ between two probability distribution functions (PDFs) m_i and m_j is defined as follows:

$$W_p^{(p)}(m_i, m_j) \equiv \inf_{\pi} \sum_{k,l} (\tilde{d}(k,l))^p \pi_{ij}(k,l), \tag{5.9}$$

where k, l in the above sum runs over the domain of the PDFS, $p \in [1, \infty)$ and $\pi_{ij}(k,l)$ are joint probability distributions whose marginals are m_i and m_j,

$$\sum_l \pi_{ij}(k,l) = m_i(k), \quad \sum_k \pi_{ij}(k,l) = m_j(l). \tag{5.10}$$

If $\tilde{d}(k,l)$ is a valid distance function satisfying all the properties of a metric then pth root of optimised $W_p^{(p)}(m_i, m_j)$ satisfies all the axioms of a distance function.

In theory of optimal transport, $\pi_{ij}(k,l)$ is usually interpreted as different ways to transport material such that the distribution function m_i is transformed to the distribution function m_j and $(\tilde{d}(k,l))^p$ is called the cost function of the transport and is interpreted as the cost paid for above transfer. In a general scenario the cost function is not restricted to be positive powers of a distance. The above optimised sum, $W_p^{(p)}(m_i, m_j)$, is defined as the minimal cost of transforming m_i to m_j. The central concept of optimal transport problem

is finding an optimal joint distribution function $\pi^*_{ij}(k,l)$ which minimises the sum defined on the RHS of Eq. 5.9.

We consider the choice $p = 2$ in Eq. 5.9 and define squared Wasserstein distances $W^{(2)}(m_i, m_j)$ between any two PDFs m_i and m_j as follows,

$$W^{(2)}(m_i, m_j) \equiv \inf_{\pi} \sum_{k,l} (\tilde{d}(k,l))^2 \pi_{ij}(k,l). \tag{5.11}$$

π_{ij} satisfies the constraints given by Eq. (5.10).

We consider the distributions, m_i and m_j, to be the distance distributions defined at any two points k_i and k_j. While $\tilde{d}(k,l)$ can be any valid distance defined between the points in the spectral parameter space, we have studied the quantum distances and the Euclidean distances. The corresponding squared Wasserstein distance between distance distributions, given by the above sum in Eq. (5.11) then gives the weighted average of all the squared distances between any two points in the spectral parameter space, with the corresponding weights given by the optimal joint probability distribution π^*_{ij}.

Optimal transport theory also gives means to interpolate between different functions and define the barycenter of a weighted family of functions, in a very general context, by the concept of a Wasserstein barycenter. Using this concept, we identify a single representative distribution function on the spectral parameter space.

We will give a detailed description of the Wasserstein distances and the Wasserstein barycenter [66, 72] particularly emphasizing their capability to give a vivid geometric description and characterisation of the many-body state, by application to the $t-V$ model in Chapter 7 and 8 respectively.

5.4 Application to the one-dimensional $t - V$ model

We apply our formalism to the system of spinless fermions in one dimension with nearest neighbour repulsion, the $t - V$ model[33, 34, 35]. For the half-filled case, the model exhibits a Mott transition. One of the main reasons for choosing the above model is that much of the motivation of our work comes from characterisation of the insulating state using quantum geometry. The power of quantum geometry is highlighted in its capability to answer the following fundamental question: which feature of the insulating state can uniformly characterise it, and in fact, differentiate it from the metallic state.

The efficiency of our new method will be well demonstrated if it is able to give characterisation of the metallic and insulating state. We hope to find some geometrical observable parallel to the localisation tensor which differentiates both the phases. Moreover, time-reversal symmetry and parity invariance are preserved in this model. Thus, we do not expect any geometric phase effects and can focus only on the quantum distances.

5.4.1 Physics of the model

The Hamiltonian in terms of the Fermion creation and annihilation operators, for a lattice of L sites, is the following:

$$H = \sum_{i=1}^{L} \left(-t \left(C_{i+1}^{\dagger} C_i + H.c. \right) + V n_i n_{i+1} \right), \tag{5.12}$$

where $n_i \equiv C_i^{\dagger} C_i$ is the operator representing the number of fermion at the i^{th} site. For the half-filled states, it holds that $\sum_i n_i |\psi\rangle = L/2 |\psi\rangle$. Using the Bethe ansatz the Hamiltonian can be solved exactly[35]. The above model can be mapped to the well known XXZ spin-$\frac{1}{2}$ model by Jordan-Wigner transformation [33]. The spin model again can be mapped onto a model of impenetrable (hard-core) bosons, known as the lattice Tonks-Girardeau gas[35].

The Fourier transform of the fermion operators are defined as usual,

$$C_k = \frac{1}{\sqrt{L}} \sum_{i=1}^{L} e^{-i\frac{2\pi}{L}ki} C_i \tag{5.13}$$

where k is an integer that we choose to be $-L/2 \leq k < L/2$. The Hamiltonian is,

$$H = -2t \sum_{k=-L/2}^{L/2-1} \cos\left(\frac{2\pi}{L}k\right) C_k^\dagger C_k + \frac{2V}{L} \sum_{k_1,k_2,k_3,k_4} \delta(k_1 - k_2 + k_3 - k_4) cos\left(\frac{2\pi}{L}(k_3 - k_4)\right) C_{k_1}^\dagger C_{k_2} C_{k_3}^\dagger C_{k_4}. \tag{5.14}$$

We choose the quasi-momenta as the spectral parameters of our formalism.

Let us first look at the two extreme interaction limits.

$V = 0$. The Hamiltonian, at $V = 0$ is,

$$H^0 = -\sum_{k=-L/2}^{L/2-1} 2t \cos\left(\frac{2\pi}{L}k\right) C_k^\dagger C_k \tag{5.15}$$

We choose L to be an even number which is not divisible by 4. Further we define $N = L/2$ (an odd number). So the half-filled ground state for a system with N fermions in this interaction limit is non-degenerate. The ground state is the non-interacting Fermi sea (FS), and is of the following form,

$$|FS\rangle = \prod_{k=-N/2-1/2}^{N/2+1/2} C_k^\dagger |0\rangle \tag{5.16}$$

where $|0\rangle$ is the empty state, defined by $C_i|0\rangle = 0, \ \forall i$.

$V = \infty$. At $V = \infty$, the Hamiltonian (Eq. (5.12)) is,

$$H_\infty = V \sum_i n_i n_{i+1}. \tag{5.17}$$

The translation symmetry is spontaneously broken, and the particles are localised at alternate sites, either all odd or all even sites leading to a charge density ordered or CDW state. In the thermodynamic limit thus we have two degenerate ground states. For finite L, however, the degeneracy splits and the symmetric combination is the ground state. We denote it by $|CDW\rangle$,

$$|CDW\rangle \equiv \frac{1}{\sqrt{2}}\left(\prod_i C^\dagger_{2i}|0\rangle + \prod_i C^\dagger_{2i+1}|0\rangle\right). \tag{5.18}$$

As soon as the interaction is turned on, or $V = 0^+$, the ground state is found to be a metallic Luttinger liquid, where we find the long-distance correlations decay as power laws, characterised by an anomalous dimension of the fermion operators[73, 74, 75]. With the increase of V a transition from the above gapless Luttinger liquid (LL) to a gapped charge-density wave (CDW) occurs at $V/t = 2$, which was analysed in detail by Shankar[76]. The translational symmetry is spontaneously broken in the above transition.

5.4.2 Distance matrices at different interaction values

Let us return back to the quantum distances. We already found that in the one band model, for translationally invariant states, the expression for the expectation values of the exchange operators is

$$\langle E(k_1, k_2)\rangle = 1 - \left\langle \left(C^\dagger_{k_1} C_{k_1} - C^\dagger_{k_2} C_{k_2}\right)^2 \right\rangle. \tag{5.19}$$

We know the exact analytic form of the ground state at the extreme limit of interactions (Eqs. (5.16,5.18)). We can thus analytically compute the above expectation values and analyse the distances. For the intermediate interaction regime we have performed exact diagonalisation on systems of size $L \leq 18$ and obtained the numerical $L \times L$ distance matrices.

Let us look at the three cases $V = 0$, $0 < V < \infty$, and $V = \infty$.

$V = 0$. We found the ground state is a simple non-interacting Fermi Sea (FS), given by Eq. (5.16). The exchange of the occupation numbers of two quasi-momenta which are both in the Fermi sea or both outside it, does not alter the state, giving an expectation value ± 1. So the corresponding distances given by Eq. (4.9) are 0.
On the contrary, when one quasi-momenta is in the Fermi sea and the other outside it, the exchange operator removes a particle from the Fermi sea and creates one outside it creating a particle-hole state orthogonal to $|FS\rangle$ and hence the expectation value of the exchange operator is 0. Thus the corresponding distances by Eq. (4.9) are 1.

$$|\langle E(n,m)\rangle_{FS}| = \begin{cases} 1 & n \in FS,\ m \in FS \\ 1 & n \notin FS,\ m \notin FS \\ 0 & n \in FS,\ m \notin FS \\ 0 & n \notin FS,\ m \in FS \end{cases}$$

The corresponding squared distances are

$$\begin{aligned} \left(d^{FS}(n,m)\right)^2 &= 1 - |\langle E(n,m)\rangle|^{\alpha} \\ &= \begin{cases} 0 & n \in FS,\ m \in FS \\ 0 & n \notin FS,\ m \notin FS \\ 1 & n \in FS,\ m \notin FS \\ 1 & n \notin FS,\ m \in FS \end{cases} \end{aligned}$$

We relabel the momenta as $n \rightarrow n, p$ with $-N/2 \leq n < N/2,\ p = \pm$ as follows,

$$n- \ = \ n, \quad -N/2 \leq n < N/2 \tag{5.20}$$

$$n+ \ = \ n+N \quad -N/2 \leq n < N/2, \tag{5.21}$$

giving us, $n- \in FS$ and $n+ \notin FS$.

Let $\mathcal{I}$ be a $N \times N$ matrix with all entries equal to 1, $\mathcal{I}_{nm} = 1$ and a 2×2 matrix, $\tau^x_{pp'} = 1 - \delta_{pp'}$. The distance matrix can thus be written in a compact form as,

$$d^{FS}(np, mp') = \mathcal{I}_{nm}\tau^x_{pp'} \ \Rightarrow \ d^{FS} = \begin{pmatrix} 0 & \mathcal{I} \\ \mathcal{I} & 0 \end{pmatrix}. \tag{5.22}$$

We find the points are highly “clustered" because the distance matrix is the same as a space with only two points seperated by a distance 1. One of the points represents all the quasi-momenta in the FS and the other one represents all the quasi-momenta outside it. This is demonstrated in the schematic figure below.

Figure 5.2: Schematic figure for the two points seperated by distance 1 as obtained from the distance matrix. The filled circle correspond to all the quasi-momenta modes inside the FS and the unshaded circle represents all the quasi-momenta modes outside it.

We also find that the distance matrix reveals a sharp Fermi surface, in the sense that the distances jump from 0 to 1 at the Fermi points.

$0 < V < \infty$**.** Numerical exact diagonalisation of the Hamiltonian, in the quasi-momentum basis, for the 18-site system, for values of interaction strength $V = 0 - 12$, gives us the quantum distance matrix.

We have chosen $\alpha = 2$ in the definition of the quantum distances in Eq. (4.9).

As soon as the interaction is turned on, $V = 0^+$, the zero distances between pairs of quasi-

momenta in the Fermi sea (and pairs outside it) become non-zero and are not all equal either. Also, the distances between quasi-momenta in the Fermi sea and outside shift slightly from 1 and are no longer all equal. The distance matrix has the following form,

$$d = \begin{pmatrix} \Delta & \Delta_e \\ \Delta_e & \Delta \end{pmatrix} \tag{5.23}$$

where Δ has all matrix elements $\ll 1$ and Δ_e has matrix elements slighlty less than 1. The matrix elements of Δ increase and those of Δ_e decrease upon increasing V. The numerical distance matices and their evolution with the interaction is shown in Fig. (5.3). For $V \geq 4$,

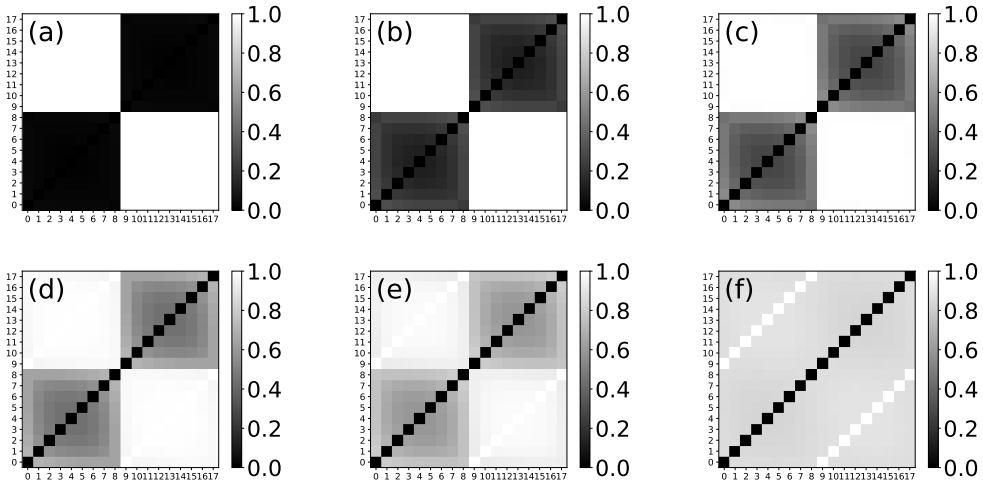

Figure 5.3: (a)-(f) Distance matrices obtained from numerical computation for interaction strengths $V = 0.1$ (a), $V = 1$ (b), $V = 2$ (c), $V = 3$ (d), $V = 4$ (e) and $V = 12$ (f).

the above block structure is no longer there, the matrix becomes homogenous with only the elements $d(i, i + \frac{L}{2}), i = 1, \cdots, \frac{L}{2}$ differing from the rest. These are features of the distances in the extreme CDW limit as we will soon find out.

$V = \infty$. We know the exact ground state given by Eq. (5.18). The corresponding expectation values of the exchange operators are,

$$|\langle E(n,m)\rangle_{CDW}| = \begin{cases} 1 & n = m \\ 0 & n = m + \frac{L}{2} \\ \frac{1}{2} & n \neq m,\ n \neq m + \frac{L}{2} \end{cases}$$

The quasi-momenta k_n, k_m are labelled by n, m in the above equation. We find that $|\langle E(k, k+\pi)\rangle| = |\langle E(n, n + \frac{L}{2})\rangle| = 0$. From Eq. (5.19) it can be inferred that this is a consequence of the particle-hole symmetry of the model, $C_k^\dagger \to C_{k+\pi}$. This will thus be true for all values of k and V.

The distance matrix elements are thus obtained as,

$$d^{CDW}(n,m) = \begin{cases} 0 & n = m \\ 1 & n = m + \frac{L}{2} \\ \sqrt{1 - \frac{1}{2^\alpha}} & n \neq m,\ n \neq m + \frac{L}{2}. \end{cases}$$

We define $c(\alpha) \equiv \sqrt{1 - 1/2^\alpha}$ and denote the $N \times N$ identity matrix by I, $I_{nm} = \delta_{nm}$. The distance matrix can then be written as,

$$d^{CDW} = c(\alpha) \begin{pmatrix} \mathcal{I} - I & \mathcal{I} - I \\ \mathcal{I} - I & \mathcal{I} - I \end{pmatrix} + \begin{pmatrix} 0 & I \\ I & 0 \end{pmatrix}. \tag{5.24}$$

Choosing $\alpha = 2$ we get $c(\alpha) = \frac{\sqrt{3}}{2}$.

So in this limit all the distances are large and more or less homogenous. There is no "clustering" feature like before. Moreover, there is no sharp change at the Fermi points.

5.4.3 Heuristic study of the properties

We find the distances in both the interaction regime are drastically different. We have heuristically studied the properties of the distances with particular interest in how it reflects the basic physics of the model.

Distances from $k = -\pi$

We first look at the the distances from a fixed point $k = -\pi$.

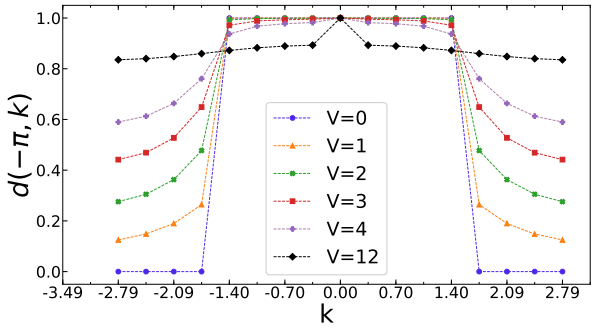

Figure 5.4: Distance $d(-\pi, k)$ between $k = -\pi$ and the other k modes in the Brillouin zone (BZ) for different values of the interaction strength V.

In Figure (5.4) we have plotted the distance $d(-\pi, k)$ for different interaction strengths. $k_F = \pm\pi/2$ are the Fermi points. The observations are:

1. Discontinuity at the Fermi points.

   $V = 0$ is characterised by a jump of the distance from 0 to 1 at the Fermi points. At large V, the discontinuity disappears. Whether the discontinuity persists for small V we will inspect in more detail soon.

2. $d(-\pi, 0) = 1$, for all values of the interaction. This is because $d(k, k+\pi) = 1$, for all values of k and V, as a consequence of the particle-hole symmetry of the model.

We examine the discontinuity at the Fermi points by plotting the difference across the Fermi points, $\delta = d(-\pi, -\frac{\pi}{2}) - d(-\pi, -\frac{\pi}{2} - \frac{2\pi}{L})$, for different system sizes in Fig. (5.5). We

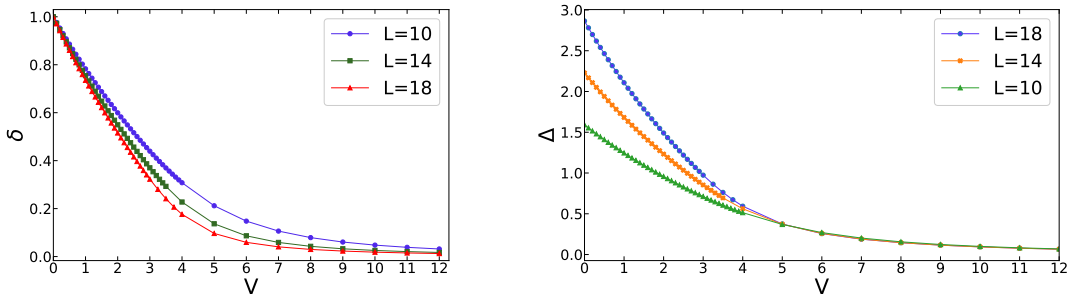

Figure 5.5: $\delta = d(-\pi, -\frac{\pi}{2}) - d(-\pi, -\frac{\pi}{2} - \frac{2\pi}{L})$ and Δ: the derivative of the distance $d(-\pi, k)$ at $k = -\pi/2$, are studied as a function of interaction strength V for different system sizes, to examine the discontinuity across the Fermi points.

also look at the numerical derivative of the distance $d(-\pi, k)$ at $k = -\pi/2$ which can be defined as follows: $\Delta = \left(d(-\pi, -\frac{\pi}{2} + \frac{2\pi}{L}) - d(-\pi, -\frac{\pi}{2} - \frac{2\pi}{L})\right) \times \frac{L}{2\pi}$.

For above small systems the discontinuity seems to persist for $V \lessapprox 2$, as we find δ is insensitive to the system size for $V \lessapprox 2$ and starts depending on the system size for larger values of V. Also, the derivative Δ should tend to a constant value as a function of L if there is no discontinuity. Which is clearly not the case in the above regime as demonstrated in Fig. (5.5). So there is a possibility of the discontinuity persisting in the thermodynamic limit for small values of V.

Properties of the triangles for different values of interaction

We study the properties of triangles with edges given by the distances, which are the fundamental geometric objects. There are three types of triangles in the system when we classify them according to the behaviour of the distances,

1. Triangles with all the vertices either inside the FS or outside it.

   In the large interaction limit these are equilateral triangles and with the decrease of interaction the edges start shrinking. Such triangles shrink to a point at $V = 0$, with all the edges being zero. This is illustrated in Fig. (5.7). Such triangles are $\left(\frac{L}{2}\right) C_3$ in number and we call these triangles "particle triangles".

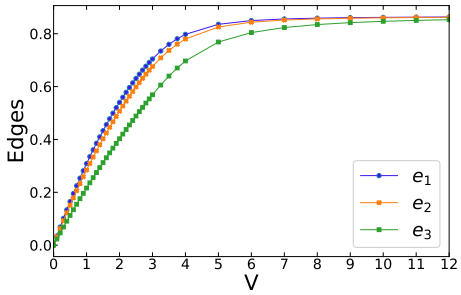

Figure 5.6: The edges $\{e_i\}, i = 1, 2, 3$, of the Particle Triangles as a function of interaction strength.

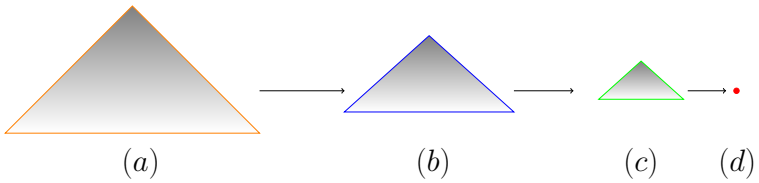

Figure 5.7: (Color online) $(a) - (c)$ Particle triangles for values of interaction strength $V = 4$ (a) (orange), $V = 2$ (b) (blue) and $V = 1$ (c) (green). $V = 0$ (d) (red) corresponds to a point.

2. Triangles with two vertices inside the FS and one outside and vice versa.

   Of the above $\frac{L}{2}(\frac{L}{2}(\frac{L}{2} - 1))$ triangles, we are excluding the triangles with edges $(i, i + \frac{L}{2})$ for now. In the large interaction limit these are equilateral triangles as well

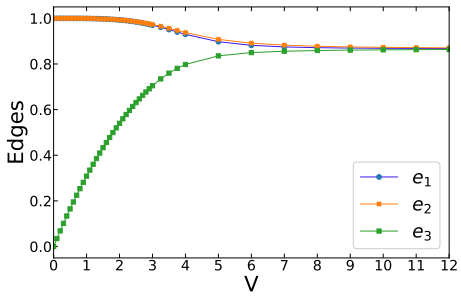

Figure 5.8: The edges $\{e_i\}, i = 1, 2, 3$, of the particle-hole triangles as a function of interaction strength.

and with the decrease of interaction one of the edges starts shrinking, while the remaining two expand. These triangles show the interesting behaviour that they become isosceles triangles at $V \sim 2$. Upon further decreasing the interaction, only one of the edge shrinks, and at $V = 0$ we have a segment. This is illustrated in

Fig. (5.9). We call such triangles “particle-hole triangles”.

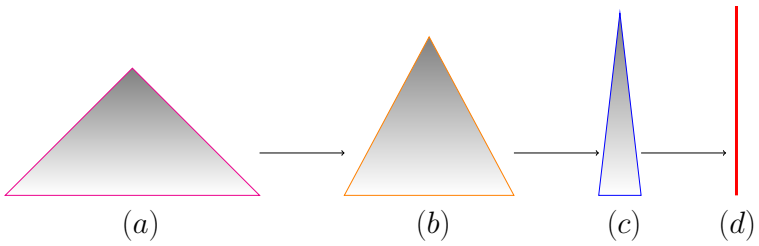

Figure 5.9: (Color online) $(a)-(c)$ Particle-hole triangles for values of interaction strength $V = 6$ (a) (purple), $V = 4$ (b) (orange) and $V = 2$ (c) (blue). $V = 0$ (d) (red) corresponds to a segment.

3. Triangles with the edge $(i, i + \frac{L}{2})$

   These traingles are also particle-hole triangles but only $\frac{L}{2} \times (L - 2)$ in number.

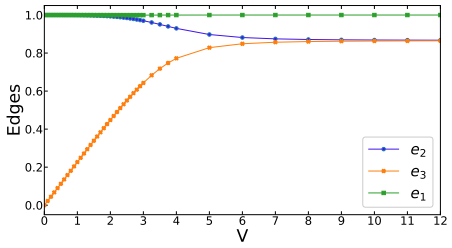

Figure 5.10: The edges $\{e_i\}, i = 1, 2, 3$, of the particle-hole triangles with the special edge $(i, i + \frac{L}{2})$ as a function of interaction strength. e_1 labels the constant edge $(i, i + \frac{L}{2})$.

They are isosceles triangles in the large interaction limit. One of the edges is independent of V, while one of the remaining two equal edges expands and the other one contracts as V decreases. It again becomes an isosceles triangle for $V \lesssim 2$, beyond which only one edge shrinks, and at $V = 0$ we have a segment like all other particle-hole triangles. This is illustrated in the Fig. (5.11).

Nearest neighbour distances

We inspect the distances between neighbouring points in the BZ, $(k, k + 1)$. The first question which comes to mind in the context of the nearest neighbour distances is: can

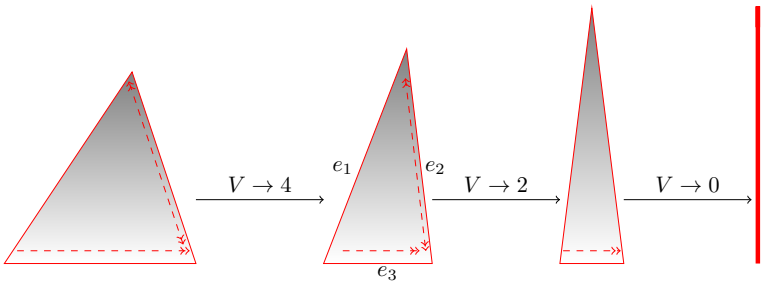

Figure 5.11: The particle-hole triangles with the edge $(i, i+\frac{L}{2}) \equiv e_1$, for different values of interactions. In the first and second figure the edge e_3 contracts and e_2 expands for $V \gtrsim 2$. After which, for $V < 2$, $e_1 = e_2$ and the isosceles triangle shrinks only by shrinking of edge e_3 and becomes a segment at $V = 0$.

we define an infinitesimal metric as discussed in the previous chapter (Eq. (3.8))?

If the distances between two quasi-momenta decrease monotonically with the separation between them, then we stand a chance. But this is hardly the case. As we already know, at $V = \infty$, almost all the points in the BZ are equidistant. The distance detween the quasi-momenta does not monotonically decrease with the BZ separation between them, even for a small value of V, as shown in Fig. (5.12). We find for the distances from a reference

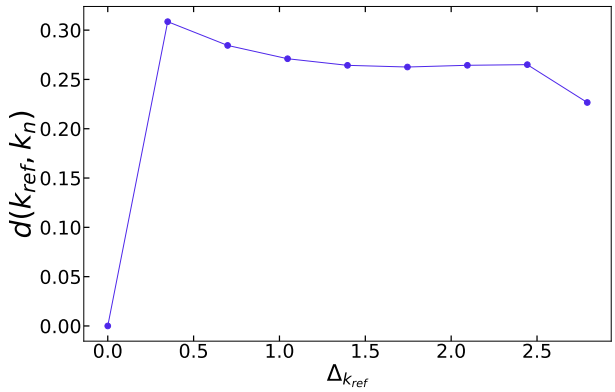

Figure 5.12: Distances between $k_{ref} = -\frac{\pi}{2}$ and other modes $k_n \in FS$, as a function of the seperation between them in the BZ, $\Delta_{k_{ref}} = k_n - k_{ref}$, for $V = 1$.

k mode $-\frac{\pi}{2}$ (k_{ref}), the distance from the closest k mode is infact having the optimum value even at a small interaction value, $V = 1$.

Thus the infinitesimal quantum metric $g(k)$, defined by $\lim_{\Delta k \to 0} d^2(k, k + \Delta k) = g(k)\Delta k^2$,

may not be well defined in this system.

Let us have a look at the behaviour of the nearest-neighbour distance $d(k_n, k_{n+1})$ for different V, which is shown in Fig. (5.13) over half the Brillioun zone. The value of n runs from 0 ($k_0 \equiv -\pi$) to $L-1$ ($k_{L-1} \equiv \pi - \frac{2\pi}{L}$) over the full BZ and we consider $k_L \equiv -\pi$.

The observations are,

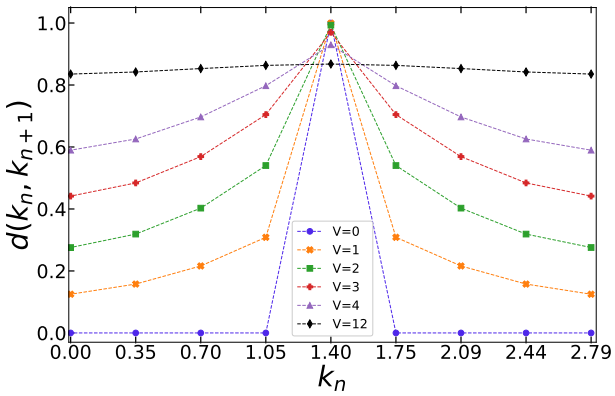

Figure 5.13: Nearest Neighbour Distance for different interaction strength V, over half the BZ.

1. $V = 0$, is characterised by is a delta function singularity at the Fermi point. All the nearest neighbour distances are zero except at the Fermi point, when one quasi-momentum is in the Fermi sea and its nearest neighbour is outside it, in which case it is equal to 1.

2. The above singularity seems to persist for low V, and slowly smoothens when V is increased at large V.

3. At $V = \infty$, all the nearest neighbour distances are equal and it can be seen that at $V = 12$ this is more or less true.

Representation on the unit circle

A pictorial representation on the unit circle constructed from the nearest neighbour distances turns out to be particularly insightful for demonstrating the clustering feature of the distances discussed in section 5.4.2.

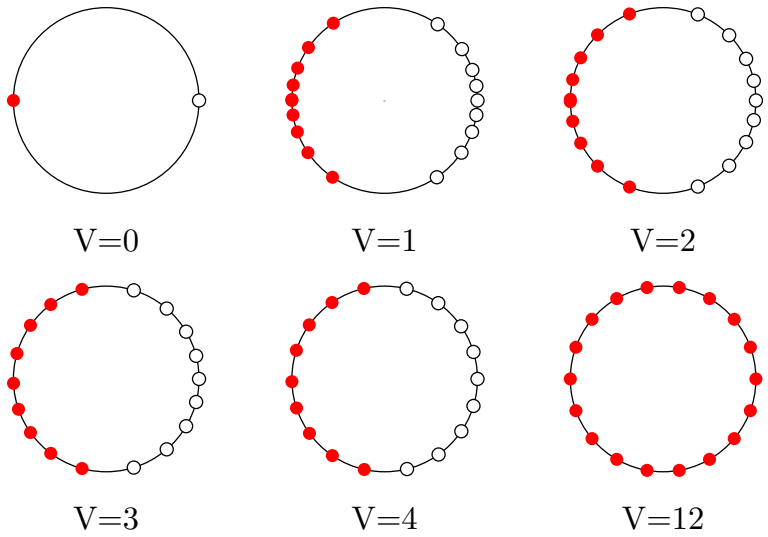

Figure 5.14: Schematic representations on the unit circle for different values of the interaction V. For each unit circle, in the first five cases, the small filled circles represent modes inside the Fermi sea and the small open circles correspond to modes outside the Fermi sea.

We begin with defining a radius, R, in terms of the sum of all the nearest neighbour distances, as follows:

$$2\pi R \equiv \sum_{i=0}^{L-1} d(k_i, k_{i+1}). \tag{5.25}$$

The radius attains the values $R = 1/\pi$ at $V = 0$ and $R = c(\alpha)L/(2\pi)$ at $V = \infty$.

Each nearest neighbour distance is represented by an angle,

$$\Delta\theta_{i,i+1} = \frac{d(k_i, k_{i+1})}{R}. \tag{5.26}$$

Finally, an angular representation is constructed for each quasi-momentum,

$$\theta_{k_i} = \sum_{j=0}^{i} \Delta\theta_{j-1,j} \tag{5.27}$$

where, $\Delta\theta_{-1,0} \equiv 0$.

The corresponding representation on the unit circle, is shown in Fig. (5.14). At $V = 0$, all the points collapse into $\theta = 0, \pi$, at small V, they spread out but the points in the Fermi sea and those outside it are well seperated. Illustrating the clustering of the points inside (or outside) the FS together. The separation starts closing for values of V between 2 and 3, and at $V \geq 4$ all points are equally spaced like the $V = \infty$ case and the separation is almost invisible. Thus the features of clustering is completely washed off.

5.4.4 Conclusions

Let us summarize the results we get from the heuristic study of the properties of the distances. We have applied exact diagonalization and looked at the quantum distances for a finite system which consequently does not show a sharp phase transition but only a crossover from the metallic to the insulating regime as an effect of the interaction V. The exact diagonalization was performed using standard sparse library in Python. It was performed to track only the first three states of the spectrum.

Our main observation is the clustering of points inside (or outside) the FS from the distances in the metallic regime which are either very small or close to 1. The distances show signals of sharp Fermi points as well. When increasing V the distances become homogenous and the above grouping is gone and discontinuities at the Fermi points are lost as well.

We have illustrated this behaviour in three ways.

- Analysis of distances from a fixed point, $k = -\pi$, to all the others showed jumps at the Fermi points at low V, which smoothen out slowly when increasing V, at large V.

- The triangles formed by the distances between three quasi momenta being fundamental geometrical objects, have been studied them in detail. The triangles are mostly equilateral with finite areas in the insulating regime. The area, however, falls rapidly in the metallic regime, leaving only points and segments at $V = 0$.

- Inspection of nearest-neighbour distances and constructing representations of the quasi-momenta modes on an unit circle has been quite insightful, with a nice pictorial demonstration of the clustering at small V and complete loss of it at large V.

In all the three cases we observe the crossover around $V = 2-4$. Since the metal-insulator transition occurs at the theoretical value $V = 2$[76], we conclude that the "clustering-declustering" feature that we observe in the distance matrix is indeed characterizing the metal-insulator crossover.

The transformation of the graph of the ground state, introduced in Sec. (5), as a function of the interaction is rather interesting.

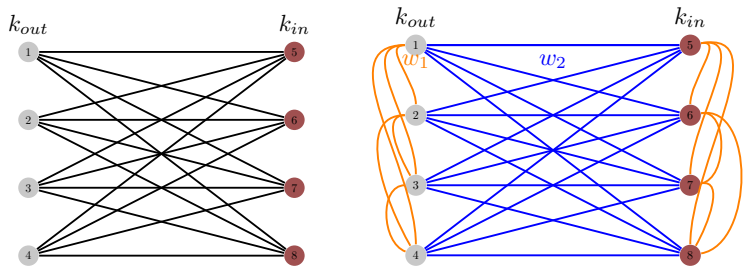

Figure 5.15: The schematic representation of the graph of ground state of the $t-V$ model at $V = 0$ (left) and $V \neq 0$ (right). The weight of the edges for vertices given by points inside (or outide) the FS is denoted by w_1 and the weight of the edges for one vertex inside the FS and one outside it is denoted by w_2. w_1 increase as a function of V, while w_2 decreases.

At $V = 0$, we have a bipartite graph with the points in the FS and outside the FS representing two group of vertices, which are disconnected amongst themselves but connected to each other. Immediately as the interaction is switched on, $V = 0^+$, the graph changes character and we have a completely connected graph. But the weights of the edges given by the distances are highly non-uniform resulting in the "clustering" of the vertices, while at large V the graph for the insulator is a complete graph with uniform connectivity or weights over all the edges. We will illustrate the efficiency of all the tools introduced in previous sections by applying them to the quantum distances of the $t - V$ model in upcoming chapters.

Chapter 6

Euclidean Embedding of the Distances

The study of the extrinsic geometry of the correlated many-body state involves the construction of vector configurations in Euclidean space, such that the vectors are separated from each other by distances prescribed by the matrix of quantum distances D (Eq. (5.1)). This brings us to the fascinating subject of distance geometry developed by mathematicians like Cayley[55], Menger[56], Bluementhal[57], Schoenberg[54] and Godel[77], which focuses on the study of geometry in terms of distances.

In the context of our work, it is interesting to understand the properties of the embedding: what is the dimension of the Euclidean space and what kind of vector configurations arise in our objective of realizing quantum distances?

A lot of researchers in other branches of science have asked similar questions. Seeking the vector configuration of points from a set of noisy or incomplete distances is a topic of active research[53]. Applications include finding $3D$ configurations of molecules from NMR data with particular success in finding the structure of proteins[78]. In the Wireless Sensor Network Localization problem (WSNL), the relative distance of sensor networks estimated by recording the power loss during a two-way exchange are used to find the positions of each sensor[79]. Multidimensional scaling, i.e., the problem of finding a set of vectors in smaller dimensions starting from a higher dimensional space, is popularly

used in data visualization[80].

Contrary to some of the popular applications listed above, the problem we have at hand is simpler, because we have the accurate and complete distance matrix D. If the distance matrix D can be an EDM, then it can be easily found by constructing the Gram matrix as per Eq. (6.10) and inspecting the eigenvalues, as a direct consequence of Schoenberg's theorem (1) discussed in Sec. (5.2). The dimension of the Euclidean space is given by the rank of the Gram matrix and the configuration of the point set in above Euclidean space is obtained by the spectral decomposition of the Gram matrix (Eq. (6.11)).

6.1 Embedding of mean field states

Before entering into the machinery of distance geometry, let us have a look at the Euclidean embedding of the distance matrices obtained from the mean-field states. For the mean field states our definition of the quantum distances reduces to the standard one in terms of overlap of the single particle wavefunctions, given by Eq. (3.8).

Let us first look at the choice $\alpha = 1$, in our definition of distances in Eq. (4.9), which gives the Hilbert-Schmidt distances for the mean field states. For a N-dimensional Hilbert space, $\mathcal{H}_N$, the matrix of Hilbert-Schmidt distances between two states $|\Psi_n\rangle$, $|\Psi_m\rangle \in \mathcal{H}_N$, is

$$(D(n,m))^2 = 1 - \mathrm{tr}\,(\rho_n \rho_m) \tag{6.1}$$

where $\rho_n \equiv |\Psi_n\rangle\langle\Psi_n|$. Let us consider the N^2 generators of $U(N)$: the identity operator I and the generators of SU(N): T^α, $\alpha = 1, \ldots, N^2 - 1$. The above generators satisfy the conditions

$$(T^\alpha)^\dagger = T^\alpha, \quad \mathrm{tr}\,(T^\alpha) = 0, \quad \frac{1}{2}\mathrm{tr}\left(T^\alpha T^\beta\right) = \delta^{\alpha\beta}. \tag{6.2}$$

We know that any linear Hermitian operator in $\mathcal{H}_N$ can be expressed as a linear combination of the generators of $U(N)$ in the fundamental representation. Then, ρ_n can then be

expressed as,

$$\rho_n = \frac{1}{N} + \vec{a}_n \cdot \vec{T}, \qquad a_n^\alpha = \frac{1}{2}\mathrm{tr}\,(T^\alpha \rho_n)\,. \tag{6.3}$$

The vector $\vec{a}$ in above equation is a real $N^2 - 1$ dimensional vector, i.e $\vec{a}_n \in \mathbb{R}^{(N^2-1)}$, since we know T^α and ρ_n are Hermitian matrices.

From the basic properties $\rho_n^2 = \rho_n$ and $\mathrm{tr}\,\rho_n = 1$,

$$\vec{a}_n \cdot \vec{a}_n = \frac{1}{2}\left(1 - \frac{1}{N}\right). \tag{6.4}$$

Equation (6.1) can be rewritten as

$$\begin{aligned} (D(n,m))^2 &= 1 - \frac{1}{N} - 2\vec{a}_n \cdot \vec{a}_m & (6.5)\\ &= |\vec{a}_n - \vec{a}_m|^2. & (6.6) \end{aligned}$$

Thus the Hilbert-Schmidt distance matrix of mean field states of systems with translational symmetry can be isometrically embedded in a finite dimensional Euclidean space, $\mathbb{R}^{(n_b^2-1)}$, for a n_b orbital model, irrespective of the system size.

Let us consider an arbitrary α in Eq. (4.9) in the definition of the distances. The distance between neighbouring points $\mathbf{k}$ and $\mathbf{k} + d\mathbf{k}$, in the limit $d\mathbf{k} \to 0$ is

$$\begin{aligned} (D_\alpha(\mathbf{k}, \mathbf{k} + d\mathbf{k}))^2 &= 1 - (\mathrm{tr}\rho(\mathbf{k})\rho(\mathbf{k} + d\mathbf{k}))^\alpha \\ &= 1 - \left(1 - |\vec{a}(\mathbf{k} + d\mathbf{k}) - \vec{a}(\mathbf{k})|^2\right)^\alpha . \end{aligned}$$

Assuming $\vec{a}(\mathbf{k})$ to be a smooth function of $\mathbf{k}$, because the wave functions $|\Psi(\mathbf{k})\rangle$ are themselves so, it holds that

$$\begin{aligned} (D_\alpha(\mathbf{k}, \mathbf{k} + d\mathbf{k}))^2 &= \alpha \frac{\partial \vec{a}(\mathbf{k})}{\partial k_\mu} \cdot \frac{\partial \vec{a}(\mathbf{k})}{\partial k_\nu}\, dk_\mu\, dk_\nu & (6.7)\\ &\equiv g_\alpha^{\mu\nu}(\mathbf{k})\, dk_\mu\, dk_\nu. & (6.8) \end{aligned}$$

This implies the distances between neigbouring points in the spectral parameters are just scaled by the factor α, in the thermodynamic limit,

$$g^{\mu\nu}_{\alpha}(\mathbf{k}) = \alpha g^{\mu\nu}_{1}(\mathbf{k}). \tag{6.9}$$

So we can conclude for $\alpha \neq 1$, although the Euclidean embedding in $(n_b^2 - 1)$ dimensional space obtained for $\alpha = 1$ will not be isometric, the shape of the embedded surface is independent of α up to a scaling factor.

6.2 Isometric Euclidean embedding

1. Construct the Gram matrix,

$$G = -\frac{1}{2}(I - \frac{1}{L^d}ee^T)D^2(I - \frac{1}{L^d}ee^T). \tag{6.10}$$

   I is the $L^d \times L^d$ identity matrix. e is a L^d-dimensional column vector with all entries equal to 1.

2. Check if it is positive semi definite (PSD) with only positive eigenvalues.

3. The rank of G, if it is PSD, corresponds to the dimension of the Euclidean space in which the distances can be embedded.

4. The configuration of the L^d embedded vectors $\{\mathbf{x}_i\}$ is obtained by diagonalization of the above real symmetric matrix G,

$$G(i, j) = \mathbf{x}_i.\mathbf{x}_j = (U\sqrt{\Lambda})(\sqrt{\Lambda}U^T). \tag{6.11}$$

Figure 6.1: Algorithm for isometric embedding of quantum distances.

The algorithm for isometric embedding of the matrix of quantum distances D is rather simple and a direct consequence of the Schoenberg's theorem (1), proposed by Isaac Schoenberg in 1935[54]. It has been detailed in Fig. (6.1). The volume of N simplices as obtained from the Cayley-Menger determinant Δ, which is constructed from the distance

matrix as follows[55, 56],

$$\Delta = Det(C_D), \tag{6.12}$$

$$C_D = \begin{bmatrix} 0 & 1 & 1 & .. & 1 \\ 1 & 0 & D_{1,2} & .. & D_{1,N} \\ \vdots & & & & \\ 1 & D_{N,1} & D_{N,2} & .. & 0 \end{bmatrix} \tag{6.13}$$

$$V_N^2 = \frac{(-1)^{N-1}}{2^N (N!)^2} \Delta, \tag{6.14}$$

should reflect the same result.

If the dimension of Euclidean embedding is obtained to be r, which is the rank of the G matrix, we should find the volume of all N simplices for $N \leq r+1$ should be nonzero and higher order simplices should be zero, as per Bluementhal's theorem (2)[57].

6.2.1 Isometric embedding of the distance matrix of $t-V$ model

We apply the above scheme to the $L \times L$ matrix of quantum distances of the half filled one-dimensional $t-V$ model, for different values of interaction V, discussed in Sec. (5.4.2). We look at the three cases, $V=0$, $V=\infty$, and $0<V<\infty$ in this section.

$V = 0$. At $V=0$, the ground state is a mean field state (the Fermi sea) with all the single particle states with energies less than zero occupied and those with energies greater than zero unoccupied. The quasi-momenta corresponding to the occupied single particle states we label as k_{in} and those for the unoccupied single particle states by k_{out}.

The distance matrix, D_{FS} obtained in Eq. (5.22) has the following form,

$$D_{FS}(k_{in}, k_{in}) = 0 = D_{FS}(k_{out}, k_{out}) \tag{6.15}$$

$$D_{FS}(k_{in}, k_{out}) = 1 = D_{FS}(k_{out}, k_{in}). \tag{6.16}$$

The Gram matrix has only one non-zero eigenvalue, $\lambda = \frac{L}{4}$ and the distance matrix can be embedded in a one dimensional Euclidean space,

$$x(k_{in}) = -0.5, \qquad x(k_{out}) = 0.5. \tag{6.17}$$

$V = \infty$**.** The matrix of the squared distances, D^2_{CDW}, using Eq. (5.24) can be written as:

$$D^2_{CDW} = \frac{3}{4}\begin{pmatrix} \mathcal{I} - I & \mathcal{I} - I \\ \mathcal{I} - I & \mathcal{I} - I \end{pmatrix} + \begin{pmatrix} 0 & I \\ I & 0 \end{pmatrix}. \tag{6.18}$$

$\mathcal{I}$ is a $N \times N$ matrix ($N = \frac{L}{2}$) with all entries equal to 1, I is the identity matrix and e is defined below equation(6.10) and $ee^T = \mathcal{I}$. The Gram matrix defined in equation(6.10) is,

$$G_{CDW} = -\frac{1}{2} A D^2_{CDW} A \tag{6.19}$$

$$A \equiv \begin{pmatrix} I & 0 \\ 0 & I \end{pmatrix} - \frac{1}{L}\begin{pmatrix} \mathcal{I} & \mathcal{I} \\ \mathcal{I} & \mathcal{I} \end{pmatrix}. \tag{6.20}$$

We find that,

$$\left[A, D^2_{CDW}\right] = 0 \;\Rightarrow\; [A, G_{CDW}] = 0 \tag{6.21}$$

Thus, A and G_{CDW} have the same eigenvectors.

Let us define a complete, orthonormal set of $\frac{L}{2}$ dimensional column vectors a^μ, $\mu = 1...\frac{L}{2}$, where $a^1 = \sqrt{\frac{2}{L}}(1, 1, \ldots, 1)^T$. A complete set of L dimensional orthonormal vectors is

then defined as follows,

$$b^i = \begin{cases} \frac{1}{\sqrt{2}} \begin{pmatrix} a^i \\ a^i \end{pmatrix} & i = 1, \ldots, \frac{L}{2} \\ \frac{1}{\sqrt{2}} \begin{pmatrix} a^{i-L/2} \\ -a^{i-L/2} \end{pmatrix} & i = \frac{L}{2}+1, \ldots, L. \end{cases} . \tag{6.22}$$

Therefore,

$$G_{CDW} b^1 = 0 \tag{6.23}$$

$$G_{CDW} b^i = \begin{cases} \frac{1}{4} b^i & i = 2, \ldots, \frac{L}{2} \\ \frac{1}{2} b^i & i = \frac{L}{2}+1, \ldots, L \end{cases} . \tag{6.24}$$

Thus,

$$(G_{CDW})_{ij} = \sum_{k=2}^{L/2} \frac{1}{4} b_i^k b_j^k + \sum_{k=L/2+1}^{L} \frac{1}{2} b_i^k b_j^k. \tag{6.25}$$

Thus the explicit solution for the embedding is found to be the L, $(L-1)$-dimensional vectors, $x_i,\ i = 1, \ldots, L$, with components, $(x_i)^n\ ,\ n = 1, \ldots, L-1$, given by

$$(x_i)^n = \frac{1}{2} b_i^{n+1}, \quad n = 1, \ldots, \frac{L}{2} - 1 \tag{6.26}$$

$$= \frac{1}{\sqrt{2}} b_i^{n+1}, \ \ n = \frac{L}{2}, \ldots, (L-1). \tag{6.27}$$

The distance matrix at $V = \infty$, can be isometrically embedded in a Euclidean space with dimension equal to $L - 1$.

$0 < V < \infty$**.** We have obtained the numerical distance matrix applying exact diagonalization for system sizes $L \leq 18$ and interaction values, $V = 0 - 12$. Applying the above scheme we find, as soon as the interaction is turned on, the exact rank of the Gram matrix

becomes thermodynamically large, i.e $L-1$ and remains so till $V = 12$. The result in the CDW limit suggests for the insulating phase the dimension of Euclidean embedding is indeed scaling as system size. But for smaller values of V this is counterintuitive.

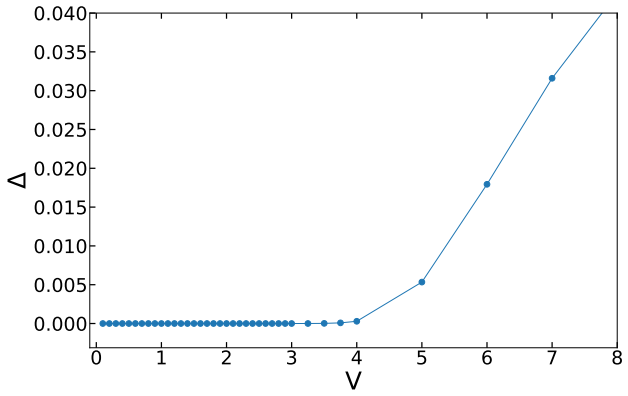

Figure 6.2: Volume of the L simplex as a function of the interaction, for 18 sites.

For small values of V, the state is not very different from the mean field state although we know that as soon as interactions are turned on, the system goes from a Fermi liquid to a Luttinger liquid. The state, though qualitatively different, still remains metallic till $V/t = 2$. Besides, we also find that the spectrum of the Gram matrix does not drastically change, the largest eigenvalue shifts very little from the previous value $\frac{L}{4}$ (at $V = 0$) and most of the smaller eigenvalues are insignificant. We look at the volume of the L simplex, in Fig. (6.2) and find that it remains very small in the metallic regime, although the exact rank is $L-1$, suggesting the effective embedding still has a lower dimensionality.

It is thus natural to ask whether the distance matrix can still be approximately embedded in a finite-dimensional Euclidean space in some precise sense, in the metallic regime.

In a more general context, we would like to visualize the embedding in lower dimensional spaces and associate "shapes" and surfaces to the distances obtained from the correlated state, for a characterisation of the extrinsic geometry. Thus even if the embedding dimension scales with the system size, if an approximate embedding scheme exists we can do

so.

There are several methods for approximate embedding of a distance matrix in a Euclidean space [58, 59, 60, 61, 62], two of which we investigate in next section.

6.3 Approximate Euclidean Embedding

We seek approximate embedding of the quantum distances into a smaller dimensional $(1-3)$ Euclidean space where visualisation of the vectors is possible. The cost that we pay is that the embedding is no longer isometric. But there are well defined concepts of quantitative estimation of the accuracy of such approximations. We consider two such approaches, the first being the truncation of the spectrum of the Gram matrix with an estimate of error[61, 62] and the second being the method of average distortion[59, 60].

6.3.1 Truncation of Gram matrix spectrum with error estimate

The effective rank of the numerical Gram matrix is very difficult to determine, because the effective zeros also manifest in the spectrum as small numerical values.
So the precise question we are asking is, how many eigenvalues from the Gram matrix spectrum we should retain or how many eigenvalues could we safely discard?

Similar questions are asked by people in data mining[61, 62] where for dimensionality reduction of huge dataset, they look into Prinicipal Component Analysis and discard the smaller eigenvalues of the covariance matrix with an error estimate or for data mining applications where people use truncated Singular Value Decomposition. We extend the most common method used in above applications, retain the first few largest singular values or eigenvalues and estimate the corresponding squared error from the ratio of the sum of the eigenvalues to the total sum of eigenvalues. Then we keep as many eigenvalues such that this error remains within a threshold value of $10\% - 20\%$.

The diagonalisation of the Gram matrix, which is a real symmetric $L^d \times L^d$ matrix, gives

$$G = U\Lambda U^T \tag{6.28}$$

where U is an orthogonal matrix and Λ a diagonal matrix. We choose a basis obtained by arranging the eigenvalues in the order of their magnitude, $\Lambda_{11} \geq \Lambda_{22} \geq \cdots \geq \Lambda_{L^d L^d}$.

Retaining only the highest q diagonal entries we obtain an approximate Gram matrix in the diagonal basis, $\tilde{\Lambda}$, where $\tilde{\Lambda}_{ii} = \Lambda_{ii},\ i \leq q$, $\tilde{\Lambda}_{ii} = 0, i > q$. The approximate Gram matrix $\tilde{G}$ with rank q will be,

$$\tilde{G} \equiv U\tilde{\Lambda}U^T. \tag{6.29}$$

We define the corresponding truncation error as,

$$E(q) = 1 - \sqrt{\frac{\sum_{i=1}^{q} \Lambda_{ii}}{\sum_{k=1}^{L^d} \Lambda_{kk}}}. \tag{6.30}$$

Let us now demonstrate the method with the $t - V$ model,

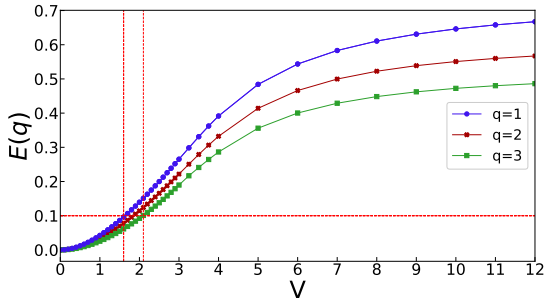

Figure 6.3: Truncation error for keeping first few (1-3) eigenvalues of G. The error for approximate embedding is less than 12% in case of embedding in one dimension $E(q = 1)$ up to $V \approx 1.5$ and for embedding in three dimension $E(q = 3)$ up to $V \approx 2$.

Fig. (6.3) clearly shows that the truncation error for retaining first few largest eigenvalues ($1 \leq q \leq 3$) is quite small, less than 12%, for $V < 2$. So an approximate embedding into smaller dimensions is indeed possible in the metallic phase. However, for $V > 2$ such

an approximation will be highly inaccurate as indicated by the error estimate. So in the insulating phase the dimension of even the approximate embedding is definitely greater than 3.

6.3.2 Average distortion

The next method of approximate embedding we follow, is that of average distortion.

The concept of distortion originated in theoretical computer science in the context of metric embedding, or defining a map from a metric space (K, d) to another simpler host metric space (H, ∂), $f : K \to H$, where the faithfulness of the embedding is measured by the distortion[58]. The distortion ϵ is an estimate of how close the distances between points in (H, ∂) resemble that in (K, d), and is defined as[59],

$$\epsilon = max_{x,y\in K} \frac{d(x, y)}{\partial(x, y)}. \tag{6.31}$$

Another global estimate of accuracy is the average distortion ϵ_{avg}, defined as follows[59, 60],

$$\epsilon_{avg} = \frac{\sum_{x,y\in K} d(x, y)}{\sum_{x,y\in K} \partial(x, y)}. \tag{6.32}$$

Let us begin with the set of L^d vectors in r dimensions (rank of G), $\{\mathbf{x_i}\}$ $(i = 1, \ldots, L^d)$, $\mathbf{x_i} \in \mathbb{R}^{(r)}$, obtained from isometric Euclidean embedding by diagonalising the Gram matrix.

We choose q of the basis vectors and look at each of the $(L^d - 1)C_q$, q-dimensional subspaces. Let $\tilde{D}(i, j)$ be the corresponding new distances in the q dimensional Euclidean space. The average distortion for each case is given by,

$$\epsilon_{avg} \equiv \frac{\sum_{i,j} D(i, j)}{\sum_{i,j} \tilde{D}(i, j)}. \tag{6.33}$$

We compute the average distortion in each case and pick the subspace that minimizes it.

We label the above minimum value of average distortion as ϵ_{min}. Lower values of average distortion could perhaps be obtained by rotating the basis set. In our application to the distance matrices of the $t-V$ model we have however considered only the choice of q of the basis vectors.

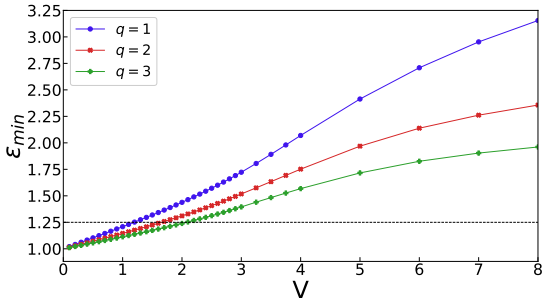

Figure 6.4: Average distortion for approximate embedding of D in lower dimensions as a function of interaction strength.

The average distortion as a function of interaction strength for $q = 1, 2, 3$ is plotted in Fig. (6.4). We find embedding with values of average distortion very close to the ideal value one is possible only for small values of interaction, $V \ll 2$. The maximum average distortion allowed corresponding to the upper bound of error 0.12 in region $V \lesssim 2$ is found to be 1.27. In the insulating phase approximate embedding in lower dimensions is not possible as indicated by the high values of average distortion.

Chapter 7

Wasserstein Distances

The geometry of the many-body state can also be studied by constructing probability distributions from the quantum distances. The central technique of our choice is the powerful theory of optimal transport[63, 64]: it is used to construct geometric observables from the distance distributions. In general, optimal transport theory gives us the necessary tools to perform a thorough analysis of the geometry of the distance distributions. In particular, it provides us with a new metric called the Wasserstein distance, which is essentially a measure of distance between probability distributions.

In this chapter we focus on the Wasserstein distances which are found to be particularly successful in capturing the phases of the many-body state. Using these distances, we obtain a very sharp characterisation of the phases of the ground state. Moreover they are interesting in our context because they are obtained by averaging over the full spectral parameter space.

7.1 Theory of Optimal Transport

The theory of optimal transport traces back its origin to the transportation problem proposed by Monge in 1781[81], where a collection of particles, distributed with a certain density, needs to be moved, such that they arrange according to a new distribution, with a given new density. The movement has to be so chosen that the average displacement is minimized. This problem remained unsolved for a vast stretch of time untill it could be cast into a nice linear form after relaxations introduced by Kantorovich in 1942[82]. He suggested for each point in the source distribution instead of defining a one-to-one map to a point in the target distribution more general movements are possible from one point in the source to multiple points in the target distribution. A general cost function is considered and the average cost of transportation is minimized rather than the average displacement, giving the following tranportation problem.

For two distributions m_i and m_j, the minimum tranportation cost $C(m_i, m_j)$ is defined as

$$C(m_i, m_j) \equiv \inf_{\pi} \sum_{k,l} c(k,l)\, \pi_{ij}(k,l), \tag{7.1}$$

where k, l in the above sum runs over the domain of the distributions, and $\pi_{ij}(k,l)$ are transportation plans which transform distribution m_i to m_j and satisfy the following constraints:

$$\sum_{l} \pi_{ij}(k,l) = m_i(k), \quad \sum_{k} \pi_{ij}(k,l) = m_j(l). \tag{7.2}$$

The central concept of above transport problem involves finding an optimal transportation plan $\pi^*_{ij}(k,l)$ such that the sum defined on the RHS of Eq. 7.1 is minimum. The transportation problem is thus a linear optimization problem under linear constraints, since the above equations are linear in $\pi_{ij}(k,l)$. Even though the duality thoery (and the corresponding dual problem) is important, we will focus on the primal problem.

7.1.1 Basic definitions

1. We construct the normalised distribution of distances m_i, from the distance matrix D as follows,
$$m_i(j) = \frac{D(i,j)}{\sum_k D(i,k)} \tag{7.3}$$

2. The system of equations (7.9-7.10) is casted as a linear programming problem:
$$W^{(p)}(i,j) = \inf_{\Pi \geq 0} \left(\tilde{D}^T \Pi\right) \tag{7.4}$$
$$A^T \Pi = \eta. \tag{7.5}$$
Where $\tilde{D}$ is a L^{2d} component column matrix defined as follows:
$$\tilde{D} = ((\tilde{d}(1,1))^p, ...(\tilde{d}(1,L^d))^p, (\tilde{d}(2,1))^p, \ldots (\tilde{d}(L^d,1))^p, ...(\tilde{d}(L^d,L^d))^p)^T, \tag{7.6}$$
Π is a L^{2d} component column matrix and η is a $2L^d$ component column matrix constructed from the two distributions m_i and m_j,
$$\eta = (m_i(1), ...m_i(L^d), m_j(1), ...m_j(L^d))^T. \tag{7.7}$$
$$A^T = \left\{\begin{array}{cccc|cccc|c|cccc} 1 & 1 & ... & 1 & 0 & 0 & ... & 0 & ... & 0 & 0 & ... & 0 \\ 0 & 0 & ... & 0 & 1 & 1 & ... & 1 & ... & 0 & 0 & ... & 0 \\ \vdots & \vdots & .. & \vdots & \vdots & \vdots & .. & \vdots & ... & \vdots & \vdots & .. & \vdots \\ 0 & 0 & ... & 0 & 0 & 0 & ... & 0 & ... & 1 & 1 & ... & 1 \\ \hline 1 & 0 & ... & 0 & 1 & 0 & ... & 0 & ... & 1 & 0 & ... & 0 \\ 0 & 1 & ... & 0 & 0 & 1 & ... & 0 & ... & 0 & 1 & ... & 0 \\ \vdots & \vdots & .. & \vdots & \vdots & \vdots & .. & \vdots & ... & \vdots & \vdots & .. & \vdots \\ 0 & 0 & ... & 1 & 0 & 0 & ... & 1 & ... & 0 & 0 & ... & 1 \end{array}\right\} \tag{7.8}$$
A^T is a $(2L^d \times L^{2d})$ matrix.

Figure 7.1: Algorithm for computation of the Wasserstein distance starting from the matrix of quantum distances D

Let us return back to the probability distributions and review the definition of the Wasserstein distances introduced in Sec. (5.3.2).

The pth Wasserstein distance between two probability distribution functions (PDFs) m_i and m_j, $W_p(m_i, m_j)$, is defined as follows:

$$W_p^{(p)}(m_i, m_j) \equiv \inf_{\pi} \sum_{k,l} (\tilde{d}(k,l))^p \pi_{ij}(k,l), \tag{7.9}$$

where k, l in the above sum runs over the domain of the PDFS, $p \in [1, \infty)$ and $\pi_{ij}(k,l)$ is joint probability distribution whose marginals are m_i and m_j,

$$\sum_l \pi_{ij}(k,l) = m_i(k), \quad \sum_k \pi_{ij}(k,l) = m_j(l). \tag{7.10}$$

The pth root of the above optimised function $W_p^{(p)}(m_i, m_j)$ satisfies all the axioms of a distance function only when $\tilde{d}(k,l)$ is a valid distance function and satisfies all the properties of a metric.

The underlying theory of optimal transport and the Wasserstein distances are widely used in solution of partial differential equations, fluid mechanics, proability theory, statistics and discrete differential geometry. The fields of application include image retrieval[83], computer vision[84], economics and finance[85], to name some.

For our problem in quantum geometry, m_i and m_j are the distance distributions defined in Eq. (5.8) of Sec. (5.3.1) in Chapter 5, at any two points k_i and k_j in the space of spectral parameter.

While $\tilde{d}(k,l)$ can be any valid distance defined between the points in the spectral parameter space, we have studied the quantum distances and the Euclidean distances (detailed later). Choosing $p = 2$ in Eq. 7.9, we have looked at squared 2-Wasserstein distances, $W^{(2)}(m_i, m_j)$, between any two PDFs m_i and m_j, defined as follows,

$$W^{(2)}(m_i, m_j) \equiv \inf_{\pi} \sum_{k,l} (\tilde{d}(k,l))^2 \pi_{ij}(k,l). \tag{7.11}$$

Here π_{ij} satisfies the constraints given by Eq. (7.10).

The corresponding squared Wasserstein distance between the distance distributions, given by the above sum in Eq. (7.11) then gives the weighted average of all the squared distances between any two points in the spectral parameter space, with the corresponding weights

specified by the optimal joint probability distribution π^*_{ij}. We discuss them in more detail alongwith the results obtained in the $t-V$ model in Sections 7.2 and 7.3.

The Ollivier-Ricci curvature which is a generalization of the Ricci curvature in a discrete setting is closely related to the 1-Wasserstein distance, $W(m_i, m_j)$, corresponding to the choice $p = 1$ in Eq. (7.9) and the distance function $\tilde{d}(k, l)$ being the quantum distances,

$$W(m_i, m_j) \equiv \inf_{\pi} \sum_{kl} D(k, l)\pi_{ij}(k, l). \tag{7.12}$$

We will discuss this in great detail in Chapter 9. We look at the Euclidean embedding of the Wasserstein distance $W(m_i, m_j)$ in Section 7.4.

7.2 Wasserstein distances defined from the quantum distances

We define squared Wasserstein distances between two distance distributions m_i and m_j by choosing the distance function in the spectral parameter space, $\tilde{d}(i, j)$, in the RHS of Eq. (7.11) to be the quantum distances.

$$W^{(2)}(m_i, m_j) \equiv \inf_{\pi} \sum_{k,l=1}^{L^d} (D(k, l))^2 \pi_{ij}(k, l). \tag{7.13}$$

Where π_{ij} satisfies the usual constraints given by Eq. 7.10.

7.2.1 Physical Interpretation

In our study of quantum geometry of many-fermion states, the kinematics of the state is being studied and hence there is no time evolution and no concept of “transport" exists.

So physically what does the Wasserstein distance mean for us?

Since our definition is derived completely from the quantum distances in Eq. (7.13), we can attempt to answer the above question by looking into physical interpretation of the Wasserstein distances in terms of quantities in the Hilbert space.

The matrix of squared distances defined in equation (4.9) can be written as,

$$(D(i,j))^2 \equiv 1 - \mathrm{Tr}\,(\rho(i,j)\rho_0\,) \tag{7.14}$$

$$\rho_0 \equiv |\psi\rangle\langle\psi| \tag{7.15}$$

$$\rho(i,j) \equiv E(i,j)|\psi\rangle\langle\psi|E(i,j) \tag{7.16}$$

We call the subspace spanned by the states $E(i,j)|\psi\rangle \equiv |i,j\rangle$ as quantum distance Hilbert space, QDH, since the distance matrix is defined in this subspace. It includes the many-body state under inspection trivially, because $E(i,i)|\psi\rangle \equiv |\psi\rangle$.

Let $\pi^*_{ij}(k,l)$ denote the optimal joint probability distribution function, for a set of distributions m_i and m_j obtained by minimising the sum defined on the RHS of Eq. 7.13. We define mixed states, $\rho'(i,j)$ in QDH by,

$$\rho'(i,j) \equiv \sum_{k,l} \pi^*_{ij}(k,l)|k,l\rangle\langle k,l|. \tag{7.17}$$

Eq. 7.13 can then be rewritten as,

$$W^{(2)}(m_i,m_j) = 1 - Tr(\rho_0\rho'). \tag{7.18}$$

The squared Wasserstein distance, $W^{(2)}(m_i,m_j)$, can thus be expressed in terms of quantities in the QDH.

7.2.2 Results for the t-V model

The Wasserstein distance defined above, compares a set of distance distributions quantitatively and gives the distance between any two distributions. We will illustrate the efficiency of the Wasserstein distances in characterising the phases of the many-body state by application to the one-dimensional $t - V$ model. In this section we discuss the results we get from analytic calculations at the extreme interaction limit and the linear programming solutions for the intermediate values of V. But first, let us inspect the distance distributions for the $t - V$ model, because they are the fundamental object of study in optimal transport theory.

The distance distribution functions

The quantum distances between two points in the BZ in one band models calculated using Eq. (4.33), can be qualitatively thought of as a measure of the difference in the occupancies at these two quasi-momenta. Maintaining consistency with above idea, our numerical results for the one dimensional $t-V$ model (Sec. (5.4.2)) showed that deep in the metallic regime ($V \ll 1$), the distances classify the quasi momenta inside the Fermi sea, which we labelled k_{in}, and those outside it, which we labelled k_{out} into two different categories. The distances between any two points both inside or outside the Fermi sea are very small (~ 0) and those between two points, where one lies inside the Fermi sea and the other outside it, are very large (1).
On the other hand, deep in the insulating regime ($V \gg 1$), the distances are rather homogenous and there is not much distinction between quasi-momenta in the Fermi sea and those outside it.

The above behaviour can be well demonstrated by the probability distributions $\{m_i(j)\}$, defined at each point in the BZ, $i = 1, \ldots, L$, constructed from normalised distribution of distances of all the points in the BZ from the above point k_i, defined as per Eq. (7.3).

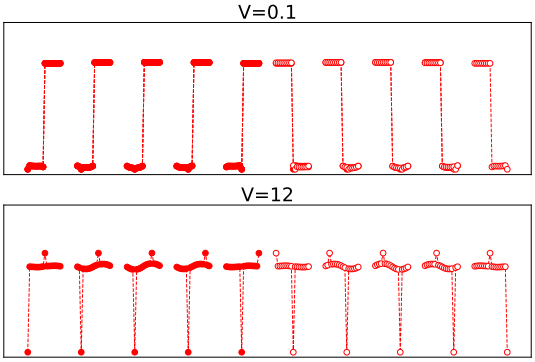

Figure 7.2: Schematic figure depicting the distribution functions, $m_i(j)$ $(i, j = 1, ..., L)$, defined at each point in the BZ for the two regimes of interaction, for 18 sites. The first five distributions depicted with filled circles represent distribution functions at alternate points for quasi-momenta modes inside the Fermi sea, $m_{k_{in}}$. While the remaining five depicted using unshaded circles represent distributions for quasi momenta modes outside it, $m_{k_{out}}$. In deep metallic regime, at $V = 0.1$, the first five distributions are completely opposite of the next five. However, for deep insulating regime, at $V = 12$, m_i are almost identical for all $k_i \in k_{in}, k_{out}$, differing only at points $i, i + \frac{L}{2}$.

The distance distributions $\{m_i(j)\}$ are completely opposite of each other for points inside the Fermi sea and points outside it and exactly identical for all points inside (or outside) the Fermi sea in the deep metallic regime. In sharp contrast to this, in the deep insulating regime, the distribution for every point in the BZ are almost identical, differing only at the points $(i, i + \frac{L}{2})$. This is illustrated in the Fig. (7.2).

Squared Wasserstein distances

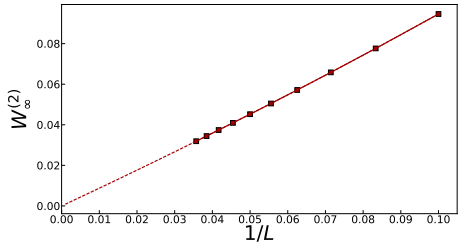

Figure 7.3: $W_\infty^{(2)}$ as a function of the inverse system size L^{-1} for system sizes $L = 10 - 28$. It is found to be linear in L^{-1} and thus vanishes in the thermodynamic limit.

Starting from the analytical quantum distances (Eqs. (5.22,5.24)), at extreme values of the

interaction, which we label as $D_{0/\infty}(i, j)$, the corresponding squared Wasserstein distances which we denote as $W^{(2)}_{0/\infty}(m_i, m_j)$, can be shown to be (calculations in Appendix),

$$\begin{aligned} W^{(2)}_0(m_i, m_j) &= (D_0(i, j))^2 \\ W^{(2)}_\infty(m_i, m_j) &= \frac{1}{\mathcal{L}}(D_\infty(i, j))^2, \end{aligned} \tag{7.19}$$

where $\mathcal{L} = \frac{\sqrt{3}}{2}(L - 2) + 1$.

Thus, calculations indicate the Wasserstein distances become zero in insulating phase in the thermodynamic limit. While, $W^{(2)}(m_{k_{in}}, m_{k_{out}})$, will most probably be large and non-zero in the metallic limit.

We further compute the Wasserstein distances numerically at $V = \infty$, choosing the distance distributions as obtained from the analytical distance matrices (Eq. 5.24) as marginals, for system sizes $L = 10 - 28$. We have studied the corresponding uniform squared distances, $W^{(2)}_\infty$, as a function of the inverse of system size in Fig. (7.3) and found it is linear in L^{-1}, and thus consistent with Eq. 7.19.

The numerical $W^{(2)}$ matrices obtained for interaction values $0 < V \leq 12$ are shown in Fig. (7.4).

In deep metallic regime, as one would expect, the matrices have a block structure. Wasserstein distances $W^{(2)}(m_{k_{in}}, m_{k_{in}})$ (or $W^{(2)}(m_{k_{out}}, m_{k_{out}})$) are very small ($\sim 0$), where both the marginals are ditributions defined at points inside (or outside) the FS, reflecting the fact that the distance distributions are almost identical.

While for the Wasserstein distances, $W^{(2)}(m_{k_{in}}, m_{k_{out}})$, where one of the marginal corresponds to the distribution defined at points inside the FS, k_{in} and the other one corresponds to the distribution defined at points outside the FS, k_{out}, are very large (~ 1), as a reflection of the fact that the distributions are completely opposite to each other.

On the contrary, in deep insulating regime the distance distributions are homogenous and almost identical so the Wasserstein distances are uniform and almost zero.

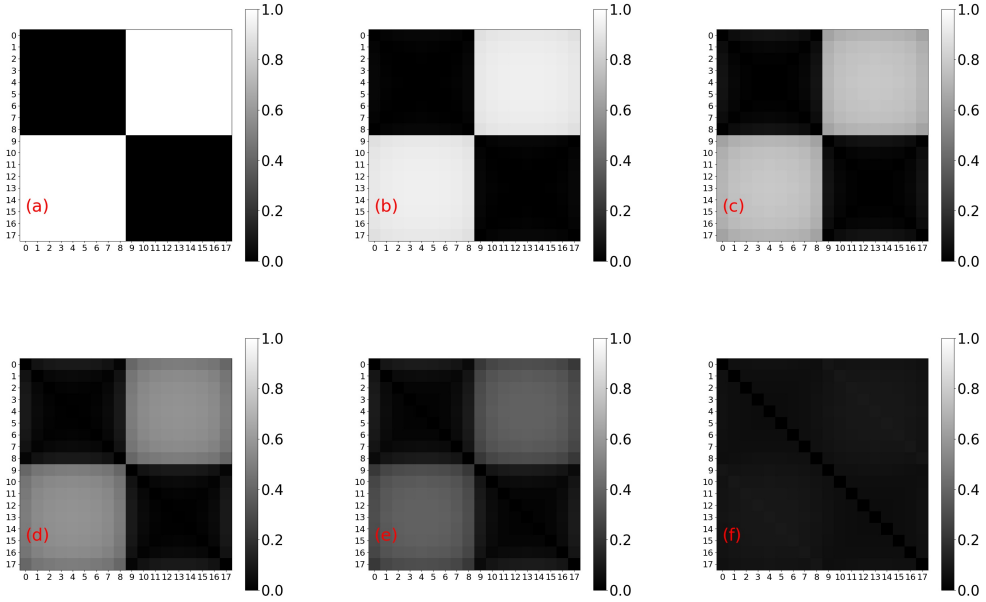

Figure 7.4: (a)-(f)Squared Wasserstein Distance matrices $W^{(2)}(m_i, m_j)$ for $L = 18$, obtained from numerical computation for interaction strengths $V = 0.1$ (a), $V = 1$ (b), $V = 2$ (c), $V = 3$ (d), $V = 4$ (e) and $V = 12$ (f). For $i < 9$, the quasi momenta modes lie inside the Fermi sea, $k_i \in k_{in}$ and for $i \geq 9$, the quasi-momenta modes lie outside it, $k_i \in k_{out}$. The deep metallic regime is characterised by $\sim 0, \sim 1$ distance values between $k_{in} - k_{in}$ ($k_{out} - k_{out}$) and $k_{in} - k_{out}$ blocks respectively. The deep insulating regime is characterised by uniform extremely small values very close to zero.

The converged optimal joint probability distribution, π^*, obtained from linear programming solutions in the metallic and insulating regime for the two different types of transport, where one of the marginal is $m_{k_{in}}$ and the other one is $m_{k_{out}}$, and where both the marginals are $m_{k_{in}}$, are shown in Fig. (7.5).

The behaviour of the distances $W^{(2)}(m_{k_{in}}, m_{k_{in}})$ as a function of the interaction strength V for different system sizes is shown in Fig. (7.6). We can expect $W^{(2)}(m_{k_{in}}, m_{k_{in}})$ to indicate the critical interaction strength for the Luttinger liquid to CDW transition, by the occurence of a peak in the thermodynamic limit.

The behaviour of the distances $W^{(2)}(m_{k_{in}}, m_{k_{out}})$ as a function of the interaction strength V, for different system sizes is shown in Fig. (7.7).

From the above figures we can conjecture in the thermodynamic limit, for $V \gtrsim 4$, in the

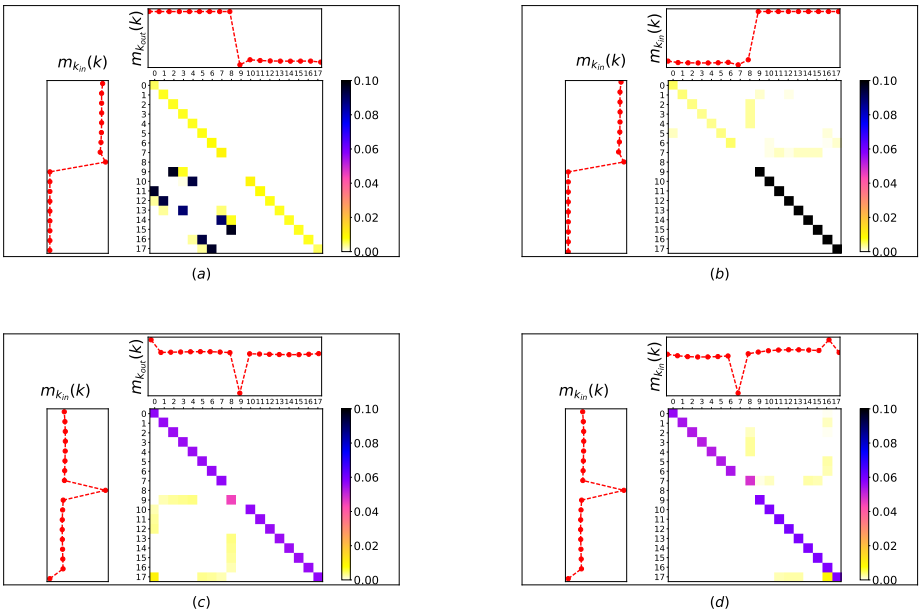

Figure 7.5: (a)-(d) The converged optimal joint probability distribution π^*_{ij}, for $L = 18$, obtained from numerical linear programming for interaction strengths $V = 1$, $i \in k_{in}$, $j \in k_{out}$ (a), $V = 1$, $i \in k_{in}$, $j \in k_{in}$ (b), $V = 8$, $i \in k_{in}$, $j \in k_{out}$ (c) and $V = 8$, $i \in k_{in}$, $j \in k_{in}$ (d). The marginals are plotted along the corresponding axis. In the insulating regime the matrix is rather sparse differing only at $i, j, i + \frac{L}{2}$ *and* $j + \frac{L}{2}$ in Figs. (c,d), in the metallic regime, $\pi^*_{k_{in},k_{in}}$ is relatively sparse in Fig. (b), but $\pi^*_{k_{in},k_{out}}$ in Fig. (a) is quite different with matrix elements having significantly larger values.

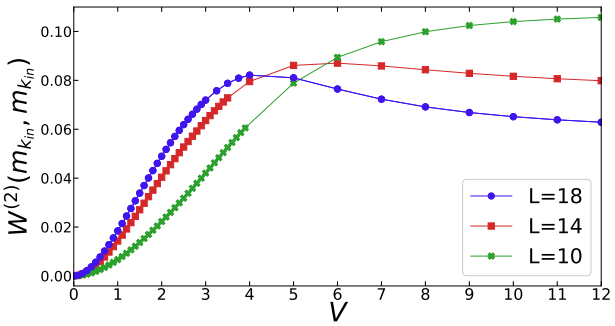

Figure 7.6: Squared Wasserstein distances between distributions defined at quasi-momenta modes inside the Fermi sea, $W^{(2)}(m_{k_{in}}, m_{k_{in}})$, as a function of the interaction strength V, for system sizes $L = 10, 14, 18$.

insulating phase the squared Wasserstein distances $W^{(2)}$ becomes zero, however, they are non-zero in the metallic phase.

The Wasserstein distances thus gives a vivid geometric description of the ground state in

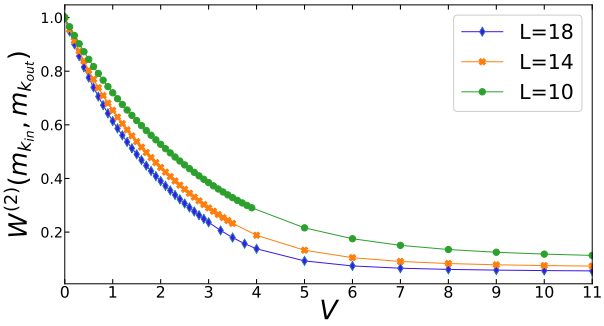

Figure 7.7: Squared Wasserstein distances between distributions defined at quasi-momenta modes inside the Fermi sea and those outside it, $W^{(2)}(m_{k_{in}}, m_{k_{out}})$, as a function of the interaction strength V for system sizes $L = 10, 14, 18$.

both the phases. It characterises the metallic phase by classifying the points inside the Fermi sea and those outside it in two different groups. Most importantly, in the thermodynamic limit, the Wasserstein distances become zero in the insulating phase while they are non-zero in the metallic phase, providing a sharp characterisation of the phases of the system.

7.3 Wasserstein distances defined from the Euclidean distances

We define squared Wasserstein distances between two distance distributions m_i and m_j by choosing the distance function in the spectral parameter space, $\tilde{d}(i, j)$, in the RHS of Eq. (7.11) to be the Euclidean distances.

$$W_E^{(2)}(m_i, m_j) \equiv \inf_{\pi} \sum_{k,l=1}^{L} (k-l)^2 \pi_{ij}(k, l), \tag{7.20}$$

where π_{ij} satisfies the constraints given by Eq. 7.10.We cannot connect $W_E^{(2)}$ to quantities in the Hilbert space like before, since the distance function is no longer derived from states in the Hilbert space. It can neither be connected to the intrinsic curvature as before.

But it is an important geometric observable for the many-body state, because it probes the geometry of the distance distribution functions, which are derived from the quantum distances. We demonstrate this by application to the $t - V$ model.

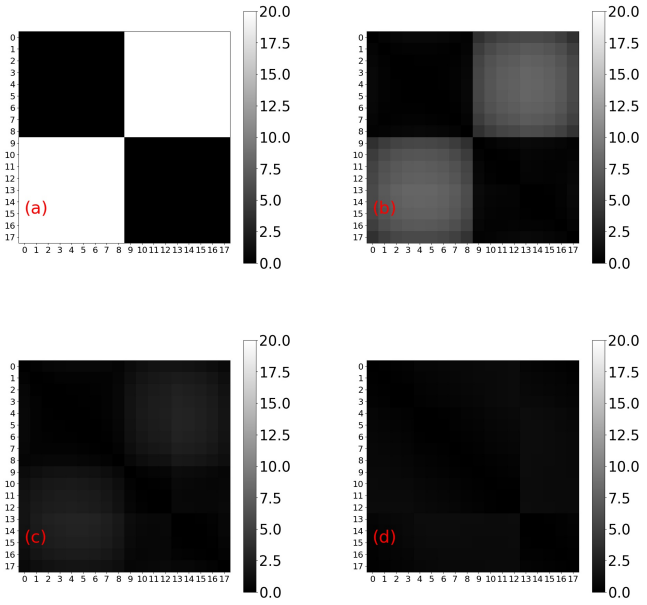

Figure 7.8: (a)-(d)Squared Wasserstein Distance matrices $W_E^{(2)}(m_i, m_j)$ for $L = 18$, obtained from numerical computation for interaction strengths $V = 0.1$ (a), $V = 2$ (b), $V = 4$ (c), and $V = 12$ (d). For $i < 9$, the quasi momenta modes lie inside the Fermi sea, $k_i \in k_{in}$ and for $i \geq 9$, the quasi-momenta modes lie outside it, $k_i \in k_{out}$. The deep metallic regime is characterised by $\sim 0, \sim 20$ distance values between $k_{in} - k_{in}$ ($k_{out} - k_{out}$) and $k_{in} - k_{out}$ blocks respectively. The deep insulating regime is characterised by uniform and extremely small values.

The numerical $W_E^{(2)}$ matrices were obtained for interaction values $0 < V \leq 12$, choosing the marginals to be the distribution functions constructed from the distance matrices obtained by performing exact diagonalization. They are shown in Fig. (7.8). The squared Wasserstein distances, $W_E^{(2)}(m_{k_{in}}, m_{k_{in}})$ (or $W_E^{(2)}(m_{k_{out}}, m_{k_{out}})$), for both the marginals being distributions corresponding to points inside or outside the FS, are very small (~ 0), while $W_E^{(2)}(m_{k_{in}}, m_{k_{out}})$ for the marginals being a distribution defined at a quasi-momenta mode inside the FS and another distribution defined at quasi-momenta mode outside it, are very large (~ 20). Whereas, in deep insulating regime the Wasserstein distances are uniform and very small.

Thus, we find the overall behaviour as one would expect, is similar to that found for the squared Wasserstein distances defined from the quantum distances.

The behaviour of both types of distances as a function of the interaction strength V, however, seems to be more revealing.

The distances $W_E^{(2)}(m_{k_{in}}, m_{k_{in}})$, as a function of the interaction strength V, for different

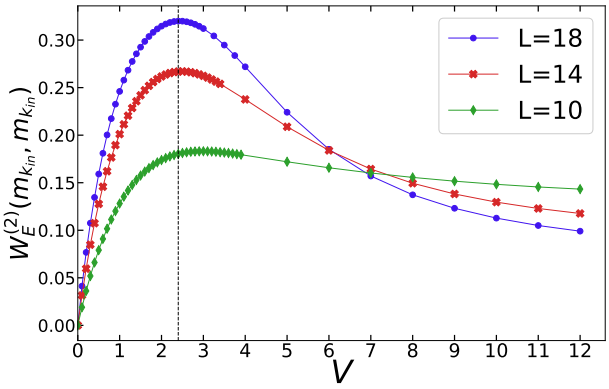

Figure 7.9: Squared Wasserstein distances between distributions defined at quasi-momenta modes inside the Fermi sea, $W_E^{(2)}(m_{k_{in}}, m_{k_{in}})$, as a function of the interaction strength V, for system sizes $L = 10, 14, 18$. The above distances show a prominent peak at $V = 2.4$, for $L > 10$.

system sizes is plotted in Fig. (7.9). These distances indicate the transition by a peak, at $V = 2.4$, which we expect to be more sharpened in the thermodynamic limit.

The distances $W_E^{(2)}(m_{k_{in}}, m_{k_{out}})$ as a function of the interaction strength V, for different system sizes is plotted in Fig. (7.10).

We find, in the regime $V \lesssim 2.4$, that $W_E^{(2)}(m_{k_{in}}, m_{k_{out}})$ scales proportionally with the system size, after which it is insensitive to system size and constant as a function of the interaction. Thus $W_E^{(2)}(m_{k_{in}}, m_{k_{out}})$ is expected to diverge in the metallic phase and remain finite in the insulating phase.

Squared Wasserstein distances obtained from the Euclidean distances in the BZ characterise the geometry of the distance distributions extremely well and thus provide a detailed geometric characterisation of the ground state in both phases.

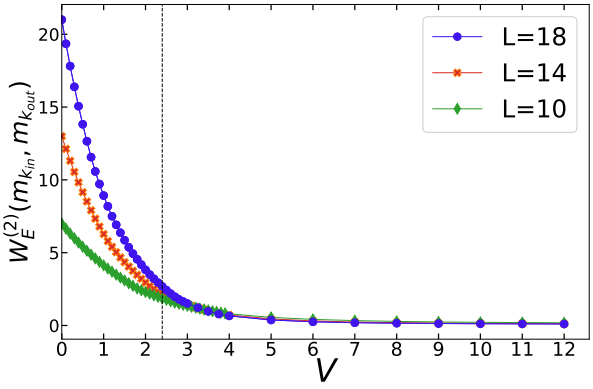

Figure 7.10: Squared Wasserstein distance between distributions defined at quasi-momenta modes inside the Fermi sea and those outside it, $W_E^{(2)}(m_{k_{in}}, m_{k_{out}})$, as a function of the interaction strength V, for system sizes $L = 10, 14, 18$. For $V \lesssim 2.4$, above distance scales proportionately with the system size, post which it is insensitive to the system size.

They sense the metal-insulator transition very strongly and indicate a critical interaction strength $V_c = 2.4$, which is very close to the theoretical value[76], $V = 2$.

A striking finding is that the distances between ditributions defined at the quasi-momenta modes inside the Fermi sea and those outside it are divergent in the metallic phase and finite in the insulating phase.

7.4 Approximate Euclidean embedding of the Wasserstein distances

The 1-Wasserstein distance or the transportation distance, $W(m_i, m_j)$, defined in Eq. (7.12), gives a new metric in the space of the spectral parameters. It will be interesting to investigate the approximate Euclidean embedding of these distances. In this section we present the results for the approximate Euclidean embedding of W in the one-dimensional $t - V$ model.

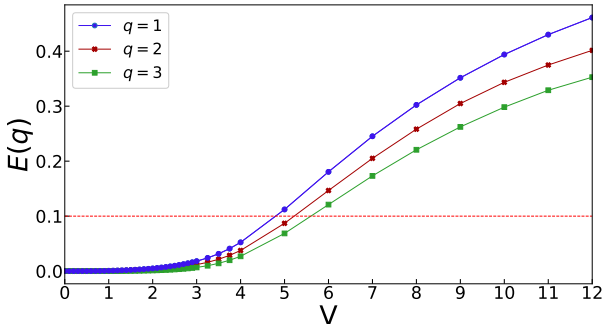

Figure 7.11: Truncation error for keeping first few $(1-3)$ eigenvalues of G as a function of the interaction strength, for approximate embedding of W.

7.4.1 Approximate embedding of W by truncation

We introduced the procedure of keeping only first few eigenvalues of G, with a truncation error in Section. (6.3.1). The result we get after repeating the same procedure for the embedding of W matrix is plotted in Fig. (7.11). The error is found to be negligible even if only one eigenvalue is retained, in the metallic regime. The errors start growing in the crossover regime and continue to grow rapidly in the insulating regime.

7.4.2 Approximate embedding of W by distortion

We have introduced the procedure of average distortion in Sec. (6.3.2) for approximate Euclidean embedding of distances. Repeating the procedure with the W matrix, the average distortion obtained for the embedding in one, two and three dimensions is plotted in Fig. (7.12).

We again find that the average distortion is almost negligible in the metallic regime, whereas it grows rapidly after $V \approx 3$. However, the distortion remains reasonably small, less than about 27%, even well into the insulating regime, up to around $V = 6$.

Thus, we can conclude that the Wasserstein distance matrix can be approximately embedded in one dimension with negligible distortion in the metallic regime. Approximate embedding in low dimensional Euclidean spaces is even possible well into the insulating

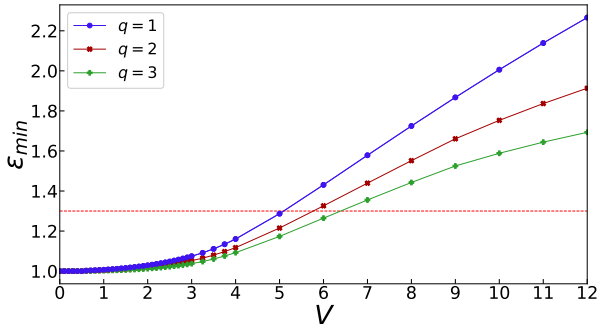

Figure 7.12: Average distortion for approximate embedding of W as a function of the interaction strength.

regime, with low distortion.

Thus, there seems to be a way to visualise the many-body correlated state, both in the metallic and in the insulating regime. We illustrate this in the next section by looking at the "shapes" obtained from the vector configurations corresponding to low average distortion in both these regimes.

7.4.3 "Shapes" of the many-body correlated state

Both the distance matrices D and W are identical at $V = 0$. The embedding again gives two mirror points k_{in} and k_{out} in one-dimension, with the following coordinates,

$$x(k_{in}) = -0.5, \qquad x(k_{out}) = 0.5. \tag{7.21}$$

The embedded vectors for $V = 1, 3$ and 6, for the three dimensional embedding is shown in Fig. (7.13). Following the usual convention, filled circles represent quasi-momenta inside the FS, k_{in} and the unshaded circles represent those outside it, k_{out}. Since all the points are not having distinct coordinates all the 18 points cannot be seen in the figure.

In Fig. (7.13-a) we have shown the embedded points at $V = 1$ (metallic regime) with very small ($< 1\%$) average distortion. We have two sets of points which are clustered around $(x, y, z) = (\pm 0.35, 0, 0)$. The set of embedded points, to a very good approximation, lie in

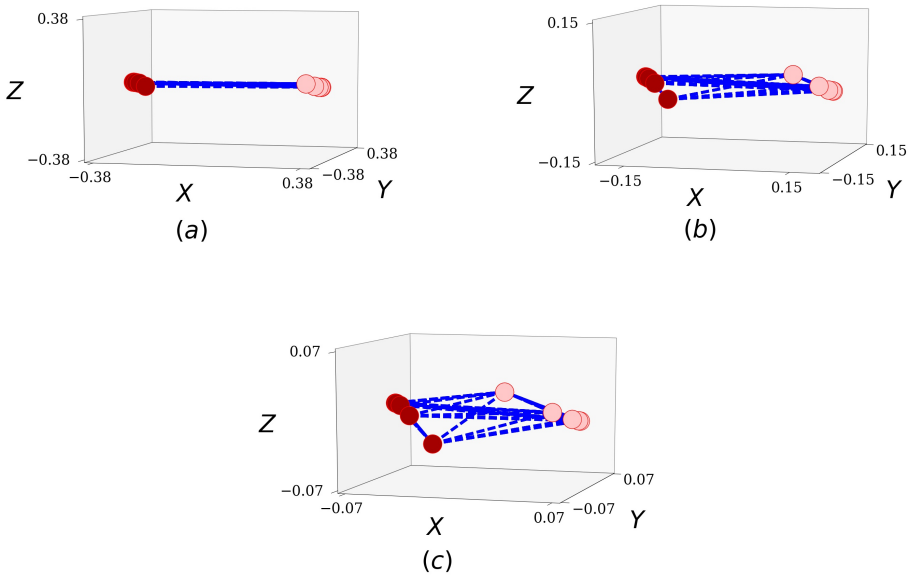

Figure 7.13: The embedded vectors of the Wasserstein distance in three dimensions. (a) $V = 1$ with average distortion $< 1\%$. (b) $V = 3$ with 3% average distortion and (c) $V = 6$ with 27% average distortion. Note that the scales of the axes are different in the three plots.

an effective one dimensional subspace as can be observed from the range of the spread in the y and z coordinates, which are 0.02 and 0.03 respectively. Thus, they are spread only over a region less that 5% of the range of the x coordinate (0.7).

In Fig. (7.13-b) we have shown the embedded points at $V = 3$ (crossover regime). The average distortion value is however higher, 3%. Although the points are all much closer to each other but the relative spread in the y and z directions have increased. The spreads in the y and z directions are now about 10% of the spread in the x direction, with ranges of the spread in the x, y and z coordinates having the values 0.36, 0.05 and 0.06 respectively.

The embedded points at $V = 6$, in the insulating regime but with rather high value of average distortion, 27%, is shown in Fig. (7.13-c). The effective one-dimensional behaviour is completely lost as can be seen from the ranges of the spread in the x, y and z. The x, y and z coordinates, have values $0.13, 0.04$ and 0.05 respectively and the spreads in the y and z directions have now increased to 30%-40% of the spread in the x direction.

7.4.4 Conclusions

1. The metallic phase is characterised by an approximate embedding dimension 1. Thus, the embedding of $W(m_i, m_j)$ distinguishes between the metallic and insulating regimes more sharply than the embedding of $D(i, j)$.

2. Moreover, $W(m_i, m_j)$ can be embedded in a finite-dimensional Euclidean space for values of $V/t \gg 2$, even in the insulating regime, with smaller error and average distortion than $D(i, j)$. Thus, characterisation of a correlated many-body state by a surface in a finite dimensional Euclidean space will be possible for large system sizes.

Chapter 8

Wasserstein Barycenter

We have studied the geometry of the distance distributions by applying optimal transport theory and introducing the Wasserstein distances between the distributions. While these distances capture the phases of the many-body state really well, there are again $(L^d)C_2$ distances to inspect for a general correlated many-body state. How to identify a single geometric observable which is able to characterise the phases?

This question led us to further application of optimal transport theory and study of Wasserstein barycenter [66, 72].

Starting from a configuration of distributions, optimal transport theory allows us to find an average representative distribution called the Wasserstein Barycenter. The generalisation of the concept of barycenter to probability distributions involve minimization of the average squared Wasserstein distances from the starting distributions instead of the minimisation of the Euclidean distances of the barycenter from all the points in a configuration of points.

The Wasserstein barycenter is a single distribution function which minimizes the average squared Wasserstein distances from all the distance distributions. The corresponding minimum average squared Wasserstein distance obtained by finding the converged Wasserstein barycenter solution is a single geometric observable which can differentiate

the metallic and insulating phases. In the insulating phase, where all the distributions are identical in the thermodynamic limit, the Wasserstein barycenter should also be trivially identical to them, and the corresponding average squared Wasserstein distances from all the distance distributions should be zero.

8.1 Basic definition and computation

The barycenter for a configuration of points usually implies the arithmetic mean of the coordinates. For a collection of points $(x_1, ..., x_p)$, the barycenter, x^*, in the Euclidean case [86], is such that the weighted average sum of squared Euclidean distance of all the points, $\sum_{i=1}^{p} \lambda_i \mid x - x_i \mid^2$, where $\lambda_i \in [0, 1]$ and $\sum_{i=1}^{p} \lambda_i = 1$, is minimised.

The above concept of barycenter can be generalized for a collection of probability distributions $\{m_i(k)\}$, defined at each point k_i $(i = 1, \ldots, L^d)$ in the spectral parameter space: essentially, optimal transport theory suggests that we replace the above weighted sum of the squared Euclidean distances by the weighted sum of squared Wasserstein distances. The Wasserstein barycenter is then a single distribution function defined on the space of spectral parameters, which minimizes the above sum [66].

To summarize, the Wasserstein barycenter, $m^*(k)$, is defined as a single function on the spectral parameter space, such that the average sum of the squared Wasserstein distances between $m^*(k)$ and each of the distributions, $W^{(2)}(m^*, m_i)$ (sum defined on the RHS of Eq. 8.1), is minimised. The average squared Wasserstein distance between the barycenter and the distance distributions is defined as the follows,

$$J(m^*) \equiv \inf_{m} \frac{1}{L^d} \sum_{i=1}^{L^d} W^{(2)}(m_i, m), \tag{8.1}$$

where we take all the weights to be uniform for simplicity. The existence of a solution or the Wassestein barycenter has been investigated by Agueh and Carlier in 2010[66].

For the computation of the Wasserstein barycenter we have used the entropic regularisation of the optimal transport problem[67] and applied Sinkhorn-Knopp's fixed point iteration algorithm[87, 88]. Entropic regularisation of the optimal transport problem involves minimising $W_\gamma^{(2)}(m_i, m)$, defined by the following equation,

$$W_\gamma^{(2)}(m_i, m) \equiv \inf_\pi \left(\sum_{ij} (D(i,j))^2 \pi_\gamma^i(i,j) + \gamma S(\pi_\gamma^i) \right) \tag{8.2}$$

$$S(\pi_\gamma^i) \equiv \sum_{kl} \pi_\gamma^i(k,l) log(\pi_\gamma^i(k,l)). \tag{8.3}$$

where $\pi_\gamma^i(i,j)$ are the joint probability distributions with marginals m_i, m and $D(i,j)$ is the matrix of the quantum distances. The second term on the RHS corresponds to the entropy of above $\pi_\gamma^i(i,j)$ matrix. A positive regularisation parameter γ is introduced, in the limit $\gamma \to 0$, we find the solution for the actual optimal transport problem given by linear programming and $W_\gamma^{(2)} \to W^{(2)}$.

It has been proved by Cuturi[67], for above minimisation problem the converged π_γ^*, has the following specific form,

$$\pi_\gamma^i(\alpha,\beta) = U^i(\alpha) K(\alpha,\beta) V^i(\beta) \tag{8.4}$$

$$K(\alpha,\beta) = e^{-D(\alpha,\beta)/\gamma} \tag{8.5}$$

where U^i and V^i are L^d dimensional arrays, solutions for which can be obtained by Sinkhorn's matrix scaling algorithm[87, 88] being applied to K.

Imposing the constraint equations on π_γ^i we get the following set of equations:

$$V^i(k) = \frac{m_i(k)}{\sum_j K(j,k) U^i(j)} \tag{8.6}$$

$$U^i(k) = \frac{m^*(k)}{\sum_j K(k,j) V^i(j)} \tag{8.7}$$

These self-consistent equations can be solved iteratively starting from an initial guess for U^i and an ansatz for m^*.

Algorithm for obtaining the solution by iterations:

1. Substitute an initial guess value for $U^i = (1, 1...., 1)$ (L^d dimensional vector with all entries 1).

2. Put in Eq. (8.6) to obtain V^i (m^i and K are obtained from D).

3. Put the following ansatz for m^*,

$$m^*(\alpha) = \prod_l \left(\sum_j K(\alpha, j) V^l(j) \right)^{1/(L^d)} . \tag{8.8}$$

4. Put in Eq. (8.7) to compute U^i.

5. Repeat the above steps until U^i, V^i converge $\forall i \in [1, L^d]$ and m^* converges as well.

The above method gives us an optimal but approximate joint distribution π^*_γ, which however is very close to the exact π^* obtained from linear programming for the small values of regularisation parameter. The advantage of the entropic regularisation is that it allows extending optimal transport to large system sizes where solving for L^{2d} constrained linear equations may not be possible.

The average of the squared quantum distances over the spectral parameter space given by above joint probability distribution π^{*i}_γ, will be very close to the squared Wasserstein distances $W^{(2)}(m_i, m)$ obtained from exact π^* by choosing very small regularisation parameters.

So after obtaining the optimal joint distribution π^{i*}_γ, by applying Sinkhorn-Knopp's fixed point iteration algorithm [87, 88], we redefine the corresponding squared regularised

Wasserstein distances $\tilde{W}_{\gamma}^{(2)}(m_i, m^*)$, as follows:

$$\tilde{W}_{\gamma}^{(2)}(m_i, m^*) \equiv \sum_{kl} (D(k,l))^2 \pi_{\gamma}^{i*}(k,l). \tag{8.9}$$

We then consider the corresponding average squared Wasserstein distance $\tilde{J}(m^*)$, between the converged barycenter m^* and all the L^d distance distributions,

$$\tilde{J}(m^*) \equiv \frac{1}{L^d} \sum_{i} \left(\sum_{kl} (D(k,l))^2 \pi_{\gamma}^{i*}(k,l) \right). \tag{8.10}$$

After the new algorithmic developments [89, 90] Wasserstein barycenters have been widely applied to various problems in machine learning like graphics[91], learning word and sentences embeddings[92], topic modeling[93], etc.

8.2 Results for the $t - V$ model

We look at the results for the one-dimensional $t-V$ model, where the distance distributions are constructed from the numerical distance matrices obtained by exact diagonalization, as before. We choose an extremely small value of the regularisation parameter, $\gamma = 0.006$, and find converged solutions for the Wasserstein barycenter. The number of iterations however varies for different values of the interaction strength V.

The Wasserstein barycenter over the BZ, for different interaction values is plotted in Fig. (8.1). We find the distribution is highly inhomogeneous over the quasi-momenta modes in the metallic phase, where the distance distributions are opposite to each other for quasi-momenta modes inside and outside the FS as observed in Sec. (7.2.2).
However, for large V, in deep insulating phase where all the distributions are more or less identical, we observe a contrasting homogenous behaviour.
Thus, the Wasserstein barycenter is found to be a single distribution function defined over the BZ, which can sense the metallic and insulating phases.

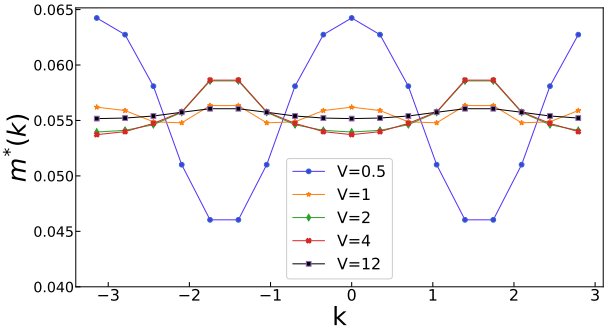

Figure 8.1: The barycenter $m^*(k)$ defined over the BZ, $k \in [-\pi, \pi)$, for different interaction values. The Fermi points are $k_f = \pm\frac{\pi}{2}$. We find that in deep metallic phase $m^*(k)$ is highly inhomogenous over the BZ and $m^*(k_f)$ is minimum. While in the deep insulating phase the distribution is flat and homogenous.

The average squared Wasserstein distance between the barycenter and the distance dis-

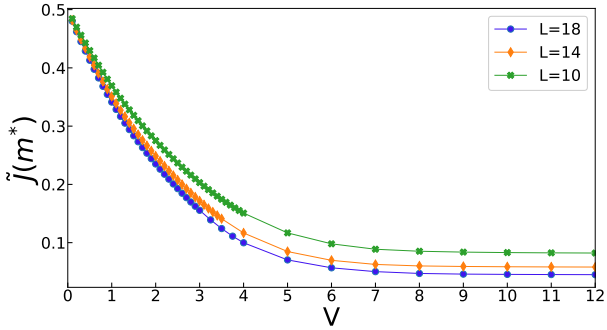

Figure 8.2: Average squared Wasserstein distance between the distribution functions and the barycenter as a function of the interaction strength, for different system sizes.

tributions, $\tilde{J}(m^*)$, as a function of the interaction strength, for the system sizes $L = 10, 14, 18$, is shown in Fig. (8.2). We find it it is insensitive to the system size in the deep metallic phase and decreases with system size in the deep insulating phase. In the metallic phase it drops abruptly, with increasing V, it is rather insensitive to V in the deep insulating phase and becomes very small.

For $V = \infty$, $\tilde{J}(m^*)$ is computed for the distributions obtained from the analytical distance matrix (5.24), for system sizes $L = 10 - 100$. We denote it as $\tilde{J}^{\infty}(m^*)$ and it is found to be linear in L^{-1}, as shown in Fig. 8.3.

Thus, from Figs. (8.2,8.3) it can be concluded that the average squared Wasserstein dis-

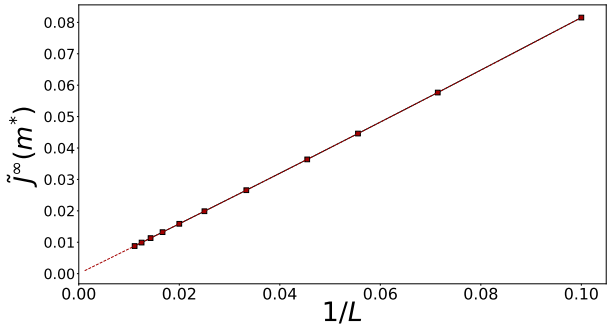

Figure 8.3: Average squared Wasserstein distance between the distribution functions and the barycenter at the extreme interaction limit, $V = \infty$ for system sizes $L = 10 - 100$, as a function of the inverse of system size.

tance between the barycenter and the distance distributions is a single geometric observable which characterises the metallic and insulating phases, because it is non-zero in the metallic phase and becomes zero in the insulating phase.

Chapter 9

Ollivier-Ricci Curvature

The intrinsic geometry of the correlated many-body state can be studied by inspecting a generalisation of the Ricci curvature in a discrete setting. This generalisation, popularly known as the Ollivier-Ricci curvature, was introduced by Ollivier in the general framework of Markov processes and metric spaces[47, 48]. Later, it was also applied in graph theory by Lin-Yau[94]. It is also closely connected to Wasserstein distances: in fact, it is defined in terms of the 1-Wasserstein distances (Eq. (7.12)).

The Ricci curvature has a rich history in geometry: it is a fundamental invariant in Riemannian geometry. In the continuous case, it is a measure of the degree to which the geometry determined by a given Riemannian metric deviates from that of ordinary Euclidean space. The Ricci curvature is usually the average of sectional curvatures of all tangent planes with some given direction. It is also closely related to the eigenvalues of the Laplace-Beltrami operator[95].

Several generalisations of the Ricci curvature in the discrete setting have been at the center of recent research activities, which not only include the Ollivier-Ricci curvature but also the Bakry-E'mery curvature[45], the entropic curvature introduced by Erbar and Maas[49], and the Forman curvature[46]. Lott-Villani-Strum used optimal transport theory to define the Ricci curvature for metric-measure spaces, using the 2-Wasserstein

distances[37].

The above generalisations, being exceedingly simple to study in discrete settings, have found wide applications in various fields: these include quantum gravity[96, 97], the study of complex biological networks[98], quantifying the systemic risk and fragility of financial systems[99], internet topology for the investigation of node degree[100], to name a few.

Let us examine how this continuous concept was adapted to the discrete setting. The main intuition used by Ollivier was that the Ricci curvature controls the amount of overlap of two distance balls in terms of their radii and the distance between their centers[50]. Without going into deep technical details, we present a brief sketch of this adaption necessary for our work.

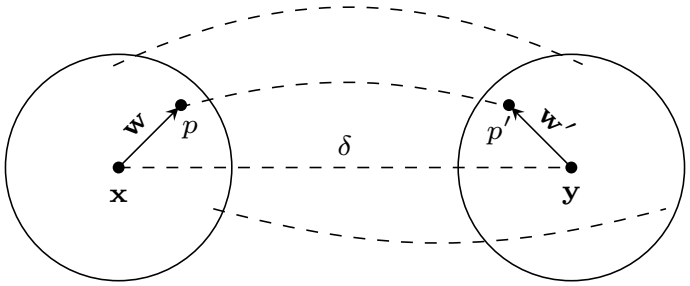

Figure 9.1: Two nearby balls, m_x^ϵ and m_y^ϵ of radius ϵ whose centres are a small distance, δ, apart, along the unit vector $\mathbf{v}$. Parallel transport of a unit vector $\mathbf{w}$ gives $\mathbf{w}'$ such that for a point $p \in m_x^\epsilon$ parallel transport along the geodesic of length δ yields a point $p' \in m_y^\epsilon$. The average distance between the points p and p' in flat space is equal to δ, while in the presence of curvature the lowest-order deviation from δ is given by Equation (9.1).

Let us consider a smooth, N-dimensional Riemannian manifold $\mathcal{M}$ and denote the local coordinates by x^μ, $\mu = 1, \ldots, N$. $g_{\mu\nu}(\mathbf{x})$ is the metric. A nearby point with local coordinates $\mathbf{y} = \mathbf{x} + \delta\mathbf{v}$ is considered, where $\mathbf{v}$ is a unit tangent vector at $\mathbf{x}$.

We look at two ϵ-balls, m_x^ϵ and m_y^ϵ around $\mathbf{x}$ and $\mathbf{y}$ which consist of the points in $\mathcal{M}$ that are at a distance $\leq \epsilon$ from $\mathbf{x}$ and $\mathbf{y}$ respectively.

If m_x^ϵ is mapped to m_y^ϵ using the Levi-Civita connection [101], the average distance be-

tween the points $p \in m_x^\epsilon$ and their images $p' \in m_y^\epsilon$, in the limit $\delta, \epsilon \to 0$, has been been shown to be[50],

$$W(m_x^\epsilon, m_y^\epsilon) = \delta\left(1 - \frac{1}{2(N+2)}\kappa(\mathbf{v}, \mathbf{v}) + O(\epsilon^3 + \delta\epsilon^2)\right). \tag{9.1}$$

In above equation $\kappa(\mathbf{v}, \mathbf{v})$ is the Ricci curvature associated with the unit vector $\mathbf{v}$. Figure (9.1) is a schematic illustration.

Extending the above idea to the discrete setting [50, 94] involves replacing the ϵ-ball, m_x^ϵ around $\mathbf{x}$ by the normalised distribution of distances of all the vertices from the vertex i,

$$m_i(j) = \frac{D(i,j)}{\sum_k D(i,k)}. \tag{9.2}$$

Moreover, the average distance W is replaced by the 1-Wasserstein distance $W(m_i, m_j)$ between two distributions m_i and m_j. Thus define

$$W(m_i, m_j) \equiv \inf_\pi \sum_{kl} D(k,l)\pi_{ij}(k,l), \tag{9.3}$$

where $\pi_{ij}(k,l)$ is a joint probability distribution defined as,

$$\sum_l \pi_{ij}(k,l) = m_i(k), \quad \sum_k \pi_{ij}(k,l) = m_j(l). \tag{9.4}$$

Recall Sec. (7.4) of Chapter 7 where we introduced this distance.

The curvature, $\kappa(i,j)$, associated with an edge $e(i,j)$ of the graph is then defined by

$$W(m_i, m_j) = D(i,j)(1 - \kappa(i,j)). \tag{9.5}$$

We can also propose a generalization of the scalar curvature at a point $\mathbf{x}$ in Riemannian manifold, for a graph [95], derived from the Ollivier Ricci curvature defined above. It is a weak invariant obtained by contracting the Ricci curvature in the Riemannian manifold.

The scalar curvature at each vertex i, $\kappa(i)$, is given by,

$$\kappa(i) = \frac{1}{\sum_k D(i,k)} \sum_j \kappa(i,j). \tag{9.6}$$

9.1 Results for the $t - V$ model

The curvature along each edge of the graph defined in Equation (9.5) and the scalar curvature defined in Equation (9.6) are computed from the 1-Wasserstein distances obtained by linear programming and the quantum distance matrix given by exact diagonalization, for the one-dimensional $t - V$ model. The quasi-momenta (taking values in the BZ), $k_l \in [-\pi, \pi)$, are given by

$$k_l = -\pi + \frac{2\pi l}{L}. \tag{9.7}$$

With every quasi-momenta mode k_l we associate the integer l which runs from 1 to L. These integers label the vertices of the graph (as per discussions in Sec. (5)).

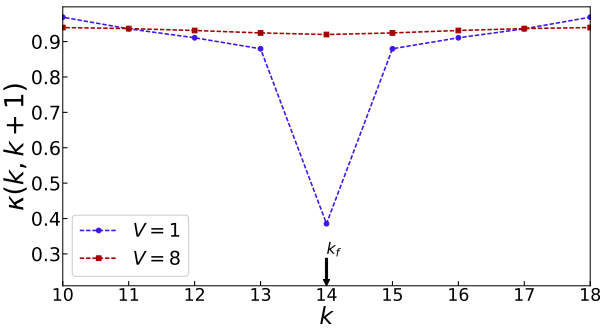

Figure 9.2: Curvatures for the nearest neighbour edges $(k, k+1)$ over half the BZ, for different interaction strengths. The integer values of k along the x axis label the vertices of the graph as per Eq. (9.7). The metallic regime is characterised by a discontinuity at the Fermi point k_f.

The values of curvatures in the metallic regime, $V \ll 2$, is highly edge-dependent and they classify the edges into two types, yet again. The edges corresponding to vertices both inside or outside the FS, $e_1 \equiv (k_{in}, k_{in})$ or (k_{out}, k_{out}), have large curvatures, whereas

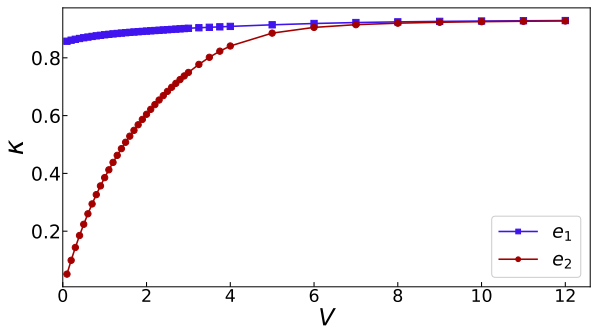

Figure 9.3: Curvatures for both type of edges e_1 and e_2 as function of interaction strength V.

the edges with one of the vertices inside the FS and another one outside it, $e_2 \equiv (k_{in}, k_{out})$ or (k_{out}, k_{in}), have small curvatures.

The insulating regime, $V \gg 2$ (as usual), is characterised by the contrasting behaviour where curvatures of e_1 and e_2 are both quite large and uniform.

We have plotted the curvature corresponding to the edges formed by vertices which are nearest neighbours in the BZ, $\kappa(k, k+1)$, in Figure (9.2). This figure shows a discontinuity in the curvature, at the Fermi point which is labelled by k_f, for $V = 1$, in the metallic regime. This discontinuity decreases smoothly as a function of interaction strength and disappears at large V. This dip in the curvature at the Fermi point in the metallic regime is a consequence of the difference in behaviour of the two types of edges. All the nearest neighbour edges $\kappa(k, k+1)$ for k, $k+1 \neq \pm k_f$ belong to e_1. In such cases the quantum distance $D(k, k+1)$ is small and the distance distributions (Eq. (9.2)) are similar to each other consequently the Wasserstein distance $W(k, k+1)$ is small. But the edge with the Fermi point k_f as one of the vertices belongs to e_2. The corresponding nearest neighbour quantum distance is large. The distance distributions are very different, consequently the Wasserstein distance is large as well. The two distance values don't differ much from each other, resulting in small values of curvature as per Eq. (9.5).

Fig. (9.3) shows the Ricci curvature of both types of edges as a function of V. The curvature of e_1 is more or less constant and has a high value at all the values of the interaction. However, the curvature of e_2 continously increases in the metallic and the

crossover regime, after which it saturates to a constant high value, roughly the same as that of e_1.

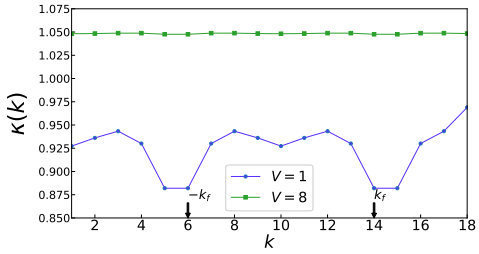

Figure 9.4: Scalar Curvature as a function of the quasi-momenta modes representing vertices of the graph. The integer values along the x axis label the vertices of the graph as per Eq. (9.7). The Fermi points are labelled by $\mp k_f$. In insulating regime the scalar curvature is uniform over all the vertices.

Fig. (9.4) shows the scalar curvature as a function of the quasi-momenta modes, in the two regimes. We find the same contrasting behaviour where the insulating phase is characterised by a uniform scalar curvature, whereas in the metallic phase the scalar curvature varies considerably for different vertices.

From the above results we can conclude the Ollivier-Ricci curvature is able to demarcate both the phases by a difference in behaviour.

Chapter 10

Summary and Outlook

We conclude this thesis by summarizing the findings and presenting future directions of work that spring from them.

The first half of the thesis introduced a new formalism for studying the quantum geometry of correlated many-body states. We know the building blocks of many-body states are the single particle states. The complete set of single particle states can be labelled by some set of parameters that we have refered to as the spectral parameters.

Our proposition, introduced in Chapter 4, is to define local geometrical observables in the space of the spectral parameters, in terms of expectation values of appropriately defined unitary operators. We have succeeded in defining valid quantum distances between pairs of points in the spectral parameter space that satisfy the triangle inequalities. The definition gives back the standard quantum distances in the mean-field states as we observed in Sec. (3.1.1).

The spectral parameters are completely general, they could be quasi-momenta, positions labelling Wannier orbitals, parameters labelling the eigenfunctions of some confining potential like in a quantum dot or an optical trap. So in parallel to the single-particle formalism already well studied in condensed matter system and discussed in Chapter 3, for

correlated electron systems we can study local geometrical properties in a space of physical parameters. Thus we gain over the existing method [9, 18] discussed in Sec. (1.2). Morever, unlike the single-particle formalism, our theory is capable of probing the quantum geometry of metallic phases as well as insulating ones.

Another advantage of our definition of the distances is, its formulation in terms of expectation values of the exchange operator. It is thus a purely kinematic definition. So it gives exclusive geometric characterisation of the ground state, unlike the previous Green's function approaches[19, 20, 21, 22, 23, 24] which involved single particle excitations. Moreover, it can easily be applied to any one-band model. In fact we have applied our method to the one-dimensional $t-V$ model using exact diagonalization and found striking results. This model is a one band model exhibiting a Mott transition. So it clearly marks out these advantages.

The implementation definitely has a wide scope because our definition of the quantum distances are in terms of the static correlation functions and can be computed applying any exact or approximate technique like perturbation theory, quantum Monte Carlo methods, DMRG and bosonisation in one dimension. The static correlation functions of interest for the one band models are the four-point correlations, while multi-orbital models will need the computation of higher-order correlation functions. In the same spirit as the work of Resta and Sorella[29], we have given a geometrical framework for studying the static correlations, which themselves characterize the many-body states. However, our correlation functions are slightly different from conventionally studied ones and thus bring in newer prospects.

The next part of the thesis focused on developing tools to study the quantum distances and construct geometrical observables from the space of distances. We have a matrix of quantum distances to begin with, or we can think of this structure as a weighted graph. We have applied tools popularly used in distance geometry and discrete differential geometry, for studying the geometry of graphs and networks, which are very popular in other applied

fields like computer vision, image processing, data mining, machine learning, the study of biological networks, finding molecular conformations in NMR, to name only a handful.

We have outlined a method to study the extrinsic geometry of the many-body state by Euclidean embedding of the distances. Even visualization in terms of shapes and surfaces in lower dimensional Euclidean space was possible by approximate embedding techniques. A particularly powerful geometric approach has been outlined, by constructing probability ditributions from the distances and introducing the theory of optimal transport to study the geometry of these distance distributions. We find geometric observables which can be obtained by averaging over the space of the spectral parameters. The Wasserstein distances, which give the distance between the distributions are proposed as geometrical observables which can capture the phases of the many-body state.

Further, parallel to the localisation tensor, optimal transport theory allows us to define a single geometric observable characterising the phases by the concept of Wasserstein barycenter. The average squared Wasserstein distance between the distance distributions and the barycenter is tracked down as such a geometric observable. This approach to study the structure of a many-body state is closely related with the machine learning approach towards data analysis, where one often has to deal with collections of samples that can be interpreted as probability distributions. One of the fundamental tasks then becomes comparing, summarising, and reducing the dimensionality of the probability distributions on a given metric space. In parallel, we generate probability distribution functions from the many body state and infer geometric properties of ground states by comparing these distributions (in terms of Wasserstein distance).

A method to study the intrinsic geometry of the many-body state has been proposed as well, by introducing the Ollivier-Ricci curvature. It is a discrete version of the Ricci curvature in terms of the Wasserstein distances, and thus has the optimal transport theory at the heart of its basic construction.

10.1 Future plans

This new formalism is at a nascent stage and has a wide scope of applications. Since much of the motivation comes from the characterisation of the metal-insulator transition and since our applications to the $t - V$ model succeed in such characterisation by using the theory of optimal transport, there is the range of applications to other models in order to find an uniform characterisation.

It will be interesting to bring in the spin degree of freedom and study the Hubbard model, where the distances can be computed by quantum Monte Carlo. A plan to investigate the one-dimensional spin chains, applying DMRG to compute the quantum distances, is under progress.

However, our proposed general scheme is very powerful. We think that if the static correlation functions are computed using any of the exact or approximation techniques (the ones listed above or even newer ones), we will be able to introduce the geometrical framework of the quantum distances and characterise the phases of any quantum state applying these new tools.

The distances for conventional tight binding models though are the usual Hilbert-Schmidt distances, but the above tools can also be used for studying basic physics in such models, which are well studied by the conventional approach to quantum geometry. Applications of this new methodology to the Haldane model is also planned for the near future.

Studying the ground state of a system is interesting from the perspective of quantum phase transitions. The formalism being based on expectation values over a state, it can be applied to any state in principle and can possibly find applications in dynamical systems as well.

Coming back to the broader theoretical picture of our formalism, the generalisation of the

geometric phases in terms of expectation value of a unitary operator was not possible by choosing the products of the exchange operators as a candidate. However, there remains the exciting possibility of finding an appropriate operator such that the additive law is satisfied.

Appendix A

Appendix

A.1 Quantum distances of general mean field states

In this section we generalise our previous results of the distance matrix for general mean field states (MFS).

We consider a general d-dimensional lattice with L unit cells in each direction. We label the sites of the unit cells by i and the sublattices by $a = 1, \dots n_B$. The sites of the lattice are denoted by $\mathbf{R}_{ia} = \mathbf{R}_i + \mathbf{r}_a$. Thus $\mathbf{R}_i$ specifies a point in the unit cell and $\mathbf{r}_a$ the locations of the sub-lattice sites with respect to that point. The fermion creation and annihilation operators are denoted by $(C^\dagger_{ia}, C_{ia})$. They satisfy the canonical anti-commutation relations. The Fourier transforms of these operators are defined as,

$$C_a(\mathbf{k}) \equiv \frac{1}{L^{\frac{d}{2}}} \sum_i e^{i\mathbf{k}\cdot\mathbf{R}_{ia}} C_{ia} \tag{A.1}$$

where $\mathbf{k} \in BZ$.

We denote the single-particle hamiltonian in the quasi-momentum space by $h_{ab}(\mathbf{k})$ and its spectrum by,

$$h_{ab}(\mathbf{k}) u^n_b(\mathbf{k}) = \epsilon^n(\mathbf{k}) u^n_a(\mathbf{k}). \tag{A.2}$$

We denote the Fermi level by ϵ_F and the number of occupied bands at $\mathbf{k}$ by $N_F(\mathbf{k})$, namely,

$$N_F(\mathbf{k}) \equiv \sum_{n=1}^{N_B} \Theta\left(\epsilon_F - \epsilon^n(\mathbf{k})\right). \tag{A.3}$$

The general mean field state is defined as

$$|u, \epsilon_F\rangle \equiv \prod_{\mathbf{k}} \prod_{n=1}^{N_F(\mathbf{k})} \left(u_a^n(\mathbf{k}) C_a^\dagger(\mathbf{k})\right)|0\rangle \tag{A.4}$$

where u denotes the full set of eigenstates, $u^n(\mathbf{k})$. We define $\Psi_{a_1,\ldots a_{N(\mathbf{k})}}(\mathbf{k})$ to be the anti-symmetrised product of the $N_F(\mathbf{k})$ single particle wave functions, $u^n(\mathbf{k})$,

$$\Psi_{a_1 \ldots a_{N_F(\mathbf{k})}}(\mathbf{k}) = \sum_P (-1)^P \prod_{l=1}^{N_F(\mathbf{k})} u^n(\mathbf{k})_{a_P(l)} \tag{A.5}$$

The general mean field state can be written in the factorised form,

$$\begin{aligned} |\Psi(\mathbf{k})\rangle &\equiv \left(\sum_a \Psi_{a_1 \ldots a_{N_F(\mathbf{k})}}(\mathbf{k}) \prod_{l=1}^{N_F(\mathbf{k})} C_{a_l}^\dagger(\mathbf{k})\right)|0\rangle_{\mathbf{k}} \\ |u, \epsilon_F\rangle &= \prod_{\mathbf{k}} |\Psi(\mathbf{k})\rangle \end{aligned} \tag{A.6}$$

where $\sum_a$ denotes the sum over all the $n_B C_{N_F(\mathbf{k})}$ combinations of the the index a and $\prod_{\mathbf{k}}$ denotes the direct product of the states defined at each point in the BZ.

A.1.1 The quantum distance matrix

Our definition of the quantum distance matrix is,

$$D^2(\mathbf{k}_1, \mathbf{k}_2) \equiv 1 - |\langle u, \epsilon_F | E(\mathbf{k}_1, \mathbf{k}_2) | u, \epsilon_F \rangle|^\alpha \tag{A.7}$$

where $E(\mathbf{k}_1, \mathbf{k}_2)$ are the exchange operators. They are unitary operators and their action of the fermion creation operators is given by,

$$E(\mathbf{k}_1, \mathbf{k}_2) C_a^\dagger(\mathbf{k}_1) E^\dagger(\mathbf{k}_1, \mathbf{k}_2) = \pm C_a^\dagger(\mathbf{k}_2) \tag{A.8}$$

$$E(\mathbf{k}_1, \mathbf{k}_2) C_a^\dagger(\mathbf{k}_2) E^\dagger(\mathbf{k}_1, \mathbf{k}_2) = \pm C_a^\dagger(\mathbf{k}_1). \tag{A.9}$$

The $\pm$ signs above depend on the ordering convention of the creation operators in the definition of the many-body states. While it is important to keep track of them for correlated states, as we will see below, due to the factorized form of MFS, the distances are independent of the signs.

The action of the exchange operator on the states is

$$\begin{aligned} E(\mathbf{k}_1, \mathbf{k}_2) |\psi(\mathbf{k}_1)\rangle \otimes |\psi(\mathbf{k}_2)\rangle = \pm \Bigg(& \sum_{aa'} \Psi_{a_1 \ldots a_{N_F(\mathbf{k}_1)}}(\mathbf{k}_1) \\ & \Psi_{a'_1 \ldots a'_{N_F(\mathbf{k}_2)}}(\mathbf{k}_2) \Bigg) \\ & \prod_{l'=1}^{N_F(\mathbf{k}_2)} C_{a'_l}^\dagger(\mathbf{k}_2) |0\rangle_{\mathbf{k}_2} \\ & \otimes \prod_{l=1}^{N_F(\mathbf{k}_1)} C_{a_l}^\dagger(\mathbf{k}_1) |0\rangle_{\mathbf{k}_1}. \end{aligned} \tag{A.10}$$

Equations (A.7), (A.8), (A.9) and (A.10) imply

$$D^2(\mathbf{k}_1, \mathbf{k}_2) = 1 - |\langle \Psi(\mathbf{k}_1)) | \Psi(\mathbf{k}_2)) \rangle|^{2\alpha} \, \delta_{N_F(\mathbf{k}_1), N_F(\mathbf{k}_2)}. \tag{A.11}$$

For $\alpha = 1$, the RHS of the above equation is the Hilbert- Schmidt distance between $\Psi(\mathbf{k}_1)$ and $\Psi(\mathbf{k}_2)$. Thus we have shown that the quantum distances of the mean field states reduce to the standard definition in terms of the overlap of wavefunctions. For $\alpha = 1$, it is exactly the Hilbert-Schmidt distance between the $N_F(\mathbf{k})$ states at $\mathbf{k}$. Our definition also implies

that the distance between two quasi-momenta with different occupation numbers is equal to 1.

A.2 The classical Ptolemy problem for $\alpha = 2$

In this section we look at the special case $\alpha = 2$ in the definition of distances in Eq. (4.9). This case is special in the sense, the proof of the triangle inequalities is interesting in this case. We encounter the classical Ptolemy problem in 3-dimensional Euclidean space.

To state the problem, we are given four normalized vectors in a Hilbert space, $\mathcal{H}$, $|\chi_\mu\rangle$, $\mu = 0, \ldots, 3$. Let $|\psi\rangle \equiv |\chi_0\rangle$ denote the correlated many-body state being studied. The remaining three states are the states generated by the action the exchange operators (introduced in Chapter 4) on it. The six distances between these four vectors are given by,

$$D_{\mu\nu} = \sqrt{1 - |\langle\chi_\mu|\chi_\nu\rangle|^2} \tag{A.12}$$

We will now prove that we can always find 4 points in a 3-dimensional Euclidean space, $\vec{x}_\mu$, such that,

$$D_{\mu\nu} = |\vec{x}_\mu - \vec{x}_\nu| \tag{A.13}$$

This reduces the problem to the classical Ptolemy problem.

We can always find a 4-dimensional subspace of $\mathcal{H}$ which contains the four vectors, $|\chi_\mu\rangle$. The physical states, forming the manifold $\mathbb{CP}_3$, are in one-to-one correspondence with the pure state density matrices,

$$\rho_\mu \equiv |\chi_\mu\rangle\langle\chi_\mu|. \tag{A.14}$$

The distances defined in Eq. (A.12) can be expressed as,

$$D_{\mu\nu} = \sqrt{1 - \mathrm{Tr}(\rho_\mu\rho_\nu)} \tag{A.15}$$

Since ρ_μ are hermitian, they can be expressed as a linear combination, with real coefficients, of the identity matrix and the 15 generators of $SU(4)$ in the fundamental representation. We denote them by, $T_\alpha,\ \alpha = 1, \ldots, 15$. They can always be chosen such that,

$$\mathrm{Tr}T_\alpha = 0, \qquad \mathrm{Tr}T_\alpha T_\beta = \delta_{\alpha\beta} \tag{A.16}$$

Thus we have,

$$\rho_\mu = a_0 I + \sum_{\alpha=1}^{15} a_\mu^\alpha T_\alpha \tag{A.17}$$

$$a_0 = \frac{1}{4}\mathrm{Tr}\rho_\mu \tag{A.18}$$

$$a_\mu^\alpha = \mathrm{Tr}T_\alpha \rho_\mu \tag{A.19}$$

The fact that, $\mathrm{Tr}\rho_\mu^2 = \mathrm{Tr}\rho_\mu = 1$ implies that,

$$a_0 = \frac{1}{4},\ \vec{a}_\mu \cdot \vec{a}_\mu \equiv \sum_{\alpha=1}^{15} a_\mu^\alpha a_\mu^\alpha = 1 - \frac{1}{16} = \frac{15}{16} \tag{A.20}$$

Note that $\rho_\mu^2 = \rho_\mu$ implies other constraints on $\vec{a}$, but these are not relevant for our proof.

Thus, we have shown that each of the physical states, ρ_μ, can be represented by a point on a 14-dimensional sphere of radius $\frac{\sqrt{15}}{4}$.

The distance $D_{\mu\nu}$ can be expressed in terms of $\vec{a}_\mu$,

$$\begin{aligned} D_{\mu\nu}^2 &= 1 - \mathrm{Tr}(\rho_\mu \rho_\nu) \\ &= \frac{15}{16} - \vec{a}_\mu \cdot \vec{a}_\nu \\ &= \frac{1}{2}|\vec{a}_\mu - \vec{a}_\nu|^2 \end{aligned} \tag{A.21}$$

Thus, if we define $\vec{x}_\mu \equiv \frac{1}{\sqrt{2}}\vec{a}_\mu$, then we have constructed four points, $\vec{x}_\mu$, in a 15-dimensional

Euclidean space such that the 6 distances between them are $D_{\mu\nu}$. Namely,

$$D^2_{\mu\nu} = |\vec{x}_\mu - \vec{x}_\nu|^2 \tag{A.22}$$

We can always find a 3-dimensional subspace of this 15-dimensional Euclidean space that contains the four points $\vec{x}_\mu$.

Hence, we have found 4 points, $\vec{x}_\mu$ in a 3-dimensional Euclidean vector space such that the 6 distances between them is $D_{\mu\nu}$. Thus the problem reduces to the classical Ptolemy problem.

A.3 Optimal transport problem at the extreme interaction limits

In this section, we present analytic proofs for the results stated in the text (Eq. s 7.19) for $W(m_i, m_j)$ in the extreme limits of the coupling. Namely, $V = 0$ and $V = \infty$.

A.3.1 $V = 0$

The distance matrix at $V = 0$ can be written as

$$D = \begin{pmatrix} 0 & \mathcal{I} \\ \mathcal{I} & 0 \end{pmatrix} \tag{A.23}$$

where $\mathcal{I}$ is the $L/2 \times L/2$ matrix with all entries equal to 1. We denote the $L/2$ component column vector with all entries equal to 1 by e. We represent the distance distributions

defined in Equation 5.8 by column vectors $m_i, m_{L/2+i}, i = 1, \ldots, L/2$,

$$m_i = \frac{2}{L}\begin{pmatrix} 0 \\ e \end{pmatrix} \quad m_{L/2+i} = \frac{2}{L}\begin{pmatrix} e \\ 0 \end{pmatrix}. \tag{A.24}$$

The constraints defining the joint probability distributions, π_{ij} can be writen in a matrix form,

$$\pi_{ij}\begin{pmatrix} e \\ e \end{pmatrix} = m_i \quad \begin{pmatrix} e^T & e^T \end{pmatrix}\pi_{ij} = m_j^T \tag{A.25}$$

The general solution to the above equations(A.25) is

$$\pi_{ij} = \frac{2}{L}\begin{pmatrix} 0 & 0 \\ 0 & P \end{pmatrix} \quad \pi_{iL/2+j} = \frac{2}{L}\begin{pmatrix} 0 & 0 \\ P & 0 \end{pmatrix}$$
$$\pi_{L/2+ij} = \frac{2}{L}\begin{pmatrix} 0 & P \\ 0 & 0 \end{pmatrix} \quad \pi_{L/2+iL/2+j} = \frac{2}{L}\begin{pmatrix} P & 0 \\ 0 & 0 \end{pmatrix},$$

where $i, j = 1, \ldots, L/2$. P is any $L/2 \times L/2$ component positive semi-definite matrix whose rows and columns sum up to 1. $P(i, j) \geq 0$, $\sum_{k=1}^{L/2} P(k, l) = 1 = \sum_{l=1}^{L/2} P(k, l)$.

The Wasserstein distances can be written in this matrix form as,

$$W(m_i, m_j) = \inf_{\pi} \mathrm{Tr}\left(D^{(2)}\pi_{ij}\right), \tag{A.26}$$

where $D^{(2)}(k, l) = (D(k, l))^2$. Using the fact that $P\mathcal{I} = \mathcal{I} = \mathcal{I}P$, it is easy to see that the RHS of the above equation is independent of P and we obtain the result stated in equation(7.19), that at $V = 0$,

$$W(m_i, m_j) = (D(i, j))^2 \tag{A.27}$$

A.3.2 $V = \infty$

The distance matrix in the limit $V = \infty$ for $\alpha = 2$ is

$$D = c\begin{pmatrix} \mathcal{I} - I & \mathcal{I} \\ \mathcal{I} & \mathcal{I} - I \end{pmatrix} + (1-c)\begin{pmatrix} 0 & I \\ I & 0 \end{pmatrix}, \tag{A.28}$$

where $c = \sqrt{3}/2$. To represent the distance distributions as column vectors, we define a set of $L/2$ component column vectors, $\chi_i, i = 1, \ldots, L/2$ whose entries are all zero except for the i^{th} one, which is equal to 1. Namely, $\chi_i(j) = \delta_{ij}$. We then have,

$$m_i = \frac{1}{\mathcal{L}}\begin{pmatrix} ce - c\chi_i \\ ce + (1-c)\chi_i \end{pmatrix}, \quad m_{L/2+i} = \frac{1}{\mathcal{L}}\begin{pmatrix} ce + (1-c)\chi_i \\ ce - c\chi_i \end{pmatrix} \tag{A.29}$$

where $\mathcal{L} = c(L-2) + 1$. We present a set of solutions to equations. We have no proof that these are the most general solutions. However, the definition of the Wasserstein distance in equation(A.26) implies that the infimum in this set provides an upper bound for $W(m_i, m_j)$. The solutions are of the form,

$$\pi_{ij} = \frac{1}{\mathcal{L}}\left(cP_{ij} + \pi'_{ij}\right) \tag{A.30}$$

where P_{ij} are $L \times L$, positive semi-definite matrices whose columns and rows sum up to 1.

$$P_{ij} \geq 0, \ \sum_{k=1}^{L} P_{ij}(k,l) = 1 = \sum_{l=1}^{L} P_{ij}(k,l) \tag{A.31}$$

π'_{ij} are,

$$\begin{aligned}
\pi'_{ij} &= \begin{pmatrix} -c\chi_i\chi_j^T & 0 \\ 0 & (1-c)\chi_i\chi_j^T \end{pmatrix} \\
\pi'_{iL/2+j} &= \begin{pmatrix} 0 & -c\chi_i\chi_j^T \\ (1-c)\chi_i\chi_j^T & 0 \end{pmatrix} \\
\pi'_{L/2+ij} &= \begin{pmatrix} 0 & (1-c)\chi_i\chi_j^T \\ -c\chi_i\chi_j^T & 0 \end{pmatrix} \\
\pi'_{L/2+iL/2+j} &= \begin{pmatrix} (1-c)\chi_i\chi_j^T & 0 \\ 0 & -c\chi_i\chi_j^T \end{pmatrix} \\
&. \qquad \text{(A.32)}
\end{aligned}$$

Equations (A.30), (A.32) and the constraint $\pi_{ij}(k,l) \geq 0, k, l = 1, \ldots, L$, implies that $P_{ij}(i,j) - 1 \geq 0$. Since the maximum value of the matrix elements of P_{ij} is 1, we have,

$$P_{ij}(i,j) = 1, \quad P_{ij}(i,k) = 0 \; \forall k \neq j, \quad P_{ij}(k,j) = 0 \; \forall k \neq i. \tag{A.33}$$

Consider the set of matrices, P^*_{ij} defined as,

$$P^*_{ij}(k,l) \equiv \delta_{kl}\left(1 - \delta_{ik} - \delta_{jl}\right) + \delta_{ik}\delta_{jl} + \delta_{il}\delta_{jk}, \tag{A.34}$$

it is straightforward to verify that P^*_{ij} satisfy all the constraints in equations (A.31) and (A.33).

Thus, equations (A.26) and (A.30) imply,

$$W(m_i, m_j) \leq \frac{1}{\mathcal{L}} \mathrm{Tr}\left(D^{(2)}\left(cP^*_{ij} + \pi'_{ij}\right)\right). \tag{A.35}$$

The RHS of the above inequality can be computed using equations (A.28), (A.32) and

(A.34). The result is,

$$\mathrm{Tr}\left(D^{(2)}\left(cP^{*}_{ij}+\pi'_{ij}\right)\right)=(D(i,j))^{2} \tag{A.36}$$

Thus, we have proved the result stated in equation 7.19, that at $V=\infty$,

$$W(m_i,m_j)\leq\frac{1}{\mathcal{L}}(D(i,j))^{2}. \tag{A.37}$$

Bibliography

[1] M. V. Berry, "Quantal phase factors accompanying adiabatic changes," *Proceedings of the Royal Society of London. A. Mathematical and Physical Sciences*, vol. 392, no. 1802, pp. 45–57, 1984.

[2] D. J. Thouless, M. Kohmoto, M. P. Nightingale, and M. den Nijs, "Quantized Hall conductance in a two-dimensional periodic potential," *Phys. Rev. Lett.*, vol. 49, pp. 405–408, Aug 1982.

[3] J. E. Avron, R. Seiler, and B. Simon, "Homotopy and quantization in condensed matter physics," *Phys. Rev. Lett.*, vol. 51, pp. 51–53, Jul 1983.

[4] Q. Niu and D. J. Thouless, "Quantised adiabatic charge transport in the presence of substrate disorder and many-body interaction," *Journal of Physics A: Mathematical and General*, vol. 17, pp. 2453–2462, aug 1984.

[5] F. D. M. Haldane, "Model for a Quantum Hall Effect without Landau Levels: Condensed-Matter Realization of the "Parity Anomaly"," *Phys. Rev. Lett.*, vol. 61, pp. 2015–2018, Oct 1988.

[6] R. Karplus and J. M. Luttinger, "Hall Effect in Ferromagnetics," *Phys. Rev.*, vol. 95, pp. 1154–1160, Sep 1954.

[7] G. Sundaram and Q. Niu, "Wave-packet dynamics in slowly perturbed crystals: Gradient corrections and Berry-phase effects," *Phys. Rev. B*, vol. 59, pp. 14915–14925, Jun 1999.

[8] F. D. M. Haldane, "Quantum geometry in conducting systems," June 2006. *PITP*-Les Houches Summer School, Quantum Magnetism.

[9] D. Xiao, M.-C. Chang, and Q. Niu, "Berry phase effects on electronic properties," *Rev. Mod. Phys.*, vol. 82, pp. 1959–2007, Jul 2010.

[10] F. D. M. Haldane, "Berry Curvature on the Fermi Surface: Anomalous Hall Effect as a topological Fermi-liquid property," *Phys. Rev. Lett.*, vol. 93, p. 206602, Nov 2004.

[11] R. D. King-Smith and D. Vanderbilt, "Theory of polarization of crystalline solids," *Phys. Rev. B*, vol. 47, pp. 1651–1654, Jan 1993.

[12] R. Resta, "Macroscopic polarization in crystalline dielectrics: the geometric phase approach," *Rev. Mod. Phys.*, vol. 66, pp. 899–915, Jul 1994.

[13] R. Resta, "The insulating state of matter: a geometrical theory," *The European Physical Journal B*, vol. 79, pp. 121–137, Jan 2011.

[14] F. D. M. Haldane, "Topology and geometry in quantum condensed matter." *PCCM/PCTS* Summer School, July 2012.

[15] N. Mukunda and R. Simon, ""quantum kinematic approach to the geometric phase. i. general formalism"," *Annals of Physics*, vol. 228, no. 2, pp. 205 – 268, 1993.

[16] V. Bargmann, "Note on Wigner's theorem on symmetry operations," *Journal of Mathematical Physics*, vol. 5, no. 7, pp. 862–868, 1964.

[17] R. Simon and N. Mukunda, "Bargmann invariant and the geometry of the Güoy effect," *Phys. Rev. Lett.*, vol. 70, pp. 880–883, Feb 1993.

[18] I. Souza, T. Wilkens, and R. M. Martin, "Polarization and localization in insulators: Generating function approach," *Phys. Rev. B*, vol. 62, pp. 1666–1683, Jul 2000.

[19] Z. Wang, X.-L. Qi, and S.-C. Zhang, "Topological Order Parameters for Interacting Topological Insulators," *Phys. Rev. Lett.*, vol. 105, p. 256803, Dec 2010.

[20] Z. Wang and S.-C. Zhang, "Simplified Topological Invariants for Interacting Insulators," *Phys. Rev. X*, vol. 2, p. 031008, Aug 2012.

[21] L. Wang, X. Dai, and X. C. Xie, "Frequency domain winding number and interaction effect on topological insulators," *Phys. Rev. B*, vol. 84, p. 205116, Nov 2011.

[22] V. Gurarie, "Single-particle Green's functions and interacting topological insulators," *Phys. Rev. B*, vol. 83, p. 085426, Feb 2011.

[23] K.-T. Chen and P. A. Lee, "Unified formalism for calculating polarization, magnetization, and more in a periodic insulator," *Phys. Rev. B*, vol. 84, p. 205137, Nov 2011.

[24] Z. Wang, X.-L. Qi, and S.-C. Zhang, "Topological invariants for interacting topological insulators with inversion symmetry," *Phys. Rev. B*, vol. 85, p. 165126, Apr 2012.

[25] W. Kohn, "Theory of the insulating state," *Phys. Rev.*, vol. 133, pp. A171–A181, Jan 1964.

[26] L. D. Landau, "On the theory of phase transitions," *Zh. Eksp. Teor. Fiz.*, vol. 7, pp. 19–32, 1937. [Ukr. J. Phys.53,25(2008)].

[27] R. Resta, "Quantum-mechanical position operator in extended systems," *Phys. Rev. Lett.*, vol. 80, pp. 1800–1803, Mar 1998.

[28] R. Resta, "Why are insulators insulating and metals conducting?," *Journal of Physics: Condensed Matter*, vol. 14, no. 20, p. R625, 2002.

[29] R. Resta and S. Sorella, "Electron localization in the insulating state," *Phys. Rev. Lett.*, vol. 82, pp. 370–373, Jan 1999.

[30] R. Resta, "Electron Localization in the Quantum Hall Regime," *Phys. Rev. Lett.*, vol. 95, p. 196805, Nov 2005.

[31] R. Resta, "Why are insulators insulating and metals conducting?," *Journal of Physics: Condensed Matter*, vol. 14, no. 20, p. R625, 2002.

[32] C. Sgiarovello, M. Peressi, and R. Resta, "Electron localization in the insulating state: Application to crystalline semiconductors," *Phys. Rev. B*, vol. 64, p. 115202, Aug 2001.

[33] C. N. Yang and C. P. Yang, "One-dimensional chain of anisotropic spin-spin interactions. I. proof of Bethe's hypothesis for ground state in a finite system," *Phys. Rev.*, vol. 150, pp. 321–327, Oct 1966.

[34] R. J. Baxter, *Exactly Solved Models in Statistical Mechanics*. Academic Press, 1982.

[35] M. A. Cazalilla, R. Citro, T. Giamarchi, E. Orignac, and M. Rigol, "One dimensional bosons: From condensed matter systems to ultracold gases," *Rev. Mod. Phys.*, vol. 83, pp. 1405–1466, Dec 2011.

[36] I. J. Schoenberg, "On Metric Arcs of Vanishing Menger Curvature," *Annals of Mathematics*, vol. 41, no. 4, pp. 715–726, 1940.

[37] J. Lott and C. Villani, "Ricci curvature for metric-measure spaces via optimal transport.," *Ann. Math. (2)*, vol. 169, no. 3, pp. 903–991, 2009.

[38] S. Ohta *Comment. Math. Helv*, vol. 82, pp. 805–828, 2007.

[39] K.-T. Sturm, "On the geometry of metric measure spaces. ii," *Acta Math.*, vol. 196, no. 1, pp. 133–177, 2006.

[40] E. Saucan, *Metric Curvatures Revisited: A Brief Overview*, pp. 63–114. 10 2017.

[41] K. F. Gauss, "General investigations of curved surfaces of 1827 and 1825," *Nature*, vol. 66, pp. 316–317, 2010.

[42] E. Saucan and E. Appleboim, "Curvature Based Clustering for DNA Microarray Data Analysis," pp. 405–412, 06 2005.

[43] A. Wald, "Sur la courbure des surfaces," *C. R. Acad. Sci. Paris*, vol. 201, pp. 918–920, 1935.

[44] A.-I. Bonciocat and K.-T. Sturm, "Mass transportation and rough curvature bounds for discrete spaces," *Journal of Functional Analysis*, vol. 256, no. 9, pp. 2944 – 2966, 2009.

[45] D. Bakry and M. Émery, "Diffusions hypercontractives," in *Séminaire de Probabilités XIX 1983/84* (J. Azéma and M. Yor, eds.), (Berlin, Heidelberg), pp. 177–206, Springer Berlin Heidelberg, 1985.

[46] R. Forman, "Bochner's method for cell complexes and combinatorial Ricci curvature," *Discrete and Computational Geometry*, vol. 29, pp. 323–374, 2003.

[47] Y. Ollivier, "Ricci curvature of Markov chains on metric spaces," *Journal of Functional Analysis*, vol. 256, no. 3, pp. 810 – 864, 2009.

[48] Y. Ollivier, "A survey of Ricci curvature for metric spaces and Markov chains," *Probabilistic Approach to Geometry*, vol. 57, 01 2010.

[49] M. Erbar and J. Maas, "Ricci curvature of finite Markov chains via convexity of the entropy," *Archive for Rational Mechanics and Analysis*, vol. 206, pp. 997–1038, Dec 2012.

[50] Y. Ollivier, *A visual introduction to Riemannian curvatures and some discrete generalizations*. AMS, 2013.

[51] L. Liberti and C. Lavor, "Six mathematical gems from the history of distance geometry," *International Transactions in Operational Research*, vol. 23, 02 2015.

[52] L. Liberti, C. Lavor, N. Maculan, and A. Mucherino, "Euclidean distance geometry and applications," *SIAM Review*, vol. 56, 05 2012.

[53] I. Dokmanic, R. Parhizkar, J. Ranieri, and M. Vetterli, "Euclidean distance matrices: A short walk through theory, algorithms and applications," *CoRR*, vol. abs/1502.07541, 2015.

[54] I. J. Schoenberg, "Remarks to Maurice Frechet's Article "Sur La Definition Axiomatique D'Une Classe D'Espace Distances Vectoriellement Applicable Sur L'Espace De Hilbert," *Annals of Mathematics*, vol. 36, no. 3, pp. 724–732, 1935.

[55] T. Crilly, "The rise of Cayley's invariant theory (1841−1862)," *Historia Mathematica*, vol. 13, no. 3, pp. 241 – 254, 1986.

[56] K. Menger, "Untersuchungen über allgemeine Metrik," *Mathematische Annalen*, vol. 100, pp. 75–163, Dec 1928.

[57] Bluemental, *Theory and Applications of Distance Geometry*. Oxford University Press, 1953.

[58] P. Indyk and J. Matousek, *Low-Distortion Embeddings of Finite Metric Spaces*. CRC Press, 2004.

[59] Y. Rabinovich, "On average distortion of embedding metrics into the line and into l1," pp. 456–462, 2003.

[60] I. Abraham, Y. Bartal, and O. Neiman, "Advances in metric embedding theory," *Advances in Mathematics*, vol. 228, no. 6, pp. 3026 – 3126, 2011.

[61] R. Gemulla and P. Miettinen, "Data mining and matrices,03− singular value decomposition," 2013. Lecture slides Max Planck Institut Informatik.

[62] T. M. Mitchell, "Reducing data dimension," 2005. Lecture slides on Machine Learning, Carnegie Mellon University.

[63] C. Villani, *Optimal Transport: Old and New*. Grundlehren der mathematischen Wissenschaften, Springer, 2009 ed., Sept. 2008.

[64] C. Villani, *Topics in Optimal Transportation*. Graduate studies in mathematics, American Mathematical Society, 2003.

[65] S. Kolouri, S. R. Park, M. Thorpe, D. Slepcev, and G. K. Rohde, "Optimal mass transport: Signal processing and machine-learning applications," *IEEE Signal Processing Magazine*, vol. 34, pp. 43–59, July 2017.

[66] M. Agueh and G. Carlier, "Barycenters in the Wasserstein Space," *SIAM Journal on Mathematical Analysis*, vol. 43, no. 2, pp. 904–924, 2011.

[67] M. Cuturi, "Sinkhorn distances: Lightspeed computation of optimal transport," in *Proceedings of the 26th International Conference on Neural Information Processing Systems - Volume 2*, NIPS'13, (USA), pp. 2292–2300, Curran Associates Inc., 2013.

[68] M. Arjovsky, S. Chintala, and L. Bottou, "Wasserstein generative adversarial networks," in *Proceedings of the 34th International Conference on Machine Learning* (D. Precup and Y. W. Teh, eds.), vol. 70 of *Proceedings of Machine Learning Research*, (International Convention Centre, Sydney, Australia), pp. 214–223, PMLR, 06–11 Aug 2017.

[69] N. Courty, R. Flamary, D. Tuia, and A. Rakotomamonjy, "Optimal transport for domain adaptation," *CoRR*, vol. abs/1507.00504, 2015.

[70] G. Buttazzo, L. De Pascale, and P. Gori-Giorgi, "Optimal-transport formulation of electronic density-functional theory," *Phys. Rev. A*, vol. 85, p. 062502, Jun 2012.

[71] C. Cotar, G. Friesecke, and C. Kluppelberg, "Density functional theory and optimal transportation with Coulomb cost," *Communications on Pure and Applied Mathematics*, vol. 66, no. 4, pp. 548–599, 2013.

[72] M. Cuturi and A. Doucet, "Fast Computation of Wasserstein Barycenters," in *Proceedings of the 31st International Conference on Machine Learning* (E. P. Xing and T. Jebara, eds.), vol. 32 of *Proceedings of Machine Learning Research*, (Bejing, China), pp. 685–693, PMLR, 22–24 Jun 2014.

[73] J. M. Luttinger, "An exactly soluble model of a many-Fermion system," *Journal of Mathematical Physics*, vol. 4, no. 9, pp. 1154–1162, 1963.

[74] F. D. M. Haldane, "General relation of correlation exponents and spectral properties of one-dimensional Fermi Systems: application to the anisotropic $S = \frac{1}{2}$ Heisenberg chain," *Phys. Rev. Lett.*, vol. 45, pp. 1358–1362, Oct 1980.

[75] F. D. M. Haldane, "'Luttinger liquid theory' of one-dimensional quantum fluids. I. Properties of the Luttinger model and their extension to the general 1D interacting spinless Fermi gas," *Journal of Physics C: Solid State Physics*, vol. 14, no. 19, p. 2585, 1981.

[76] R. Shankar, "Solvable model of a metal-insulator transition," *International Journal of Modern Physics B*, vol. 04, no. 15n16, pp. 2371–2394, 1990.

[77] K. Gödel, *K. Gödel Collected Works*. Oxford University Press: Oxford, 1953.

[78] W. Braun, "Distance geometry and related methods for protein structure determination from NMR data," *Quarterly Reviews of Biophysics*, vol. 19, no. 3-4, pp. 115–157, 1987.

[79] G. H. Forman and J. Zahorjan, "The challenges of mobile computing," *Computer*, vol. 27, pp. 38–47, Apr. 1994.

[80] G. Saporta, "The analysis of proximity data. b. s. everitt and s. rabe-hesketh, arnold, london, 1997," *Statistics in Medicine*, vol. 18, no. 4, pp. 491–492, 1999.

[81] G. Monge, "Memoire sur la theorie des deblais et des remblais," *In Histoire de lAcademie Royale des Sciences de Paris*, pp. 666–704, 1781.

[82] L. V. Kantorovich, "On translocation of masses," *USSR AS Doklady. New Serie.*, vol. 37, pp. 227–229, 1942.

[83] Y. Rubner, C. Tomasi, and L. J. Guibas, "The earth mover's distance as a metric for image retrieval," *International Journal of Computer Vision*, vol. 40, pp. 99–121, Nov 2000.

[84] K. Ni, X. Bresson, T. Chan, and S. Esedoglu, "Local histogram based segmentation using the Wasserstein distance," *International Journal of Computer Vision*, vol. 84, pp. 97–111, Aug 2009.

[85] "A probability metrics approach to financial risk measures, by svetlozar t. rachev, stoyan v. stoyanov, and frank j. fabozzi, 2011, oxford, uk: Wiley blackwell, 392 pp. isbn: 978-1-4051-8369-7," *Journal of Risk and Insurance*, vol. 83, no. 2, pp. 505–510, 2016.

[86] K.-T. Sturm, "Probability measures on metric spaces of nonpositive curvature, heat kernels and analysis on manifolds," *Graphs, and Metric Spaces*, pp. 357–390, 01 2002.

[87] R. Sinkhorn and P. Knopp, "Concerning nonnegative matrices and doubly stochastic matrices.," *Pacific J. Math.*, vol. 21, no. 2, pp. 343–348, 1967.

[88] P. A. Knight, "The sinkhorn-knopp algorithm: Convergence and applications," *SIAM J. Matrix Anal. Appl.*, vol. 30, pp. 261–275, Mar. 2008.

[89] M. Cuturi and A. Doucet, "Fast computation of Wasserstein barycenters," in *Proceedings of the 31st International Conference on Machine Learning* (E. P. Xing and T. Jebara, eds.), vol. 32 of *Proceedings of Machine Learning Research*, (Bejing, China), pp. 685–693, PMLR, 22–24 Jun 2014.

[90] J.-D. Benamou, G. Carlier, M. Cuturi, L. Nenna, and G. Peyré, "Iterative Bregman Projections for Regularized Transportation Problems," *SIAM Journal on Scientific Computing*, vol. 2, no. 37, pp. A1111–A1138, 2015.

[91] J. Solomon, F. de Goes, G. Peyré, M. Cuturi, A. Butscher, A. Nguyen, T. Du, and L. Guibas, "Convolutional Wasserstein distances: efficient optimal transportation on geometric domains," *ACM Trans. Graph.*, vol. 34, pp. 66:1–66:11, July 2015.

[92] B. Muzellec and M. Cuturi, "Generalizing point embeddings using the Wasserstein space of elliptical distributions," in *Proceedings of the 32Nd International Conference on Neural Information Processing Systems*, NIPS'18, 2018.

[93] H. Xu, W. Wang, W. Liu, and L. Carin, "Distilled Wasserstein learning for word embedding and topic modeling," *CoRR*, vol. abs/1809.04705, 2018.

[94] Y. Lin, L. Lu, and S.-T. Yau 2011.

[95] J. Jost and S. Liu, "Ollivier's Ricci curvature, local clustering and curvature-dimension inequalities on graphs," *Discrete Comput. Geom.*, vol. 51, pp. 300–322, Mar. 2014.

[96] C. A. Trugenberger, "Random holographic "large worlds" with emergent dimensions," *Phys. Rev. E*, vol. 94, p. 052305, Nov 2016.

[97] C. A. Trugenberger, "Combinatorial quantum gravity: geometry from random bits," *Journal of High Energy Physics*, vol. 2017, p. 45, Sep 2017.

[98] R. P. Sreejith, J. Jost, E. Saucan, and A. Samal, "Forman curvature for directed networks," 2016.

[99] R. S. Sandhu, T. T. Georgiou, and A. R. Tannenbaum, "Ricci curvature: An economic indicator for market fragility and systemic risk," *Science Advances*, vol. 2, no. 5, 2016.

[100] C.-C. Ni, Y.-Y. Lin, J. Gao, X. Gu, and E. Saucan, "Ricci curvature of the internet topology," *2015 IEEE Conference on Computer Communications (INFOCOM)*, pp. 2758–2766, 2015.

[101] M. d. T. Levi-Civita, "Nozione di parallelismo in una varietà qualunque e conseguente specificazione geometrica della curvatura riemanniana," *Rendiconti del Circolo Matematico di Palermo (1884-1940)*, vol. 42, pp. 173–204, Dec 1916.